Defluidization of Silica sand or Clay particle beds by Palm Empty Fruit Bunch (EFB) ashes addition in Bubbling Fluidized Bed (BFB) process

Presented by

Student ID: T172C603

Name: PRIMA Zuldian

Department of Environmental Engineering Science

Graduate School of Science

Gunma University

2021

CONTENTS

CHAPTER III. **Agglomeration and Defluidization of Silica sand and Bentonite Particles Processes influenced by superficial velocity (1.5 U_{mf}) with thermal treatment temperature at 700, 750 and 800ºC**

CHAPTER IV. Identification of agglomeration mechanism based on reaction and distribution particle pores

LIST OF FIGURES

LIST OF TABLES

Abstract

Generation of Empty Fruit Bunch (EFB) in Indonesia is so large as promising biomass which can be utilized for a renewable energy resource by gasification process. However, alkaline concentration in EFB is high and will need a proper treatment to avoid slagging formation during reaction. A function of bentonite as particular of clay is not only as support catalyst but also as a potential natural inhibitor to avoid agglomeration. Currently, no investigation data regarding agglomeration between bentonite and EFB ash makes this study important to elucidate the applicability for a fluidized bed biomass gasification process. Higher allowance of ash concentration in a bed and longer maintenance intervals of fluidized beds in typical operation condition are expected for a bentonite fluidized bed gasification.

In Chapter I overview of slagging formation, fluidization system, and current study regarding agglomeration and defluidization are described. Furthermore, a brief information related to a newly developed fluidized bed pilot plant for EFB by applying bentonite particles relevant to this study are also informed in the chapter.

Agglomeration and defluidization behaviors in a bentonite particle fluidized bed by adding EFB ash at different temperatures with a typical superficial velocity is studied in Chapter II in comparison with those in a silica sand bed. The result in this chapter showed that bentonite particles can provide stable fluidization in wider region in comparison with silica sand. From the viewpoint of an application to the new pilot plant, bentonite application could maintain stable fluidization with around 3.5 wt.% of EFB ash concentration in the bed up to 800ºC. Meanwhile, a silica sand bed reached defluidization state after several EFB ashes addition in operation at 800ºC.

In Chapter III, in order to reduce gas consumption in a fluidized bed system, a comparison of agglomeration and defluidization behaviors of both bentonite and silica sand fluidized beds are studied in lower superficial velocity than Chapter II. The purpose of this chapter is to identify the impact of velocity affect to characteristics of agglomerates and capability to maintain fluidization. This study showed that the bentonite reached defluidization in lower ash addition than that in silica sand at treatment 800ºC. The reverse phenomena might be caused by lower mixing intensity of fluidized bed resulted from lower superficial velocity less than Chapter II. Channelling phenomena as an indicator of adhere ability of bed materials were also investigated. The results showed that bentonite particles had a high adhere ability at lower velocity, but the agglomerates were relatively weak to be easily broken.

Chapter IV discusses detailed mechanisms of agglomeration and defluidization formation based on the characteristics of bed residue after the operation. Specific surface area, pore size distribution, X-ray diffraction analysis (XRD), scanning electron microscopic observation (SEM) and energy dispersive X-ray analysis (EDX) were carried out to understand the microstructure of agglomerates. Specific surface of bentonite agglomerates was slightly increased by temperature increment in comparison with silica sand. However, the difference of both surface area of agglomerates was not significant. Decrement of peak intensity of silica (SiO_2) were observed in XRD analysis at 800^oC significantly in silica sand but slightly in bentonite. It might be caused by the difference of formation of silicates. Microstructure measurement showed that some incomplete coating and melting layers had been formed on that surface enabling to reach easier degradation than silica sand during fluidization was taking place.

Chapter V concludes that a fluidized bed of bentonite particles has higher stability to provide enough performance for EFB gasification based on the discussion in the previous chapters.

Acknowledgment

CHAPTER I

General Introduction

1.1. Background

1.1.1 Slagging formation in the thermal conversion process

A serious problem in a fluidized bed reactor at a high temperature can be caused by sintering bed particles which can decrease fluidization performance significantly (Daizo and Octave, 1991). That problem is called slagging or slag formation. Slag behavior is affected by the properties of both gaseous and solid phases, reactor wall structure, fluid dynamic, and operating conditions. At elevated temperature viscosity of slag decreased logarithmically, and at lower temperature crystallization or the separation of immiscible liquid may cause a dramatic increase in velocity. Slag viscosity strongly depends on temperature and chemical compositions, and it could be raised by the increment of operational gasification temperature (Wang and Massoudi, 2013). The slagging phenomenon is initiated by a transformation mechanism in biomass combustion where during that process, volatile organo-metallic compounds (containing C, V, etc) are first released followed by devolatilization. After that, some alkali and alkali earth elements (e.g. Hg, A, and Se) diffused out from the char. When the temperature decreases, volatile components nucleate and condense to form submicron-sized particles and condense on residual fly ash (Niu $et.al.$, 2016). The slagging from biomass combustion was formed when a high concentration of K and Na through nucleation, condensation, and reaction results in severe ash-related problems such as alkali-induced slagging, silicate melt-induced slagging and agglomeration.

The slagging formation is shown in **Figure 1-1**. In that figure, alkali metals did complex chemical reactions and transformations. That alkali released as KOH aerosol, KCl aerosol, K_2SO_4 aerosol, NaCl aerosol, and other compounds. At the time when temperature decreases, some alkali metal aerosols grow and form submicron ash particles. These aerosols will condense on the heating surface to form a sticky initial slagging layer, and on the surface of the fly ash to form a sticky layer too by reaction with SiO_2 and Fe_2O_3 contained in ash (Garba $et.al.$, 2012). The presence of sand or SiO_2 has a high

tendency to increase the slagging formation and melting ash reaction in all biomass studies (Lindstrom *et.al.*, 2008). The condensation on the heating surface and fly ash is relevant to the term of fouling and slagging formation (Niu *et.al.,* 2016).
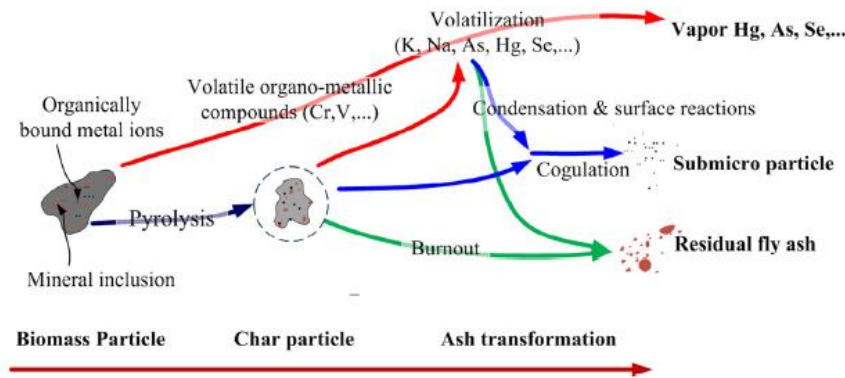
Figure 1-1. Schematic diagram of ash formation and transformation mechanism in biomass combustion

1.1.2 Alkaline of biomass as a source of the problem in the thermal conversion process

Currently, biomass utilization is relevant to renewable resources as fossil substitution coming from agricultural residues, forestry, industry residues, plantations, and energy crops as an energy source. The utilization of biomass is already successfully combusted via direct combustion and co-combustion technology, as well as gasification and pyrolysis (Mlonka *et.al.*, 2019). The unwanted problem comes from inorganic elements which form complex compounds in gaseous, liquid, and solid phases during thermal biomass conversion related to slagging and fouling process. The potency of ash containing inorganic elements from biomass is significantly lower than fossil fuel as coal (Mlonka *et.al.*, 2019), but the characteristic of nature biomass has much heterogeneity and depends on biomass origin and processing. So, the difficulty of mechanism and prevention unwanted effect will be more difficult than coal in combustion system too.

The biomass ash mainly consists of calcium, silicon potassium and phosphorus, and chlorine. Alkali metals especially K and Na will react with chlorine to make the most unwanted processes (Mlonka *et.al.*, 2019). Alkali metals in biomass mainly exist in three forms, namely organic form (e.g. R-COO-K+), inorganic salts (e.g. KCl, K_2SO_4), and mineral form (e.g. K_2O_3Si), in which a small amount of bounded potassium is stable and

non-volatile during thermal conversion. The release of alkali metals occurs through complex reactions influenced by the content of inorganic species, density, shape, the particle size of biomass, fuel to air ratio, heating rate, and temperature. During temperature increment, the organic alkali metals start to release. When the temperature is high enough, inorganic alkali metals start to release too (Cao *et.al.*, 2016).

1.1.3 The potency of Empty Fruit Bunch (EFB) utilization in thermal conversion

Biomass is defined as a broad range of materials that are biological in nature and can be used to produce various forms of energy (Miles *et.al.*,1993). Currently, biomass waste is the primary source of fuel used in biomass power plant facilities. Biomass waste for energy is provided from urban wood, fuelwood, wood by-products, and waste wood. Fuelwood is produced on private wood lots, national forest, and state wood lots. Woods by-products are resulted from liquor and sawdust, while wood waste is obtained from cull logs, hogged bark, and manufacturing scrap wood.

The palm tree is biomass that is used to produce vegetable oil. Since the demand is very high, so the supply should be high too. In 2010-2014, the total share of Palm tree plantations was dominated in South-East Asia, South America, and West Africa. Indonesia, Malaysia, Thailand, Nigeria, Colombia, Papua New Guinea including other countries become some of the highest Crude Palm Oil (CPO) producers in the world with the share were 48.44%, 35.60%, 8.08%, 3.29%, 1.81%, 1.78% and 1% (Indonesian palm tree outlook 2016). Empty Fruit Bunch (EFB) is agricultural residue or palm tree waste which is a big current issue since the effort to utilize it becomes a more beneficial commodity. It has increased continually along with the increase of CPO with a total amount of around 21% of Fresh Fruit Bunch cultivation. EFB consists of several fibers, namely 45.95% cellulose, 16.49% hemicellulose, 22.84% lignin, and high alkaline. Treatment of EFB is only incinerated and the ash (high in K_2O) is applied in oil palm plantation (Rosenani and Hoe, 1996), as one of the thermal conversion application having less risk, inexpensive, and the highest potential among short term options for realizing biomass utilization (Gaba and Iodache, 2011). Another treatment is the direct combustion process to only produce steam and then generate electricity by a steam turbine with relatively low efficiency in small to middle-scale plants (Aruga *et.al.*, 2011). Furthermore,

the treatment of EFB has been started in thermal conversion technology to generate raw syngas as a useful product for many purposes like fuel and chemicals. However, recently most EFB is still returned to the fields as an organic fertilizer and a green mulch to the palm (Rosenani and Hoe, 1996). Therefore, the effort to enhance the utilization of EFB from the waste become a commercial commodity as environmental-friendly material and renewable energy source is important and needed to be developed because EFB is the potential to be developed due to high availability. However, the presence of alkaline in EFB becomes a challenge that needs to be minimized so that thermal treatment can run well.

1.2 Fluidization process as outstanding technology to achieve high efficiency

The presence of alkali metal in combustion and gasification may give a negative effect on the overall efficiency. The function of fluidized bed may be deteriorated by agglomeration of bed particles due to low melting eutectic alkali salt mixtures. Fluidized catalytic cracking (FCC) unit operated in 1940. Fluidized beds typically are more complex to design, build and operate than other types of reactor like packed-bed and stirred-tank reactors. Furthermore, it is more difficult to be scaled up, easy to form erosion and attrition caused by moving particle, and easier to entrain solid particle reducing the mass transfer process. However, fluidized bed processes are promising technology, which can easily gasify feedstock in non-uniform shape including fibrous materials, and can produce syngas excluding nitrogen by application of a dual-bed system (Visser *et.al.*, 2008), as shown in **Figure 1-2**.
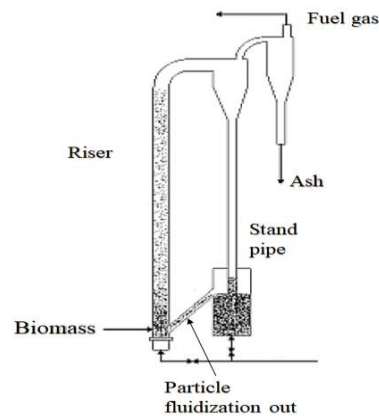
Figure 1-2. Dual-bed system fluidized bed process (Visser *et.al.*, 2008)

The fluidized bed already becomes outstanding technology with high efficiency having superior heat transfer until 10 times faster than a packed-bed reactor, easily moves solid particles, and has an ability to process material with a wide particle size distribution. Another benefit, the catalyst can be added or removed easily during operation especially in FCC circulating fluidized bed application (Cocco et.al., 2014).

1.3   Agglomeration and defluidization process as an unwanted state during fluidization process.

Inorganic alkali compounds like Na, K, Ca and Mg contained in EFB were general elements promoting alkali-silicate reaction which is initiated by the formation of deposition on the wall, agglomerate formation in the bed, and finally defluidization state (Novianti *et.al.*, 2015). Agglomeration formation is highly affected by bed material and operating conditions. Agglomeration and defluidization formation will significantly increase with operational temperature increment and the increase of experimental time (Li *et.al.*, 2011). Some methods have been developed to detect agglomeration and defluidization reactor consist of average pressure drop measurement of the bed, the measurement of standard deviation or variance of differential pressure fluctuation to detect defluidization onset, and transient power spectral density methods. Another method is temperature measurement based on two thermocouple performances at a certain vertical distance apart. When agglomeration is formed, the difference value will increase caused by sensitivity increment as the behavior towards defluidization. (Serrano *et.al.*, 2014).

1.4   Utilization of silica sand and bentonite role particles to inhibit and extend defluidization process

Silica sand which is dominated by Silicon dioxide (SiO_2) is ideal for being used in fluidized beds because of the high hardness and low cost. The defluidization time will be extended by velocity increment. High velocity in the bed will lead to better mixing of the particles and increase force acting on agglomerates. The increase of gas velocity could extend defluidization time, but it cannot avoid defluidization state (Li *et.al.*, 2011).

The application of clay particles as bed materials potentially gives several benefits. Clay minerals consist of illite, smectite, vermiculite, and kaolinite main groups in which smectite group having montmorillonite subgroup have been well known as a useful solid acid catalyst. Bentonite is a kind of natural clays consists of montmorillonite as the main constituent, which has been used in many industrial applications (Nagendrappa, 2002; Onal, 2009). The potential of bentonite bed material for tar reduction in fluidized bed biomass gasification has been already proven by Noda (Reiji Noda *et.al.*, 2009). Clay is sticky and plastic when containing moisture at room temperature but easily becomes hard by thermal treatment. Therefore, it is easy to prepare the appropriate size of granules by a conventional granulation process. The clay minerals usually contain aluminum silicates. When heating up, a mixture of alkalis and aluminum silicates, alkali aluminosilicates will be formed instead of the formation of alkali silicates. Because alkali aluminosilicates have higher melting points in comparison with alkali silicates, high resistance to agglomeration is expected during reaction with EFB ash.

The main problems of fluidized bed gasification of biomass with clay bed material are agglomeration and defluidization caused by interaction between biomass ash and bed materials. Therefore, this work has the purpose to simulate agglomeration and defludization behavior in a fluidized bed gasification process to understand stable operating conditions in various temperatures and EFB ash addition in bentonite granule beds and to elucidate the advantage of clay bed material against silica sand.

1.5   Development of fluidized bed gasification system in Indonesia

Since 2011, there had been 9 pilot plants gasification in Indonesia constructed with the fixed-bed system having capacity 3 until 7 MW. All plants used coal as raw material to produce syngas for electricity generation only. However, those plants had stopped. One of the big problems was the incapability of plants to manage tar emission resulted from a fixed-bed system.

Fluidized bed application is a promising technology that can reduce tar pollution, increase carbon conversion by almost 80 wt.% which might produce a higher syngas rate than the fixed-bed system. So, that is very relevant with the situation in Indonesia to develop technology that can handle those problems above. The concept of fluidized bed

system which had been developed in Indonesia was a circulating fluidized bed gasifier using clay catalyst, namely bentonite. Since clay has catalytic effects and high silica content, so it could be used in gasification. This concept was environmental-friendly starting from the utilization of natural clay (bentonite), conversion of EFB into syngas, releasing carbon oxide for supporting internal plant mechanism, and utilization of bed residue having rich alkaline as nutrients to sustain biomass resources production. The brief concept was explained in **Figure 1-3.**
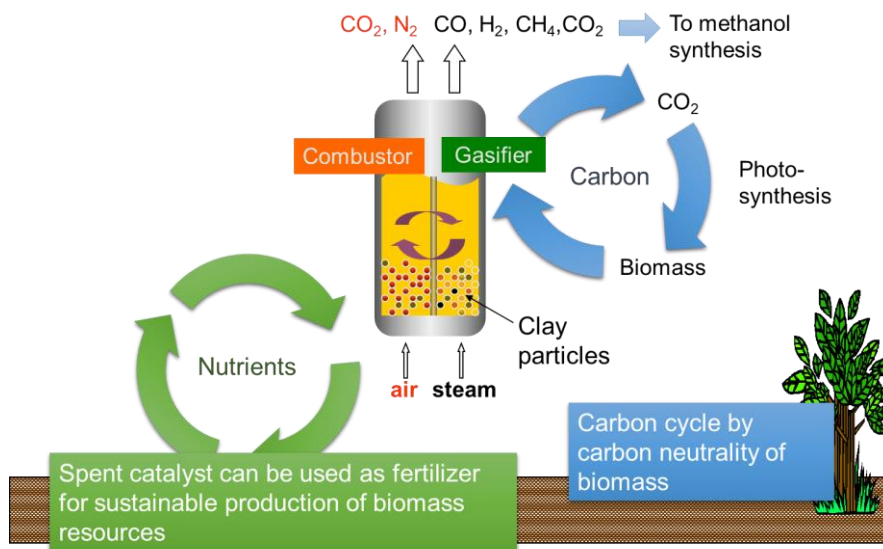
Figure 1-3. Concept of a clay catalyst circulating fluidized bed gasifier

Currently, there are two pilots fluidized bed technology which is called as loop-seal Circulating Fluidized Bed system. Both systems are shown in **Figure 1-4** consist of two compartments enabling to do gasification and combustion processes in the same operation time. It had been installed to be operated as the cold system which will simulate loop-seal fluidized bed gasification and the hot model system as the mini scale of the fluidized plant which will operate at thermal temperature. The syngas will be used in power generation to generate electricity around 50 kW with a feeding rate few hundred EFB/day.

Relevant to the study at Gunma University, that operation was similar. It would be operated between temperatures 700 and 800°C with air fluidization intensity around 4.3 U_{mf}. The U_{mf} adjustment was relevant to literature that suggested velocity adjustment on bubbling fluidization process which should be less than $10U_{mf}$ (Daizo and Octave, 1991). The raw material was EFB as residue from some palm oil plants in Indonesia, while the

natural clay in the form of Na-bentonite as bed particle which that resource could be mined from several areas in Java Island, Indonesia as shown in **Figure 1-5**.

(a).
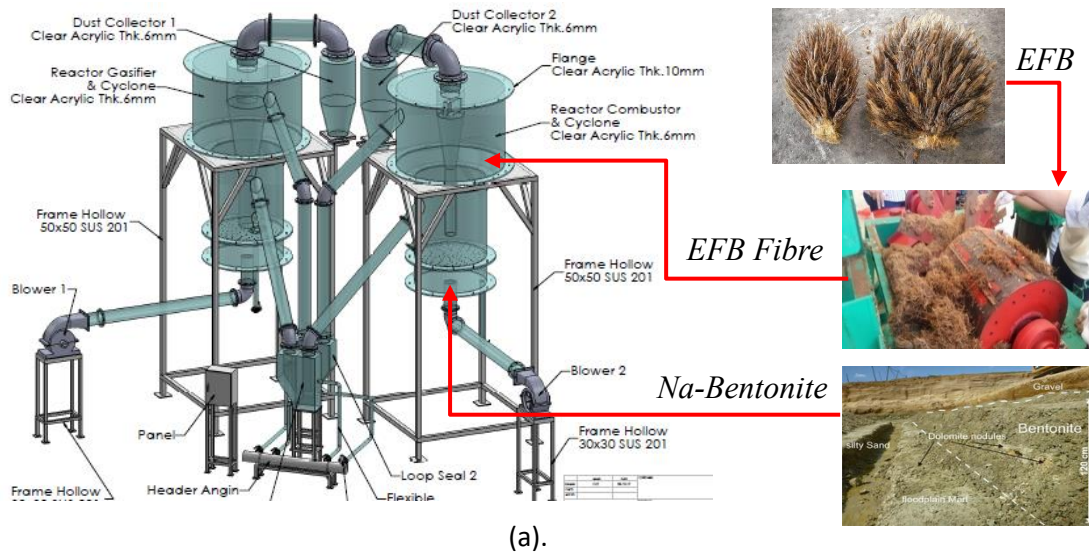
(b). Cold model

(c). Hot model

Figure 1-4. Loop-seal circulating fluidized bed mechanism (a), for cold model (b) and hot model systems (c)

Figure 1-5. Dissemination of Na-bentonite location in Indonesia

Utilization of bentonite will be used by considering that function as a solid acidic catalyst which has high availability of resources and cheaper than synthetic catalysts.

1.6 Purpose of study

Since the availability of EFB is very abundant, so it can guarantee the sustainability of thermal conversion process like gasification for a long time. Utilization of EFB by using a Fluidized bed is still rare and still limited in research only, not for commercial purposes. Application of clay in biomass fluidized bed gasification had already been proved to reduce tar and increase the efficiency of operation. However, the reaction between alkali and silicate contained in biomass and bed material has the potency to form an agglomeration process which can lead to the slagging formation. Therefore, agglomeration and defluidization study of bed material is very important, and study of bentonite as one type of clay group in fluidization has never carried out before.

This study aimed to analyze the mechanism of agglomeration and defluidization formation as the comparison between silica sand and bentonite affected by EFB ash mass increment at temperatures 700, 750, and 800°C under several superficial velocities. Based on differential pressure and standard deviation of pressure, then agglomeration state and defluidization onset could be detected after several ashes-rich potassium additions. Therefore, the threshold of potassium content between fluidization and agglomeration process could be identified. In this study, the mechanism of sticky agglomeration was observed based on elemental measurement from XRF data. Therefore, this study would elucidate not only the effect of alkaline mass addition against fluidization state threshold but also would predict the sticky level of agglomerates formed in bed residue. Furthermore, measurement of silicate components, distribution of pore size, and microscopic observation on agglomerates surface based on XRD, BET, SEM, and mapping area with SEM-EDX measurements were also carried out to predict agglomeration mechanism.

References

Aruga, Kazuhiro & Murakami, Ayami & Nakahata, Chikara & Yamaguchi, Reiko & Yoshioka, Takuyuki. (2011). *Discussion on Economic and Energy Balances of*

Forest Biomass Utilization for Small-Scale Power Generation in Kanuma, Tochigi Prefecture, Japan. Croatian Journal of Forest Engineering. 32.

Cao, W., Li, J., Luo, L., & Zhang, X. (2016). *Release of alkali metals during biomass thermal conversion. Archives of Industrial Biotechnology*, 1(1), 1-3. http://www.alliedacademies.org/articles/release-of-alkali-metalsduring-biomass-thermal-conversion.html

Center of data and agricultural-information system. *Palm Tree Outlook*. Indonesian Ministry of agriculture. 2016

Cocco, Ray & Karri, Sb & Knowlton, Ted. (2014). *Introduction to Fluidization*. Chemical Engineering Progress. 110. 21-29.

Daizo Kunii, Octave Levenspiel, *CHAPTER 4 - The Dense Bed: Distributors, Gas Jets, and Pumping Power*, Editor(s): Daizo Kunii, Octave Levenspiel, Fluidization Engineering (Second Edition), Butterworth-Heinemann, 1991, Pages 75

Gaba, Aurel & Iordache, Stefania. (2011). *Reduction of Air Pollution by Combustion Processes*. 10.5772/16959.

Garba MU, Ingham DB, Ma L, Porter RTJ, Pourkashnian M, Tan HZ, et al. *Prediction of potassium chloride sulfation and its effect on deposition in biomass-fired boilers*. Energy Fuel 2012;26:6502.

Li, Shiyuan & Qinggang, Lu & Haipeng, Teng. (2011). AGGLOMERATION DURING FLUIDIZED-BED COMBUSTION OF BIOMASS.

Lindström, Erica & Öhman, Marcus & Backman, Rainer & Boström, Dan. (2008). *Influence of Sand Contamination on Slag Formation during Combustion of Wood Derived Fuels*. Energy & Fuels - ENERG FUEL. 22. 10.1021/ef700772q.

Miles, T R, Miles, Jr, T R, Baxter, L L, Jenkins, B M, and Oden, L L. *Alkali slagging problems with biomass fuels*. United States: N. p., 1993. Web.

Mlonka-Mędrala, Agata & Magdziarz, Aneta & Gajek, Marcin & Nowińska, Katarzyna & Nowak, Wojciech. (2019). *Alkali metals association in biomass and their impact on ash melting behaviour*. Fuel. 261. 10.1016/j.fuel.2019.116421.

Nagendrappa, Gopalpur. (2002). *Organic synthesis using clay catalysts*. Resonance. 7. 66. 10.1007/BF02836172.

Niu, Yanqing & Tan, Houzhang & Hui, Shi. (2016). *Ash-related issues during biomass combustion: Alkali-induced slagging, silicate melt-induced slagging (ash fusion), agglomeration, corrosion, ash utilization, and related countermeasures*. Progress in Energy and Combustion Science. 52. 1-61. 10.1016/j.pecs.2015.09.003.

Novianti, Srikandi & Nurdiawati, Anissa & Zaini, Ilman & Prawisudha, Pandji & Sumida, Hiroaki & Yoshikawa, Kunio. (2015). *Low-potassium Fuel Production from Empty Fruit Bunches by Hydrothermal Treatment Processing and Water Leaching*. Energy Procedia. 75. 588. 10.1016/j.egypro.2015.07.460.

Önal, M. (2009). *Physicochemical properties of bentonites: an overview*.

Reiji Noda, Tomoyuki Ito, Nao Tanaka, Masayuki Horio, *Steam Gasification of Cellulose and Wood in a Fluidized Bed of Porous Clay Particles*, JOURNAL OF CHEMICAL ENGINEERING OF JAPAN, 2009, Volume 42, Issue 7.

Rosenani A.B., Hoe S.F. (1996) *Decomposition of oil palm empty fruit bunches in the field and mineralization of nitrogen*. In: Van Cleemput O., Hofman G., Vermoesen A. (eds) Progress in Nitrogen Cycling Studies. Developments in Plant and Soil Sciences, vol 68. Springer, Dordrecht. https://doi.org/10.1007/978-94-011-5450-5_20

Serrano García, Daniel & Sánchez-Delgado, S. & Sobrino, C. & Marugan-Cruz, Carolina. (2015). *Defluidization and agglomeration of a fluidized bed reactor during Cynara cardunculus L. gasification using sepiolite as a bed material.* Fuel Processing Technology. 131. 10.1016/j.fuproc.2014.11.036.

Wang, Ping & Massoudi, Mehrdad. (2013). *Slag Behavior in Gasifiers. Part I: Influence of Coal Properties and Gasification Conditions*. Energies. 6. 784-806. 10.3390/en6020784.

Visser, H. & Hofmans, H. & Huijnen, H. & Kastelein, R. & Kiel, J.. (2008). *Biomass Ash – Bed Material Interactions Leading to Agglomeration in Fluidised Bed Combustion and Gasification*. 10.1002/9780470694954.ch20.

CHAPTER II

Agglomeration and Defluidization of Silica Sand and Bentonite Particles Processes influenced typical velocity intensity (4.3 U$_{mf}$) with thermal treatment temperature at 700, 750 and 800ºC

2.1   Introduction

Empty Fruit Bunch (EFB) is still a big current issue since the effort to utilize it become a more beneficial commodity has increased continually as long as the increase of Crude Palm Oil (CPO) production in tropical countries. However, from 100 wt.% of CPO production in **Figure 2-1** was produced around 21 wt.% EFB residue too as unused material containing high alkaline and still be categorized as waste or pollutant. Currently, the treatment of EFB has been started in thermal conversion technology to generate raw syngas as a useful product for many purposes like fuel and chemicals. However, some alkaline will make the slagging problem as the negative impact thermal reaction between alkaline and oxide which will settle in the fixed bed. As the effort to reduce this problem is fluidization bed, as outstanding technology which can increase efficiency and reduce tar production.
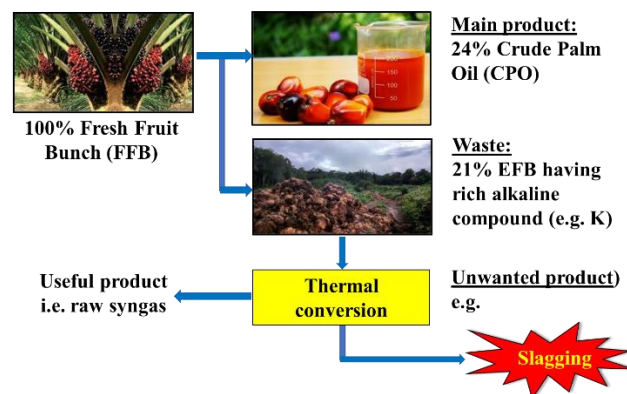
Figure 2-1. Potential slagging formation from EFB utilization

The key of fluidization is the velocity to ensure all of the bed particles can distribute optimally inside the cross-section area to contact with among of bed particles. The utilization of particle fluidization is needed to support conversion whose role is not only

to maximize momentum and chemical reaction but also to inhibit the agglomeration and defluidization formation during thermal reaction involving EFB since biomass-rich alkaline has a high tendency to form agglomeration. Therefore, the treatment and the use of particle fluidization are important to maintain fluidization for a longer time.

2.2 Experimental

2.2.1 Materials

2.2.1.1 Silica sand and bentonite particles

Particle fluidization in this study consist of silica sand and bentonite. Both particles were obtained from local manufacture consist of heterogeneous sizes, namely 0.4 wt.% of 212 µm, 12.2 wt.% of 150 µm, 43.1 wt.% of 106 µm, 30.2 wt.% of 75 µm, 10.9 wt.% of 53 µm, 2.3 wt.% of 45 µm, 0.8 wt.% of 38 µm and 0.1 wt.% of 26 µm. Silica sand consisted of some oxide compounds like SiO_2, Al_2O_3, Fe_2O_3, CaO, Na_2O, K_2O, and TiO_2. Bentonite was obtained in heterogeneous size and consist of some oxides too, namely 75.78 wt.% of SiO_2, 12.83 wt.% of Al_2O_3, 1.44 wt.% of Fe_2O_3, 0.02 wt.% of CaO, 2.70 wt.% of MgO, 2.63 wt.% of Na_2O, and 0.18 wt.% of K_2O.
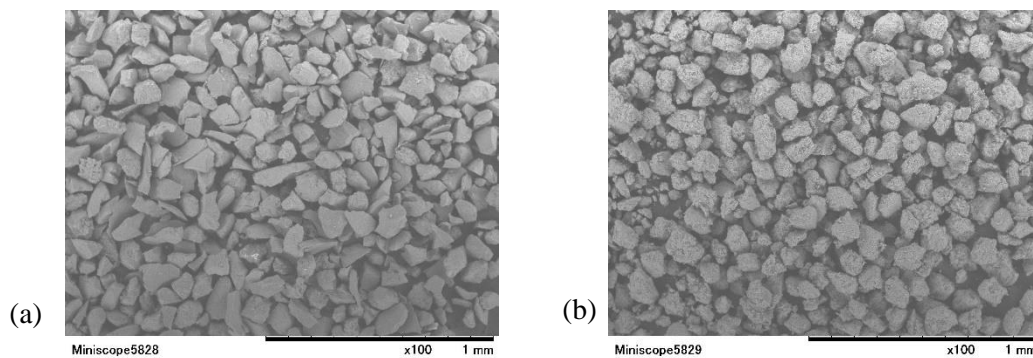
Figure 2-2. +88-125 µm silica sand (a) and bentonite (b) particles

Pre-treatment of both particles involving particle preparation consisted of grinding, milling, and sieving was required to obtain identical size +88-125 µm, in **Figure 2-2**. In the case of bentonite, a lot of fine particles still remained in the top layer. Fine particles were urgent to be removed because it can be easily moved up towards discharge line even

though it was fluidized in low velocity making bed particles mass will decrease rapidly at the beginning of fluidization. Therefore, an elutriation step was carried out to obtain the proper size by sieving 45 wt.% of fine particles. **Figure 2-3** shows the elutriation process where fine particles will be separated based on different densities under superficial velocity raising bubbling fluidization. The process was carried out for 30 minutes and stopped when fine particles coming from the bed has been fully discharged.

Figure 2-3. Bubble system for elutriation process

Degradation mass measurement was carried out to know the condition of particles at high temperature 700°C. As shown in **Figure 2-4**, thermogravimetry (Netzsch TG-DTA2000s) measurement confirmed that very small degradation on silica sand but high degradation amount 10.9 wt.% of mass on bentonite.
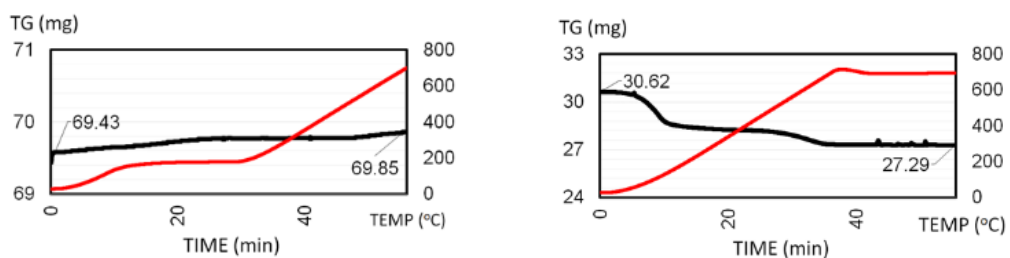
Figure 2-4. TG-DTA measurement on silica sand (left) and bentonite (right) sides.

The degradation process involved 4 steps started from endothermic reaction marked by getting quick mass loss up to temperature $200^{\circ}C$ corresponding to the dehydration process. The second stage was marked by constant mass loss followed by a quick mass loss in the third stage in the range temperature $500\text{-}750^{\circ}C$. The third step is related to the evolution of structural water involving breakdown and reorganization of ions, and the fourth step is an exothermic reaction where no mass changes at temperature $> 750^{\circ}C$ (Cuadros et.al., 1994).

Minimum fluidization velocities (U_{mf}) of both particles in normal or room temperature has been measured by observation in bubbling column resulting in U_{mf} of 0.009 and 0.008 m/s for silica sand and bentonite, respectively. In this study, all of the fluidization was set to the same intensity as 4.3 times of U_{mf} at room temperature condition. The elements inside both particles were quantified by an X-Ray Fluorescence analyzer (Shimadzu EDX-7000) in helium gas atmosphere.

2.2.1.2 Empty Fruit Bunch (EFB) ash

Malaysian EFB in pellet shape was used in this study. That biomass was converted into ash to obtain inorganic matters only when organic matters contained in tar and char were fully separated. Placing in a muffle furnace, ashing operation was started from room temperature to $700^{\circ}C$. At that temperature, the ash might be already formed completely. The step operation was the first step to increase the temperature from room to ashing temperature for 2 hours. Then, the temperature was adjusted to be $700^{\circ}C$ for 2 hours to ensure all of the pellets have obtained sufficient thermal treatment to be converted into ash. The cooling step was carried out for 2 hours to remove vaporized organic compounds in the furnace. The result of the ashing process can be seen in **Figure 2-5**.

(a)   (b)   (c)
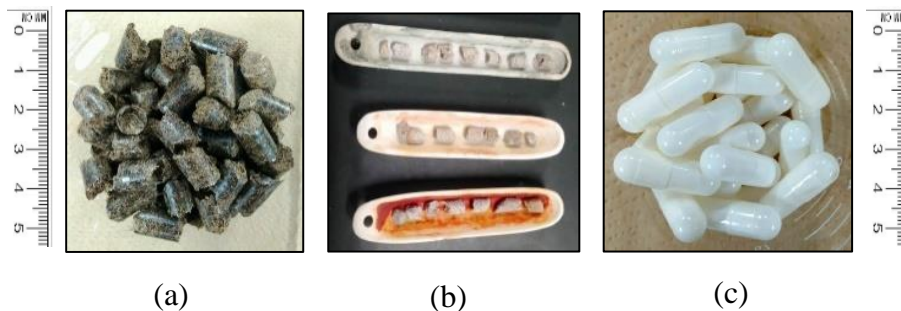
Figure 2-5. Malaysian EFB chip (a), EFB ash (b), Cellulose capsule (c)

EFB ash powder has low density making that particle was very easy to fly up in a fluidization state, but difficult when introduced into the BFB column. Cellulose capsule was used in the experiment for placement of ashes to make sure the ash can attain bed side perfectly to react with particle fluidization. That capsule sample was bought from local manufacture containing 89.2 wt.% of Hydroxypropyl methylcellulose, 6.5 wt.% of water, 2 wt.% of TiO_2, 1.3 wt.% of Carrageenan, and 1 wt.% of KCl. Analysis by TG showed that the capsule was degraded until 86.2 wt.% under Nitrogen atmosphere at 700°C, **Figure 2-6**. Elemental measurement using X-Ray Fluorescence analyser (Shimadzu EDX-7000) in Helium atmosphere showed that residue contains some inorganic elements like Ti (67.07 %), K (14.33 %), Na (13.56 %), S (3.96 %), Ru (0.80 %), P (0.24 %), Cu (0.21 %), Fe (0.14 %), Ni (0.09 %), Si (0.10 %) and Nb (0.04 %). The presence of alkaline components like K, Na, S, and P elements may affect melting behavior during thermal treatment but the amounts are too low to influence the interaction between ash and med materials.
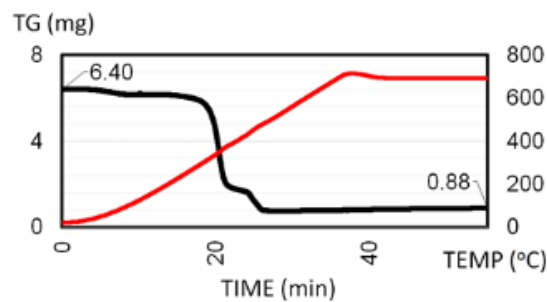
Figure 2-6. TG-DTA measurement on cellulose capsule at temperature 700°C.

2.2.2 Apparatus

The main apparatus used in this work was the Bubbling Fluidized Bed (BFB) system consist of bed column and tubular filter as main parts. The height of the column was 570 mm, and the round perforation size of the bed column was customized having 1 mm innermost and 5 mm outermost diameter which was covered by thermal insulation (ceramic fiber) to retain bed particles for easy cleaning of accumulated deposit caused by coating of particle grains and melt formation of ash components promoting agglomeration. The agglomeration formed in this perforation is easier to be removed than the smaller size

because the agglomeration formation can occur easily by contacting with ash particle even the ash size is less than or equal to 10 µm (Liu et.al., 2009). Three ball valves on the top function as a nozzle for inputting encapsulated EFB ash. Encapsulated EFB ash was inputted from the reactor top with 15 min intervals supported by N_2 to avoid backflow and ensure the capsule could reach the bed. Detail scheme of the apparatus is shown in Figure 2-7.

(a)   (b)   (c)   (d)
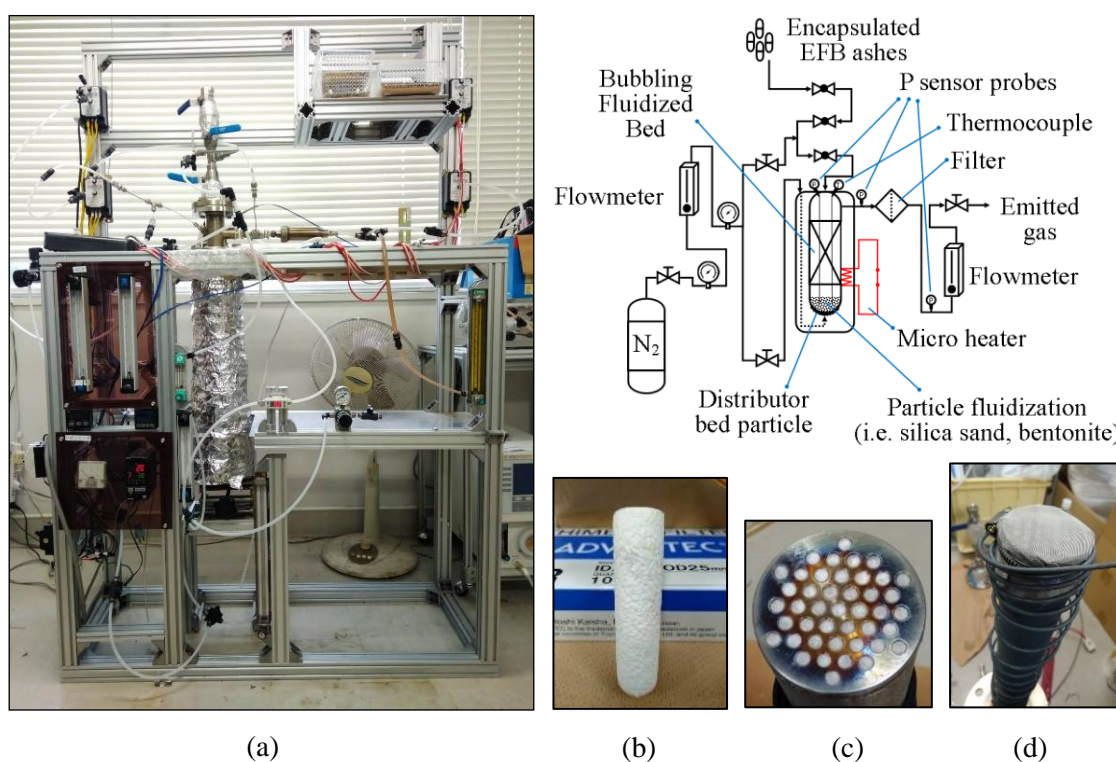
Figure 2-7. Thermal BFB treatment apparatus and scheme (a), thimble filter (b), 1 mm grate bar perforated distributor (c) supported by metal retainer (d)

Three pressure sensor probes were placed above distributor (P_1) as a differential from the freeboard area, and in discharged line before and after thimble filter location (P_2), (P_3). These pressures were recorded by a data logging system during experiments. A thermocouple was placed in the BFB chamber to maintain and adjust the bed temperature. A tubular filter cartridge and thimble filter were installed at the BFB discharge line to sieve the light or fine particles from the apparatus.

2.3. Method

2.3.1 Measurement of mass change before and after thermal treatment

The mechanism is shown in **Table 2-1**. The BFB operation was commenced by placing and heating up with around 65 g of bed particles (m1.1) to reach two levels of temperature at 750 and 800 °C. During heating up, the initial bentonite bed particle was easy to associate making weak granulation. The plasticity property of bentonite makes granulation was possible to be formed when moisture was still available. That granulation can inhibit fluidization when fluidization started. Therefore, the heating up process supported by fluidization was important for thermal conversion using bentonite.

Table 2-1 Mass balance estimation method in bed and discharged particles

	Bed residue particle (g)	Symbol	Calculation method
1	1. Bed particle input mass	$m_{1.1}$	from raw data
	2. Total EFB ash addition mass	$m_{1.2}$	from raw data
	3. Total cellulose capsule mass	$m_{1.3}$	from raw data
	4. Total bed particle mass before pyrolysis	$m_{1.4}$	$m_{1.1} + m_{1.2} + m_{1.3}$
	5. Total bed particle mass after pyrolysis	$m_{1.5}$	from raw data
	6. Total accumulated bed particle	$m_{1.6}$	$m_{1.5} - m_{1.4}$
	Discharged particles (g)		
2	1. The mass before pyrolysis	$m_{2.1}$	from raw data
	2. The mass after pyrolysis	$m_{2.2}$	from raw data
	3. Total accumulated filter particle	$m_{2.3}$	$m_{2.2} - m_{2.1}$
	Total mass loss (g)		
The difference of mass change between bed and discharged particles		m_{loss}	$m_{1.6} - m_{2.3}$

The fluidization was created by N_2 supply with a superficial velocity of 4.3 U_{mf} at room temperature from a perforated distributor. When bubbling fluidization state had been reached, capsulated EFB ash consists of EFB ash ($m_{1.2}$) and empty cellulose capsule ($m_{1.3}$) was fed in stages. Total mass before operation ($m_{1.4}$) was the total of ($m_{1.1}$), ($m_{1.2}$), and ($m_{1.3}$). The total mixture remained in bed particle ($m_{1.6}$) was a difference of mass change before ($m_{1.4}$) and after operations ($m_{1.5}$). The mass change ($m_{2.3}$) because entrained fine particles and accumulation of aerosol particulates along bubbling fluidization stage (V) remained in discharge line including tubular filter ($m_{2.1}$, $m_{2.2}$) was measured as well. Therefore, total mass loss (m_{loss}) as the difference between the mass change in bed reactor ($m_{1.6}$) and thimble filter ($m_{1.5}$) can be determined.

2.3.2 Determination of agglomeration and defluidization stages

2.3.2.1 According to pressure difference analysis

Data record from logging system (GRAPHTEC-midi LOGGER GL220) interconnected to pressure transmitter (SETRA-Model 264, +/- 12000 Pa range) over experiment was calculated to obtain averaged pressure difference data.
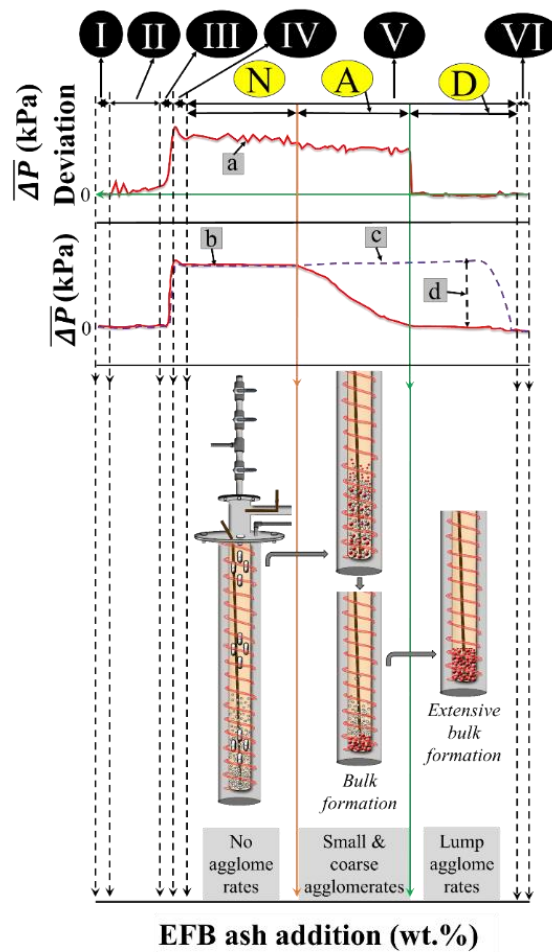
Remarks :
I : Fixed bed at room temperature a : ΔP Deviation
II : Fixed bed during heating up b : $\overline{\Delta P}$
III : Fixed bed at $T_{operation}$ c : $\overline{\Delta P}_{FB}$
IV : Smooth fluidized bed with N_2 supply d : $\overline{\Delta P}_{loss}$
V : Bubbling fluidized bed at $T_{pyrolysis}$
N : Normal fluidization zone
A : Agglomeration zone
D : Defluidization zone
VI : Fixed bed after being stopped N_2 stage

Figure 2-8. Illustration of agglomeration and defluidization formation stages against EFB ashes addition

The measurement method was shown in **Figure 2-8** started from (I) Fixed bed stage at room temperature for ± 0.25 h, (II) Fixed bed stage during heating up (± 1-2.5 h), (III) Fixed bed stage at high temperature (± 0.25 h), (IV) Smooth fluidized bed stage with N_2 supply (± 0.13-0.27 h), (V) Bubbling fluidized bed stage at high temperature (± 15-25 h), (VI) Fixed bed stage after N_2 stopped (± 0.25 h). The sampling of the EFB ash process was only carried out in bubbling fluidization state (V) with the repeated introduction of 1 capsule in 15 minutes intervals. In stage V, the fluidization behavior of bed materials could be classified into three cases like normal fluidization (N), agglomeration (A), and defluidization (D) according to changes of the differential pressure and its standard deviation.

When a fluidized is normally formed, an averaged differential pressure ($\overline{\Delta P}$) between bottom and freeboard of fluidized beds is ideally expressed as **Equation 1**.

$$\overline{\Delta P}_{\text{FB}} = \frac{m_{bed\ particle} \times gravitation\ constant\ (G)}{A_{BFB}} \quad (1)$$

In this experiment, $\overline{\Delta P}$ were measured by a differential pressure sensor between probes at bottom and freeboard for silica sand beds and as a difference of two pressure sensors located at bottom and freeboard for bentonite particle beds. Both pressure measurements have enough resolution to observe changes of ΔP based on manometer calibration in **Figure 2-9**. Zero adjustment of the sensors was carried out for $\overline{\Delta P}$ to be zero (*0 Pa*) in stage I.

(a)

(b)

(c)
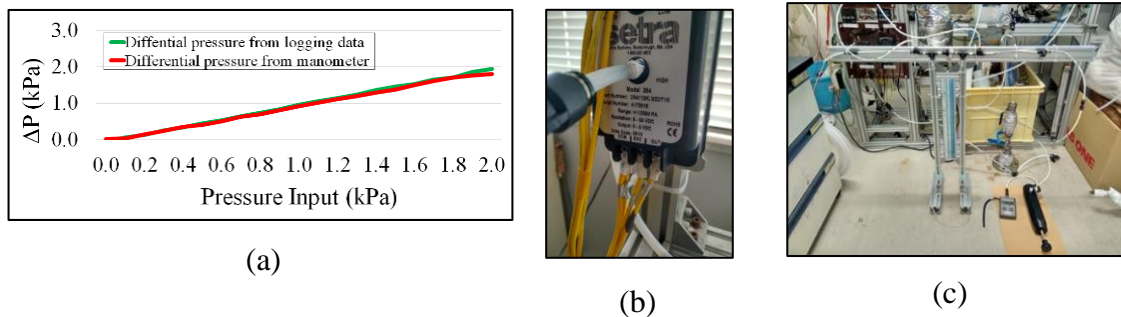
Figure 2-9. A calibration curve (a) between differential pressure of pressure sensor (b) and U-tube manometer (c)

Typical behavior of $\overline{\Delta P}$ is illustrated in **Figure 2-8**. Bubbling fluidization state should run normally when $\overline{\Delta P}$ gradual increase of bed particle mass increment according to **Equation 2**. However, when agglomeration takes place in a bed, a ($\overline{\Delta P}$) should be below from the theoretical one ($\overline{\Delta P}_{theorem}$) because agglomerates sink to the bottom to be supported not only by a drag force of gas but also the bottom wall. Feeding of encapsulated EFB ash containing alkali and alkali earth metal compounds starts reacting with bed materials to form agglomerated particles. Since the drag force caused by agglomerates may be insignificant, the pressure decrement roughly corresponds to the weight of agglomerates formed inside. After agglomeration started, agglomerates are gradually built up to produce bulk agglomerates. The bulk agglomerates may be difficult to move up then settled at the bottom of the column, while small particles were still possible to move up. Therefore, defluidization bed particles might be preceded by agglomeration formation on the bottom side. When bulk formation keeps taking place to reach the wall, defluidization of the bed takes place. The bed behaves as a fixed bed in defluidization condition. Therefore, defluidization was identified by the decrease of pressure fluctuation calculated by the standard deviation of pressure signals in **Equation 2** based on the square root of variance between ΔP and $\overline{\Delta P}$ for 15 minutes (n) observation time. Standard deviation from normal fluidization to defluidization condition is depicted as $\overline{\Delta P}_{deviation}$ curve in **Figure 2-8**.

$$\Delta P_{\text{deviation}} = \sqrt{\frac{\sum(\Delta P - \overline{\Delta P})^2}{n-1}} \qquad (2)$$

Agglomeration is highly dependent on the adhesion property of bed particles. High adhesive materials will be easier to reach defluidization. Defluidization can be marked by lower pressure fluctuation than that during fluidization which should correspond to the level after N_2 gas has been stopped.

Identification of agglomeration and defluidization were analyzed according to U_{mf} measurement of bed materials after getting some ashes with various mass. In this study, U_{mf} measurement was conducted on fixed bed condition at room temperature, bed material after heat-up treatment, bubbling fluidization after 0.025 g x 10 times addition, 0.05 g x 10 times addition, 0.25 g x 5 times addition, and 0.5 g x 5 times addition.

Furthermore, fixed bed condition after N_2 input stopped at operation temperature and fixed bed condition after cooling down were carried out too. U_{mf} measurement was determined according to linear prediction between velocity and different pressure (ΔP) as slope and intercept variables. The ΔP equation as the differential pressure between P_1 which is located on distributor and P_2 located in discharge line before the filter can result in some behaviors during U_{mf} analysis which predict status or particle condition to reach fluidization stage by applying the same adjusted velocity from. The prediction of the U_{mf} curve in **Figure 2-10** shows some probable appearances. U_{mf} will run well when the curve was similar to the appearance in number 1. In that state, no agglomerates formed around P_1 and P_2 nozzle probes which indicates pressure measurement has run well. When P_1 was run well but the P_2 nozzle was partially or completely closed by volatile agglomerates, so the ΔP will increase significantly during velocity increment as shown in number 2. When there were agglomerates around P_1, bed particles were still moving up and P_2 still running in a normal state, then the appearance might be the same as number 3. Condition in number 3 leads to the change of fluidization condition from normal to be smooth-fluidization state. Meanwhile, the condition in number 4 predicted some agglomerates have been completely closed P_1 and P_2 probes. That condition indicated that the defluidization state has been formed.
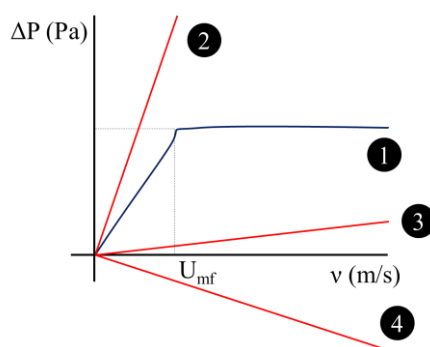
Figure 2-10. The prediction of U_{mf} appearance according to P_1 and P_2 condition during thermal treatment

2.3.2.2 According to elemental measurement analysis

The measurement of elemental composition was analyzed by XRF on the remaining mixture of bed and filter particles. These data were calculated to identify chemical

characteristics and melting behavior of coating layer on bed materials which would be sensitive with the presence of calcium and potassium in fuel. Visser et al. in **Figure 2-11** summarized two different routes for agglomeration namely "coating-induced" and "melt-induced" agglomeration. The coating-induced agglomeration is resulted from the interaction between ash forming elements in the vapor phase (aerosol) and bed particles forming covered strata consist of two or three layers (Visser, 2004). Based on their discussions, since Si, K, and Ca elements were contained in EFB ash as shown in **Table 2-3** and **Figure 2-14** most possible structure of coating were considered to be three layers: the innermost layer consisting of Si, K, and Ca, intermediate layer were Si and Ca, and outmost layer were Ca, Si, P, K, and S.
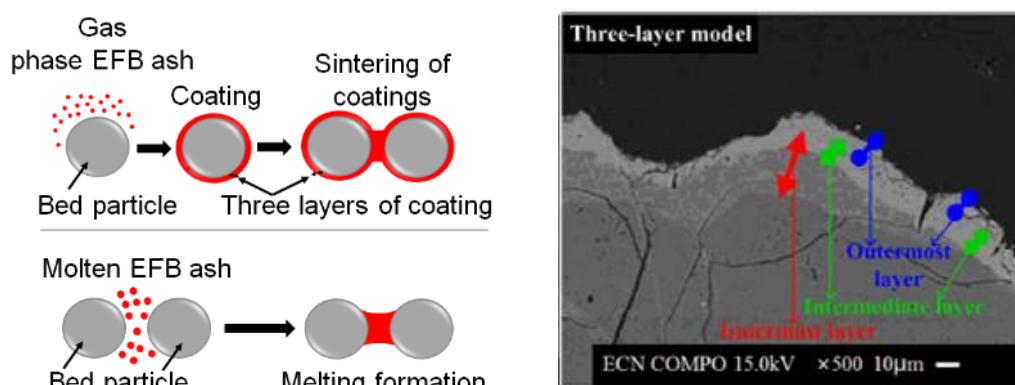
Fig. 2-11 The coating-induced (a), melt-induced agglomeration steps between ash and grains particle (b), a three layers coating agglomeration model (c) (adapted from references Visser, 2004; Visser *et.al.*, 2008)

In "melt-induced" agglomeration, bed particles adhere together via a molten phase of solid-alkali metal species because of the high local peak temperature while "coating-induced" agglomeration is presented on the surfaces of bed material grains. There is a close relationship between both routes where a neck formation may occur between the coating-induced process of individual grains. The neck formation will initiate agglomeration followed by partial defluidization of bed leading to reach local peak temperature which will start melt-agglomeration formation with bed material grains (Vissel, 2004). **Figure 7** illustrates the steps of agglomeration formation which consider the gradual ash addition as well.

An evaluation to predict bed agglomeration was carried out by referring to agglomeration indicators calculation (Visser, 2004). The first indicator (I_1) predicts agglomeration formation based on alkali-silicate reaction, the second indicator (I_2) predicts the formation of a refractory outer coating, and the third indicator (I_3) predicts potential agglomeration from alkali-silicate melt phase as shown in Equation 3, 4, and 5. The presence of Alumunium (Al) gives potency to reduce agglomeration formation if the ratio of Al/Si is still high (Li *et.al.*, 2013; Niu *et.al*, 2014). The ratio of I_1 reflects that an excess of alkali metals over sulfur and chloride leads to the formation of alkali metal silicates. It should be larger than 1 to assume the S and Cl in that fuel will completely react with bed particles (Visser, 2004). Gradual increment of indicator I_1 leads to form a sticky layer on particles when containing alkaline like potassium and sodium (Niu *et.al*, 2016). The comparison Na, K against S, and Cl showed that the conversion of biomass that released from biomass had been alkaline compound in the form KCl, K_2SO_4 aerosols as shown in **Figure 1-1.** When condensation takes place on the bed particle, then the alkali-silicate reaction had been initially formed while released some S and Cl elements. The increase in K and Na will support strengthening the binding of agglomerates to reach the stickier formation. Relevant to the previous statement, (Mu et.al., 2012) explained that the sticky layer was formed by rapid-aerosol condensation on the surfaces which capture solid ash particle with high melting points. When flue gas temperature decreases, the main transformation paths are homogenous nucleation or heterogeneous condensation to form typical eutectic mixtures which gradually formed at low melting points. The second indicator (I_2) is related to the stickiness of the outer layer on the particle. It will increase if indicator I_2 should be more than 1. That ratio was related to the increase of thickness resulted in the inner reaction (I_1) and outer coating deposition because the presence of Ca, P, and Mg having a non-sticky structure but a higher refractory rim and melting point. The formation between inner and outer layers should balance to withstand the integrated agglomerates. Therefore, the increase of I_2 should automatically increase the level of agglomerates stickiness. The third indicator (I_3) is related to the melting properties of the outer layer on particles. When the indicator exceeds one, the molten ash layer will be produced on a particle instead of coating the outer layer by high local peak temperature in a gasifier. Therefore, agglomeration formation based on indicators I_1 and I_2 becomes a trigger to establish I_3. Although this indicator was established for fixed bed

reactors, it may give us some information even in fluidized bed reactor. I_4 is an indicator for inhibition of agglomeration formation. The high value of I_4 promises to reduce agglomeration formation. In this study, the above analysis was carried out to compare the mechanisms of agglomerate formation between silica sand and bentonite particles.

$$I_1 = (Na+K)/(2S + Cl) > 1 \qquad (3)$$

$$I_2 = (Na+K+Si)/(Mg+P+Ca) > 1 \qquad (4)$$

$$I_3 = K/Si > 1 \qquad (5)$$

$$IF \quad K > 3g/kg \text{ fuel}; Si > 2g/kg \text{ fuel}$$

$$K_2O + SiO_2 > 50 \text{ wt.\% fuel ash}$$

$$I_4 = Al/Si \qquad (6)$$

2.4. Result and discussion

2.4.1 Agglomeration and defluidization behavior of silica sand particles against EFB ash added at 700°C

Mass balance analysis in **Table 2-2** showed around sixty-five grams (65.06g) of silica sand was first placed to be fluidized under velocity 4.3 U_{mf}. Encapsulated ashes consist of 4.53 g ash powder and 3.22 g empty capsules had been added 30 times with the total accumulated bed particle mass was 72.80 g. Total bed particle after the operation was 52.16 g which was sieved into several sizes dominated by +88-125, +177-250, +350, +125-177, +297-350, and +250-297 µm respectively, from which agglomerated particles as particle size having a larger size than the initial bed particle was still low.

During operation, there was 20.64 g fine bed particles had entrained toward the discharge line. Meanwhile, the accumulation of discharged particle mass as different between discharge line mass before and after the operation was 15.80 g. The difference between entrained particles and discharged particles indicated the mass loss which had attained 4.84 g.

Agglomeration and defluidization measurement could be analyzed according to the result as shown in **Figure 2-12**. In fixed bed stage as initial stage (I) observation had $\overline{\Delta P}$

deviation 5 Pa. During heating up in stage II, there was an increment of $\overline{\Delta P}$ deviation might be caused by the vaporization process of moisture in the heating zone during the early time of gradual temperature increment for 1.5 h.

Table 2-2. Mass balance of thermal BFB treatment involving silica sand utilization at 700°C, 4.3 U_{mf}

Parameter	Value
Bed residue particle	
1. Silica sand input mass ($m_{1.1}$)	65.06 g
2. Total ash EFB addition mass ($m_{1.2}$)	4.53 g
3. Total cellulose capsule mass ($m_{1.3}$)	3.22 g
4. Total accumulated bed particle ($m_{1.4}=m_{1.1}+m_{1.2}+m_{1.3}$)	72.80 g
5. Total bed particle mass after operation ($m_{1.5}$)	52.16 g
5.1. +350µm particle size	2.31 g
5.2. +297-350µm particle size	1.34 g
5.3. +250-297µm particle size	0.21 g
5.4. +177-250µm particle size	2.85 g
5.5. +125-177µm particle size	1.64 g
5.6. +88-125µm particle size	42.18 g
5.7. -88µm particle size	1.63 g
6. Total emitted bed particle mass ($m_{1.6} = m_{1.5}-m_{1.4}$)	20.64 g
Disharged particle	
1. Discharge line before operation ($m_{2.1}$)	699.90 g
2. Discharge line after operation ($m_{2.2}$)	715.70 g
3. Total discharged filter particle mass ($m_{2.3}=m_{2.2}-m_{2.1}$)	15.80 g
Total mass loss	
The difference of entrained bed and discharged particles mass ($m_{loss}=m_{1.6}-m_{2.3}$)	4.84 g

By introducing high superficial velocity (4.3 U_{mf}) then, bubbling fluidization stage (V) had been started and deviation increased becoming 61 Pa and $\overline{\Delta P}$ fluctuation attained 292 Pa, while $\overline{\Delta P}_{FB}$ measurement was 337 Pa. Total fed ashes in this stage (V) were 6.96 wt.% of initial silica sand bed particle 65.06 g.

Figure 2.12 showed that fluidization was run normally which $\overline{\Delta P}$ deviation kept increasing with the value 93 Pa and $\overline{\Delta P}$ fluctuation kept stable until last ash addition with insignificant $\overline{\Delta P}$ decrement of 270 Pa. Some agglomerates had been started with minimum $\overline{\Delta P}$ fluctuation was 162 Pa. However, the bed particle back fluctuated again indicating agglomerates were not so sticky and still could be eroded during fluidization. Bed residue and discharged particles after operation were shown in **Figure 2-13**. Small agglomerates had formed in various sizes around 1-5 mm in bed residue (a) with 15.8 g discharged particle had been accumulated as well (b). Sieved particle +350 µm (c) showed

clearer agglomerates including some incomplete capsules degradation having the mass of 2.31 g. Smaller agglomerates from +297-350 until -88 µm were also already sieved, from which the highest agglomerate was 42.18 g for size +88-125 µm.
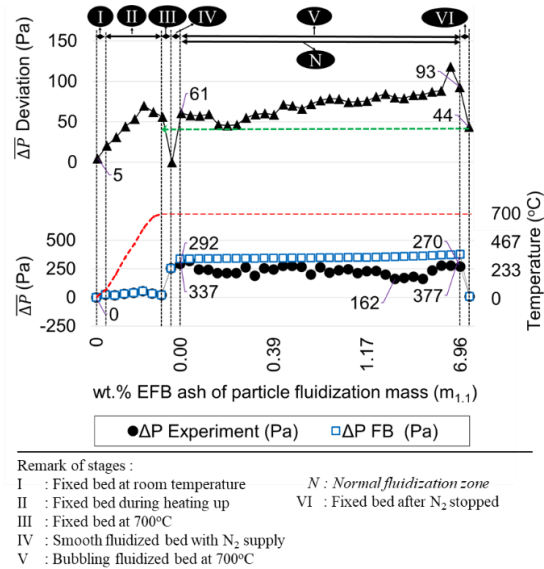
Figure 2-12. Agglomeration and defluidization analysis on silica sand at 700°C, 4.3 U_{mf}

Analysis of elemental compositions of sieved bed residue and discharged particles after operation 700°C were explained in **Table 2-3** and **Figure 2–14**, from which agglomeration mechanisms were considered based on agglomeration indicator measurement results in **Table 2-4**. Agglomeration indicator I_1 based on calculation from

(a). Bed residue   (b). Discharged particle   (c). +350µm
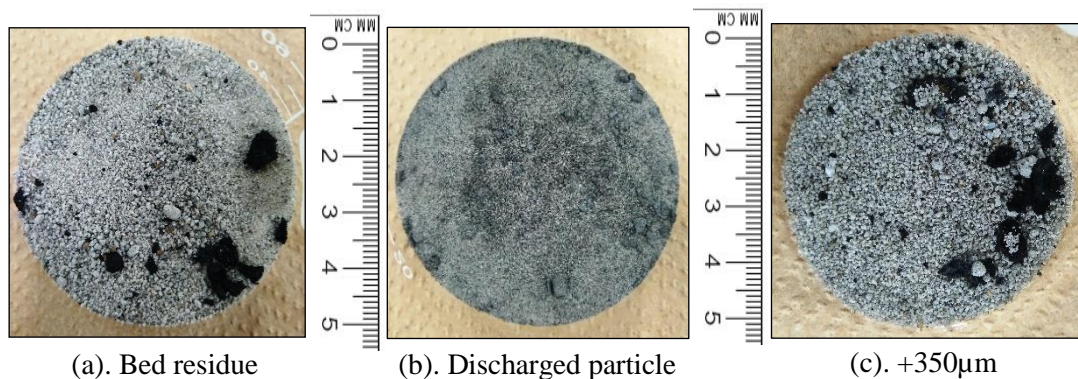
Figure 2-13. Silica sand bed residue, discharged and sieved bed residue at T=700°C, 4.3 U_{mf}

Equation 1 showed that silica sand had a high tendency to react with alkaline contained in all BFB chamber to form alkali-silicate molecules involving potassium, sodium, and SiO_2. The highest indicator was 11.13 with particle size +88-125 µm. Indicator I_1 will promote sticky agglomerates, so the stickies agglomerates were formed in that size too. Meanwhile, the other sizes had lower value and the potency to attain high strength becoming lower too in range 3.79-8.83. In the fact, all of indicators I_1 were higher than 1 indicating agglomerates had been formed. However, fluidization with a typical velocity (4.3 U_{mf}) can degrade agglomeration started from coating the outer layer formed during thermal treatment at 700°C.

Table 2-3 Composition of wt.% mixture of silica sand materials based on XRF measurement under treatment and ashing processes temperature at 700°C

| Elements | Bed residue particles | | | | | | | Discharged particles | Silica sand | EFB ash |
| | +350µm | +297-350µm | +250-297µm | +177-250µm | +125-177µm | +88-125µm | -88µm | | | |
					T =700°C					T = 700°C
K	16.16%	14.36%	14.34%	13.54%	12.55%	13.41%	16.95%	16.22%	6.98%	48.64%
Ca	7.36%	7.20%	6.41%	6.48%	5.51%	5.43%	6.68%	8.76%	3.66%	18.95%
Si	64.26%	65.42%	66.99%	68.11%	66.91%	68.57%	59.48%	56.23%	80.21%	13.26%
Mg	0.00%	0.00%	0.00%	0.00%	0.00%	0.00%	0.00%	0.83%	0.00%	2.56%
Al	5.32%	6.89%	5.07%	6.05%	6.67%	9.09%	8.11%	6.60%	6.89%	1.17%
Cl	0.50%	0.40%	1.33%	0.32%	0.57%	0.49%	2.73%	3.84%	0.00%	3.99%
S	0.66%	0.65%	0.64%	0.64%	0.48%	0.36%	0.87%	1.61%	0.26%	2.29%
P	0.65%	0.50%	0.75%	0.50%	0.35%	0.05%	0.55%	1.88%	0.00%	1.92%
Fe	3.46%	3.04%	2.92%	2.63%	3.76%	1.41%	2.58%	0.00%	1.16%	4.71%
Na	0.00%	0.00%	0.00%	0.00%	0.00%	0.00%	0.00%	2.47%	0.00%	1.30%
Ti	0.84%	0.70%	0.96%	1.13%	2.36%	0.82%	1.34%	0.17%	0.50%	0.32%
Others	0.80%	0.84%	0.60%	0.62%	0.85%	0.37%	0.70%	0.44%	0.00%	0.89%
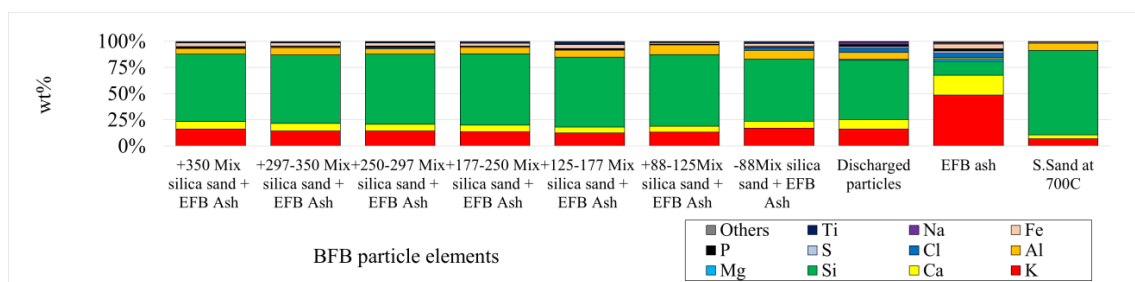
Fig. 2-14 Comparison of alkaline and dominant elements in a mixture of silica sand at 700°C, thermal silica sand, and EFB ash

Indicator I_2 corresponded to the increase of agglomerates coating. Bed particle with size +88-125 µm was the highest too with an I_2 value was 14.95 while other bed particle

sizes were lower in range 10.04-13.57. The highest I_2 value was relevant to the I_1 value. It showed that a high sticky level of agglomerates had the function to support high coating formation. In contrast, the high coating will be difficult to be formed when the low sticky level was dominant. Since fluidization kept taking place over treatment, then distribution thermal should be run well, so potency to attain rapid local temperature increment was low. Therefore, the potency to attain agglomeration caused by the melting of alkali was minimum. That condition was relevant to the analysis of indicator I_3, from which that agglomeration reaction was low to form in all of size bed residue. The lowest Indicator I_3 was contained in particle size +125-177 µm. Since particle had low of I_3 but high for I_1 and I_2, showed the agglomeration contained in the bed might be small, because the bulk agglomerates were not attained yet as condition promoting local peak temperature to lead agglomeration by melting process. The role of Aluminium to inhibit agglomeration was low in all BFB material according to indicator I_4 measurement. So, it supported agglomeration formation too.

Table 2-4 Summary of agglomeration indicator (I_1-I_4) from a mixture of BFB material with silica sand utilization at 700ºC, 4.3 U_{mf}

Indicator agglomeration	Bed residue particle							Discharged particle
	+350µm	+297-350µm	+250-297µm	+177-250µ	+125-177µm	+88-125µ	-88µm	
	$T_{pyrolysis} = 700ºC$							
I_1	8.83	8.44	5.49	8.44	8.20	11.13	3.79	2.30
I_2	10.04	10.36	11.36	11.70	13.57	14.95	10.56	6.32
I_3	0.25	0.22	0.21	0.20	0.19	0.20	0.28	0.29
I_4	0.08	0.11	0.08	0.09	0.10	0.13	0.14	0.12

2.4.2 Agglomeration and defluidization behavior of silica sand particles against EFB ash added at 750ºC

According to the mass balance measurement in **Table 2-5**, an amount of 65.02 g silica sand had been fed together with 4.52 + 3.33 g encapsulated ashes, so the total bed material should be 72.87 g. Total bed material after thermal treatment at 750ºC decreased to 45.39 g showing the total emitted bed particle was 27.48 g. Meanwhile, measurements of

accumulated mass in discharged line before and after operation were 699.9 g and 715.7 g. Which means the total amount of discharged filter particle was 22.10 g.

Defludization analysis based on differential pressure was shown in **Figure 2-15**. Started from analysis fixed bed condition at room temperature in stage I with stable deviation at 5 Pa, heating up, until reached fluidization stages under superficial N_2 velocity (II-V) with $\overline{\Delta P} = 330$ Pa and $\overline{\Delta P}$ deviation $= 72$ Pa. During fluidization, the total amount of ash addition was 6.96 wt.% of initial bed particle 65.02 gr in **Table 2-5**. In this stage, both average pressure deviation and average differential pressure were run normally where $\overline{\Delta P}$ deviation kept moving and always be higher than the deviation in fixed bed stage (I) until ashes addition by 0.12 wt.% of initial bed material.

Table 2-5 Mass balance of thermal BFB treatment involving silica sand at 750°C, 4.3 U_{mf}

	Parameter	Value
	Bed residue particle	
	1. Silica sand input mass ($m_{1.1}$)	65.02 g
	2. Total ash EFB addition mass ($m_{1.2}$)	4.52 g
	3. Total cellulose capsule mass ($m_{1.3}$)	3.33 g
	4. Total accumulated bed particle ($m_{1.4}= m_{1.1}+m_{1.2}+m_{1.3}$)	72.87 g
1.	5. Total bed particle mass after operation ($m_{1.5}$)	45.39 g
	5.1. +350µm particle size	3.19 g
	5.2. +297-350µm particle size	0.40 g
	5.3. +250-297µm particle size	0.16 g
	5.4. +177-250µm particle size	8.22 g
	5.5. +125-177µm particle size	5.12 g
	5.6. +88-125µm particle size	10.51 g
	5.7. -88µm particle size	17.80 g
	6. Total emitted bed particle mass ($m_{1.6} = m_{1.5}-m_{1.4}$)	27.48 g
	Discharged particle	
	1. Discharged line before operation ($m_{2.1}$)	699.60 g
2.	2. Discharged line after operation ($m_{2.2}$)	721.70 g
	3. Total discharged filter particle mass ($m_{2.3}=m_{2.2}-m_{2.1}$)	22.10 g
	Total mass loss	
	The difference of entrained bed particle and discharged particle mass ($m_{loss}=m_{1.6}-m_{2.3}$)	5.38 g

However, the agglomeration phenomenon was identified after that according to a gradual increment of $\overline{\Delta P}_{loss}$ until the end of ashes addition. Agglomerates in bed material might be bigger and stickier than the operation result at 700°C. The incapability of bed particles to maintain normal fluidization was the reason. When larger agglomerates formed, potency agglomerates formation might be higher and stronger. So, degradation of agglomerates was difficult, even more difficult in further ashes addition. While $\overline{\Delta P}$

deviation was still higher than stage (I), then fluidization was still taking place with lower performance.
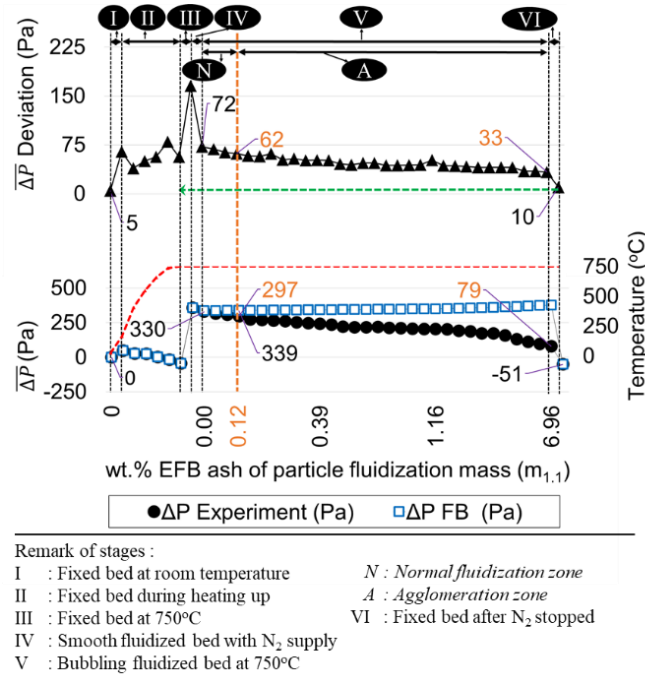
Figure 2-15. Agglomeration and defluidization analysis on silica sand at 750°C, 4.3 U$_{mf}$

Bed material and discharged particles were showing **Figure 2-16**. Several small and coarse agglomerates had been formed in spherical form with a diameter of less than 1 cm (a). Sieving treatment showed clearer coarse agglomerated particles image for +350µm particle size (c).

(a). Bed residue	(b). Discharged particle	(c). +350 µm
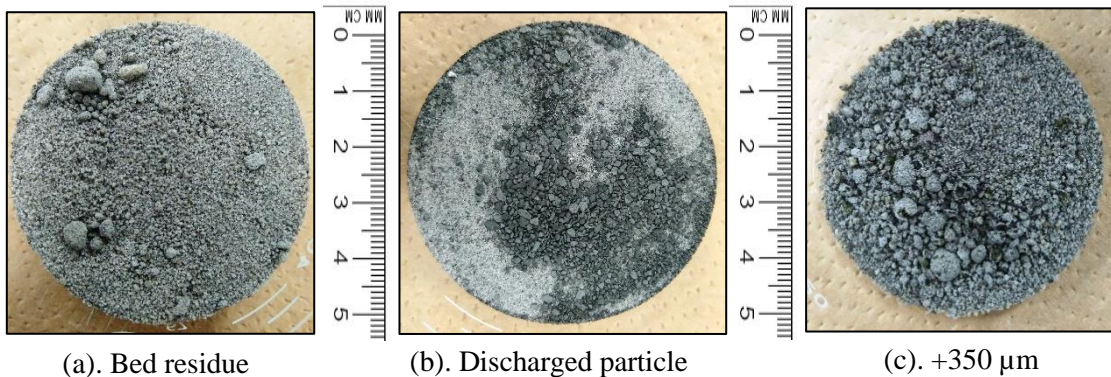
Figure 2-16. Silica sand bed residue, discharged particles, and sieved bed residue from operation at T= 750°C, 4.3 U$_{mf}$

According to mass balance data in **Table 2-5**, total coarse agglomerates in +350 µm size was 3.19 g while separated small agglomerates were distributed into few different masses mainly contained 8.22 g of +177-250 and 5.12 g of +125-177 µm particle size.

Elemental compositions of residue in the column and discharged particle after operation at 750°C as shown in **Table 2-6** and **Figure 2-17**. Agglomeration mechanism based on indicator I_1 in Table 2-7 showed in the case of operation at 750°C, three of the stickiest agglomerates were formed in +88-125, +125-177, and +177-250 µm bed particles with the indicator (I_1) of those particles were 11.61, 10.52, and 10.51 respectively. Which means those particles were the highest level of stickiness in bed residue particle.

Table 2-6 Composition of wt.% mixture of silica sand materials based on XRF measurement under treatment and ashing processes temperature at 750°C

Elements	Bed residue particles							Discharged particles	Silica sand	EFB ash
	+350µm	+297-350µm	+250-297µm	+177-250µm	+125-177µm	+88-125µm	-88µm			
				T =750°C						T = 700°C
K	19.25%	16.83%	15.65%	13.58%	12.73%	14.95%	15.34%	11.21%	6.59%	48.64%
Ca	8.20%	7.53%	7.04%	5.86%	5.11%	5.51%	6.40%	5.04%	3.28%	18.95%
Si	57.98%	61.66%	65.12%	69.08%	70.04%	66.58%	63.35%	69.42%	81.80%	13.26%
Mg	0.28%	0.00%	0.00%	0.00%	0.00%	0.00%	0.00%	0.00%	0.00%	2.56%
Al	5.02%	4.69%	4.99%	6.16%	6.57%	9.38%	9.26%	8.07%	6.34%	1.17%
Cl	0.00%	0.00%	0.00%	0.00%	0.00%	0.34%	1.05%	1.97%	0.00%	3.99%
S	1.15%	1.23%	1.17%	0.65%	0.61%	0.47%	0.66%	0.63%	0.21%	2.29%
P	0.79%	0.75%	0.68%	0.33%	0.23%	0.07%	0.17%	0.41%	0.00%	1.92%
Fe	4.32%	4.44%	3.20%	2.26%	2.20%	1.40%	1.90%	1.99%	0.98%	4.71%
Na	0.00%	0.00%	0.00%	0.00%	0.00%	0.00%	0.00%	0.00%	0.00%	1.30%
Ti	0.94%	1.02%	0.94%	1.06%	1.75%	0.77%	1.08%	0.79%	0.37%	0.32%
Others	2.07%	1.84%	1.20%	1.02%	0.76%	0.52%	0.79%	0.47%	0.43%	0.89%
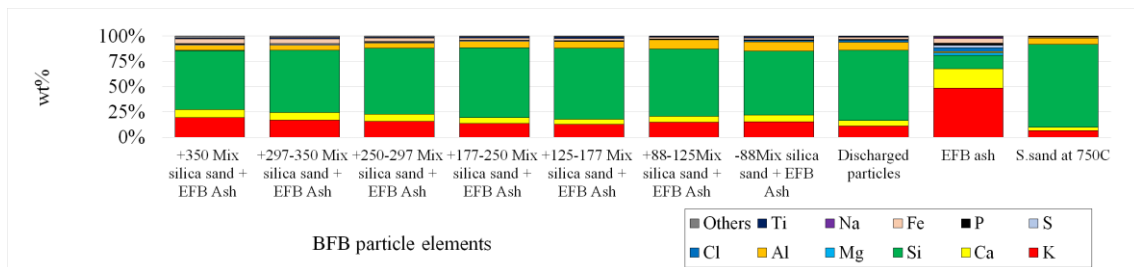
Fig. 2-17 Comparison of alkaline and dominant elements in a mixture of silica sand at 750°C, thermal silica sand, and EFB ash

According to indicator I_2, since those particles were the stickiest agglomerates, then the highest outer coating formation might be formed in those particles too. That indicator was relevant with the result that is shown in **Table 2-7**, in which the results were 14.62, 15.50,

and 13.36. Meanwhile, based on I_3, I_4 measurements, agglomeration was not achieved. So, the capability of bed particles to maintain a fluidization state was low.

Table 2-7 Summary of agglomeration indicator (I_1-I_4) from a mixture of BFB material with silica sand utilization at 750ºC, 4.3 U_{mf}

Indicator agglomeration	+350µm	+297-350µm	+250-297µm	+177-250µm	+125-177µm	+88-125µm	-88µm	Discharged particles
				Bed residue particles				
				$T_{pyrolysis} = 750^oC$				
I_1	8.36	6.83	6.71	10.51	10.52	11.61	6.46	3.47
I_2	8.33	9.48	10.47	13.36	15.50	14.62	11.98	14.79
I_3	0.33	0.27	0.24	0.20	0.18	0.22	0.24	0.16
I_4	0.09	0.08	0.08	0.09	0.09	0.14	0.15	0.12

2.4.3 Agglomeration and defluidization behavior of silica sand particles against EFB ash added at 800ºC

The total amount of accumulated bed particles including fed ashes was 72.97 g as shown in **Table 2-8**. Total bed particle mass after the operation was 45.49 g, total discharged particle mass was 23.30 g, and total mass loss was 4.19 g.

Table 2-8 Mass balance of thermal BFB treatment involving silica sand at 800ºC, 4.3 U_{mf}

Parameter	Value
Bed residue particle	
1. Silica sand input mass ($m_{1.1}$)	65.09 g
2. Total ash EFB addition mass ($m_{1.2}$)	4.53 g
3. Total cellulose capsule mass ($m_{1.3}$)	3.36 g
4. Total accumulated bed particle ($m_{1.4}= m_{1.1}+m_{1.2}+m_{1.3}$)	72.97 g
5. Total bed particle mass after operation ($m_{1.5}$)	45.49 g
5.1. +350µm particle size	3.71 g
5.2. +297-350µm particle size	1.17 g
5.3. +250-297µm particle size	0.24 g
5.4. +177-250µm particle size	6.22 g
5.5. +125-177µm particle size	4.23 g
5.6. +88-125µm particle size	23.26 g
5.7. -88µm particle size	6.67 g
6. Total emitted bed particle mass ($m_{1.6} = m_{1.5}-m_{1.4}$)	27.49 g
Sintering Filter	
1. Discharge line before operation ($m_{2.1}$)	699.60 g
2. Discharge line after operation ($m_{2.2}$)	722.90 g
3. Total discharged filter particle mass ($m_{2.3}=m_{2.2}-m_{2.1}$)	23.30 g
Total mass loss	
The difference of entrained bed and discharged particles mass ($m_{loss}=m_{1.6}-m_{2.3}$)	4.19 g

According to pressure difference analysis in **Figure 2-18**, starting from $\overline{\Delta P} = 0$ Pa and $\overline{\Delta P}$ deviation was 3 Pa. Heating up of bed particle was conducted in stage II to reach a preset temperature at 800°C. Fluidization stage IV was started from smooth fluidization to reach bubbling fluidized bed V with $\overline{\Delta P} = 244$ Pa, $\overline{\Delta P}$ deviation = 90 Pa. After the second feeding of EFB ash corresponding to 0.08 wt.% of ash in the initial bed material ($m_{1.1}$), agglomeration had taken place to form agglomerates gradually by ash feeding. At 0.39 wt.% of ash content, decreased $\overline{\Delta P}$ was once recovered maybe caused by disintegration of bulk agglomeration but was continued to decrease after the recovery. From pressure fluctuation, bubbling fluidization stage V continued to stably run until 1.55 wt.% of ash in the fluidized bed. Equal or above 1.55 wt.% of ash, pressure fluctuation rapidly dropped to be around zero. Therefore, the defluidization condition was confirmed after 1.55 wt.% of ash addition.
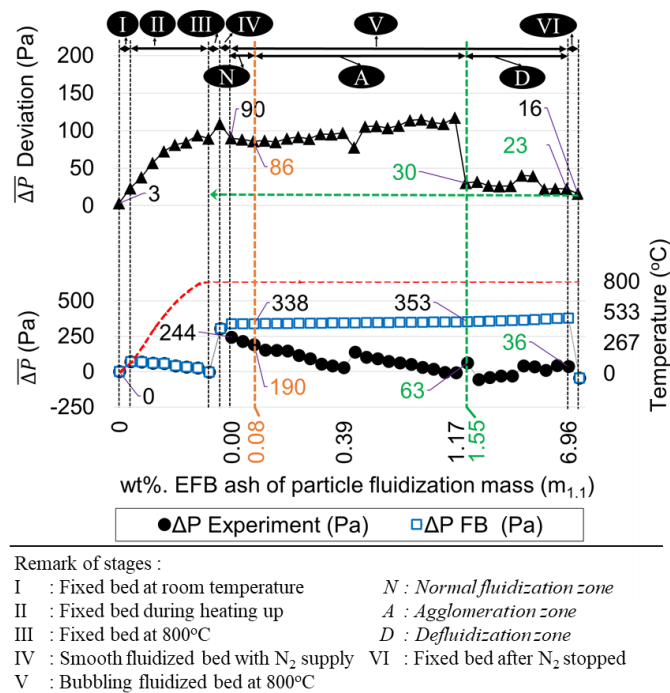
Figure 2-18. Agglomeration and defluidization analysis on silica sand at 800°C, 4.3 U_{mf}

Bed residue and discharged particles collected by a filter were shown in **Figure 2-19**. Extensive agglomerates had been formed in bed chamber (a) covering all cross-bed areas. Bed materials were taken out by manual treatment like knocking while pouring out

the agglomerates ((a).2). Some agglomerates were degraded by that treatment making the appearance looked like it contains smaller particles as shown in +350 µm particle size with agglomerate mass was 3.71 g.

| (a). before taking out | (b). Bed residue | (c). Discharged particle | (d). +350 µm |
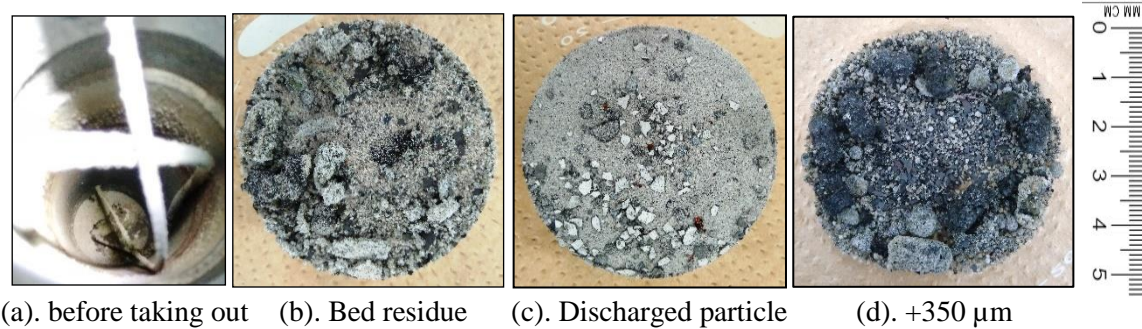
Figure 2-19 Silica sand bed residue before and after taking out, discharged particles, and sieved bed residue at T= 800ºC, 4.3 U$_{mf}$

Discharged particles were separated from the discharge line too (a).2. Mechanical sieving treatment of bed residue was carried out to obtain various sizes, in which +88-125, +177-250, +125-177 µm had three of the highest masses, with the mass of 23.26 g, 6.22 g, 4.23 g respectively.

Table 2-9. Composition of wt.% mixture of silica sand materials based on XRF measurement under treatment and ashing processes temperature at 800ºC

Elements	Bed residue particles							Discharged particles	Silica sand	EFB ash
	+350µm	+297-350µm	+250-297µm	+177-250µm	+125-177µm	+88-125µm	-88µm			
	T =800°C									T = 700°C
K	11.07%	10.17%	10.21%	11.06%	9.23%	11.52%	8.73%	9.56%	6.84%	48.64%
Ca	3.83%	4.57%	4.36%	4.55%	3.90%	5.10%	4.01%	4.51%	3.42%	18.95%
Si	44.01%	53.88%	58.04%	66.03%	66.37%	67.94%	62.72%	71.50%	80.94%	13.26%
Mg	0.00%	0.00%	0.00%	0.00%	0.00%	0.00%	0.00%	0.00%	0.00%	2.56%
Al	4.77%	5.43%	5.48%	6.43%	6.74%	9.11%	8.58%	8.22%	6.71%	1.17%
Cl	0.37%	0.40%	0.39%	0.23%	0.28%	0.32%	0.91%	1.90%	0.00%	3.99%
S	0.35%	0.23%	0.49%	0.58%	0.31%	0.22%	0.37%	0.34%	0.30%	2.29%
P	0.47%	0.45%	0.38%	0.33%	0.05%	0.00%	0.16%	0.21%	0.00%	1.92%
Fe	19.86%	16.70%	13.35%	6.94%	8.93%	3.30%	9.60%	2.30%	1.07%	4.71%
Na	0.00%	0.00%	0.00%	0.00%	0.00%	0.00%	0.00%	0.00%	0.00%	1.30%
Ti	0.65%	0.85%	0.74%	0.98%	1.12%	1.02%	1.70%	0.85%	0.45%	0.32%
Others	14.61%	7.33%	6.55%	2.87%	3.07%	1.48%	3.21%	0.62%	0.26%	0.89%

Based on **Table 2-9** and **Figure 2-20**, agglomeration indicators (I$_1$-I$_4$) were measured. Indicators (I$_1$ and I$_2$) from estimation in **Table 2-10** showed that the results after operation at 800ºC were mostly higher than the temperature at 700ºC and 750ºC indicating that

sticky level and agglomerates size formation were also stronger and bigger consisted of small, coarse until lump agglomerated particles.
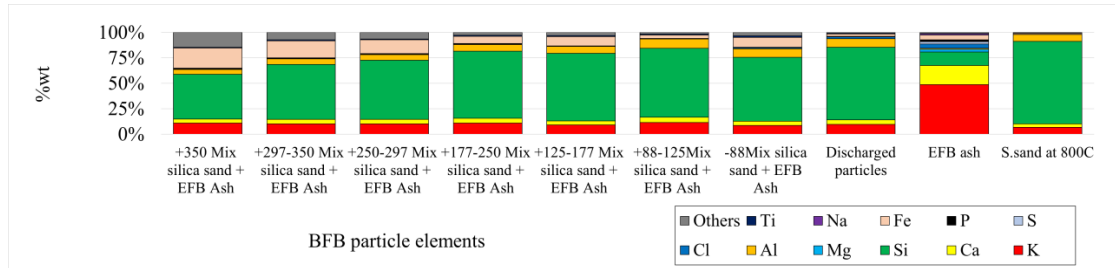
Fig. 2-20 Comparison of alkaline and dominant elements in a mixture of silica sand at 800°C, thermal silica sand, and EFB ash

Meanwhile, the result of Indicator I_3 and I_4 were insignificant like operation at 700 and 750°C which kept promoting agglomeration. High indicator value (I_1 and I_2) in +350 μm agglomerate size were 10.32 and 12.80 at 800°C compared to the same indicator at 700°C (8.83 and 10.04) and 750°C (8.36 and 8.33) already result in different strength, in which small increment of Indicator (I_1) and (I_2) was taking place at 700, 750°C had been produced strong agglomerates leading defluidization formation like at 800°C.

Table 2-10 Summary of agglomeration indicator (I_1-I_4) from a mixture of BFB material with silica sand utilization at 800°C, 4.3 U_{mf}

Indicator agglomeration	Bed residue particles							Discharged particles
	+350μm	+297-350μm	+250-297μm	+177-250μm	+125-177μm	+88-125μm	-88μm	
	$T_{pyrolysis} = 800^oC$							
I_1	10.32	12.00	7.43	8.00	10.12	15.18	5.31	3.71
I_2	12.80	12.76	14.39	15.80	19.15	15.59	17.14	17.18
I_3	0.25	0.19	0.18	0.17	0.14	0.17	0.14	0.13
I_4	0.11	0.10	0.09	0.10	0.10	0.13	0.14	0.12

Among the elements that are constructing equation I_1, sulfur becomes an important element that can inhibit the alkali-silicate reaction. The presence of low sulfur in +350 μm bed particles was causing high potency to form sticky agglomerates promoting defluidization.

2.4.4 Agglomeration and defluidization behavior of bentonite particles against EFB ash added at 700ºC

There was 25.66 g emitted particles from the bed chamber and 12.10 g accumulated discharged particles with the amount of filter particle was 12.10 g. The high mass loss during fluidization in a typical superficial velocity state was 13.56 g.

Table 2-11 Mass balance of thermal BFB treatment involving bentonite at 700ºC, 4.3 U_{mf}

Parameter	Value
Bed residue particle	
1. Bentonite input mass ($m_{1.1}$)	65.02 g
2. Total EFB ash addition mass ($m_{1.2}$)	3.04 g
3. Total cellulose capsule mass ($m_{1.3}$)	7.47 g
4. Total accumullated bed particle ($m_{1.4}=m_{1.1} + m_{1.2} + m_{1.3}$)	75.53 g
5. Total bed particle mass after operation ($m_{1.5}$)	49.87 g
5.1. +350µm particle size	0.42 g
5.2. +297-350µm particle size	0.08 g
5.3. +250-297µm particle size	0.03 g
5.4. +177-250µm particle size	0.25 g
5.5. +125-177µm particle size	1.24 g
5.6. +88-125µm particle size	45.00 g
5.7. -88µm particle size	2.84 g
6. Total emitted bed particle mass ($m_{1.6}=m_{1.5}-m_{1.4}$)	25.66 g
Discharged particle	
1. Discharge line before operation ($m_{2.1}$)	699.90 g
2. Discharge line after operation ($m_{2.2}$)	712.00 g
3. Total mass change of filter particle ($m_{2.3}=m_{2.2}-m_{2.1}$)	12.10 g
Total mass loss	
The difference of entrained bed and discharged particles mass ($m_{loss}=m_{1.6}-m_{2.3}$)	13.56 g

Operation at 700ºC in **Figure 2-21** showed that fluidization was running in a normal state. It was shown by $\overline{\Delta P}$ deviation which kept be stable from the initial fluidization state (9.84 Pa) until the last EFB ash addition at 9.31 Pa. While $\overline{\Delta P}$ fluctuation was kept running in good performance from $\overline{\Delta P}$ = 329 Pa until 442 Pa. The particle resulted in operation showed that normal fluidization state was taking place over all of ashes addition.
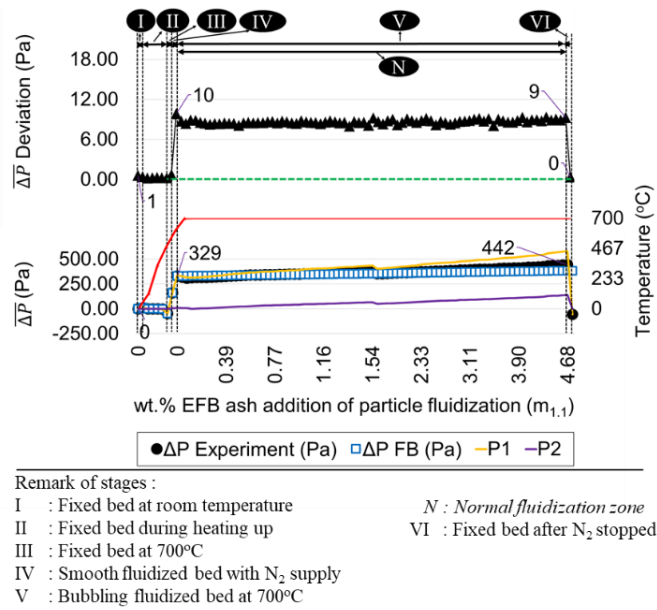
Figure 2-21. Agglomeration and defluidization analysis on bentonite at 700°C, 4.3 U_{mf}

Observing sieved bed particles especially for size +350 µm showed that the agglomeration was small too. The sieved particle in **Figure 2-22** was dominated by +88-125 µm particle around 45 g, in **Table 2-11**. That means around 92% bed particle was still there in the same size as the beginning operation.

(a). Bed residue (b). Discharged particle (d). +350µm
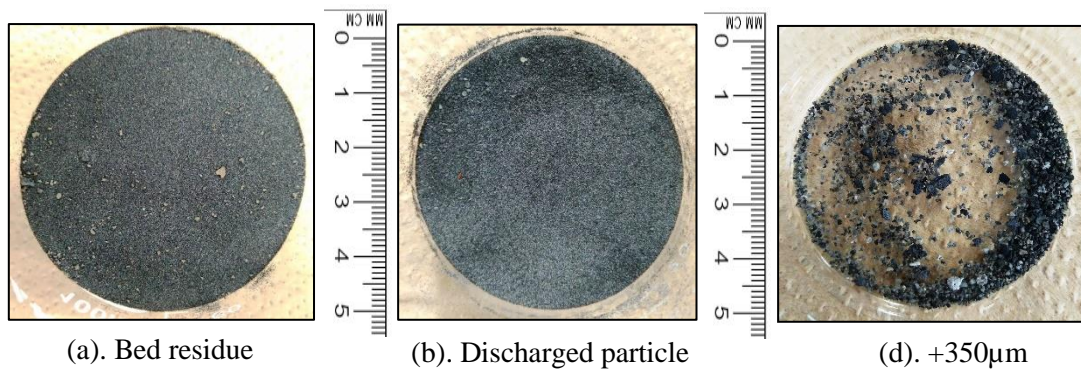
Figure 2-22. Bentonite bed residue, discharged and sieved particles at T= 700°C, 4.3 U_{mf}

Table 2-12 and **Figure 2-23** showed that the alkaline contained in bed residue particle had increased from the beginning around 1.57 and 86 wt.% for K and Na become 2 until several which promoted potency of agglomeration formation.

Table 2-12 Composition of wt.% mixture of bentonite materials based on XRF measurement under treatment and ashing processes temperature at 700°C

Elements	Bed residue particles								Bentonite	EFB ash
	+350μm	+297-350μm	+250-297μm	+177-250μm	+125-177μm	+88-125μm	-88μm	Discharge		
	T =700°C									T = 700°C
K	5.09%	3.67%	3.15%	5.34%	4.73%	6.61%	6.81%	6.89%	1.57%	48.64%
Ca	18.09%	18.04%	18.95%	8.18%	12.32%	4.20%	6.02%	6.54%	3.86%	18.95%
Si	49.49%	51.65%	50.04%	61.00%	56.18%	67.11%	64.14%	59.55%	71.51%	13.26%
Mg	2.22%	2.04%	2.32%	2.26%	2.53%	2.11%	2.10%	2.49%	2.35%	2.56%
Al	2.87%	2.33%	2.73%	8.59%	6.98%	10.35%	10.14%	9.18%	11.25%	1.17%
Cl	0.36%	0.42%	0.44%	0.26%	0.27%	0.29%	0.64%	1.05%	0.05%	3.99%
S	1.40%	1.49%	1.34%	0.84%	0.96%	0.47%	0.69%	1.03%	1.35%	2.29%
P	3.62%	3.81%	3.50%	1.10%	1.94%	0.00%	0.50%	1.01%	0.00%	1.92%
Fe	13.71%	13.10%	14.14%	9.59%	11.53%	7.19%	7.17%	9.16%	6.94%	4.71%
Na	0.00%	0.00%	0.00%	0.00%	0.00%	0.00%	0.00%	0.00%	0.00%	1.30%
Ti	0.87%	0.71%	0.86%	1.03%	1.00%	1.16%	1.16%	2.40%	0.60%	0.32%
Others	2.29%	2.75%	2.54%	1.83%	1.58%	0.53%	0.63%	0.71%	0.51%	0.89%
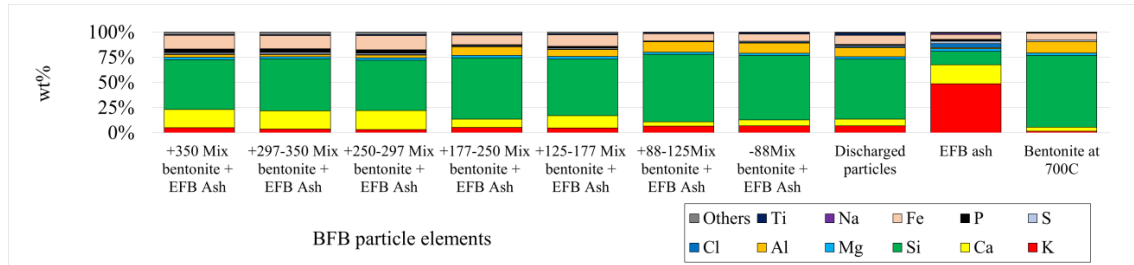
Figure 2-23. Comparison of alkaline and dominant elements in a mixture of bentonite at 700°C, thermal bentonite, and EFB ash

However, based on the prediction of agglomeration mechanisms (I_3-I_4) that agglomeration formation might be already started to produce a very small amount of agglomeration but not so sticky and not so big. So, the bed particle becomes more erodible.

Table 2-13 Summary of agglomeration indicator (I_1-I_4) from a mixture of BFB material with bentonite utilization at 700°C, 4.3 U_{mf}

Indicator agglomeration	Bed residue particles							Discharged particles
	+350μm	+297-350μm	+250-297μm	+177-250μm	+125-177μm	+88-125μm	-88μm	
	$T_{pyrolysis} = 700°C$							
I_1	1.61	1.08	1.01	2.75	2.17	5.38	3.35	2.22
I_2	2.28	2.32	2.15	5.75	3.63	11.69	8.23	6.62
I_3	0.10	0.07	0.06	0.09	0.08	0.10	0.11	0.12
I_4	0.06	0.05	0.05	0.14	0.12	0.15	0.16	0.15

Since that agglomeration was insignificantly disturbing fluidization state, then the presence of that agglomeration can be ignored because the BFB system could still run in a good performance.

2.4.5 Agglomeration and defluidization behavior of bentonite particles against EFB ash added at 750ºC

Table 2-14 showed the mass balance measurement. Total bentonite was 65.02 g, and the total number of encapsulated ashes addition was 10.25 g consist of 3.03 g EFB ashes and 7.22 g cellulose capsules. Total bed material after pyrolysis was 49.73 g while 25.33 g left bed chamber during operation into the discharge line. The total accumulated discharged particle was 12.20 g, which means around 13.33 g particles, as the difference between bed and discharge line particles had been lost.

Table 2-14 Mass balance of thermal BFB treatment involving bentonite at 750ºC, 4.3 U_{mf}

	Parameter	Value
	Bed residue particle	
	1. Bentonite input mass ($m_{1.1}$)	65.02 g
	2. Total EFB ash addition mass ($m_{1.2}$)	3.03 g
	3. Total cellulose capsule mass ($m_{1.3}$)	7.22 g
	4. Total accumulated bed particle ($m_{1.4}=m_{1.1}+m_{1.2}+m_{1.3}$)	75.26 g
	5. Total bed particle mass after pyrolysis ($m_{1.5}$)	49.73 g
1.	5.1. +350µm particle size	0.73 g
	5.2. +297-350µm particle size	0.11 g
	5.3. +250-297µm particle size	0.03 g
	5.4. +177-250µm particle size	0.25 g
	5.5. +125-177µm particle size	0.39 g
	5.6. +88-125µm particle size	42.98 g
	5.7. -88µm particle size	5.23 g
	6. Total emitted bed particle ($m_{1.6}=m_{1.5}-m_{1.4}$)	25.53 g
	Discharged particle	
	1. Discharge line before operation ($m_{2.1}$)	699.90 g
2.	2. Discharge line after operation ($m_{2.2}$)	712.10 g
	3. Total discharged filter particle mass ($m_{2.3}=m_{2.2}-m_{2.1}$)	12.20 g
	Total mass loss	
	The difference of entrained bed and discharged particles mass ($m_{loss}=m_{1.6}-m_{2.3}$)	13.33 g

Time history of $\overline{\Delta P}$ and $\overline{\Delta P}$ deviation was shown in **Figure 2-24**. In stage (I) to (V), the increase of $\overline{\Delta P}$ deviation was observed from 3 Pa to 112 Pa and $\overline{\Delta P}$ from 0 until 337

Pa. Feeding capsulated ashes in stage (V) was carried out with the total by 4.66 wt.% of initial bed particle mass (m$_{1.1}$), **Table 2-14**.
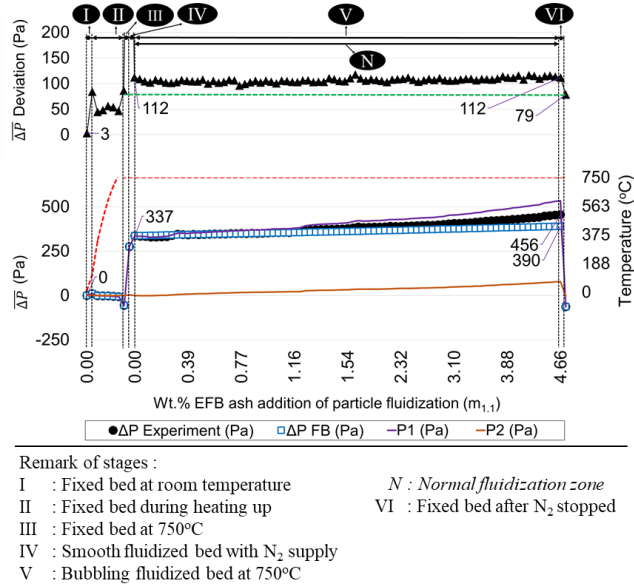
Figure 2-24. Agglomeration and defluidization analysis on bentonite at 750°C, 4.3 U$_{mf}$

Operation at 750°C showed that normal fluidization was performed from the beginning until the last addition, in which $\overline{\Delta P}$ deviation =112 Pa was almost the same with initial deviation in stage V. Furthermore, $\overline{\Delta P}$ was stable to increase without pressure loss. It was confirmed by comparison among of pressure differences from which $\overline{\Delta P}$ = 456 Pa was still higher than $\overline{\Delta P}_{FB}$ = 390 Pa.

(a). Bed residue   (b). Discharged particle   (c). +350µm
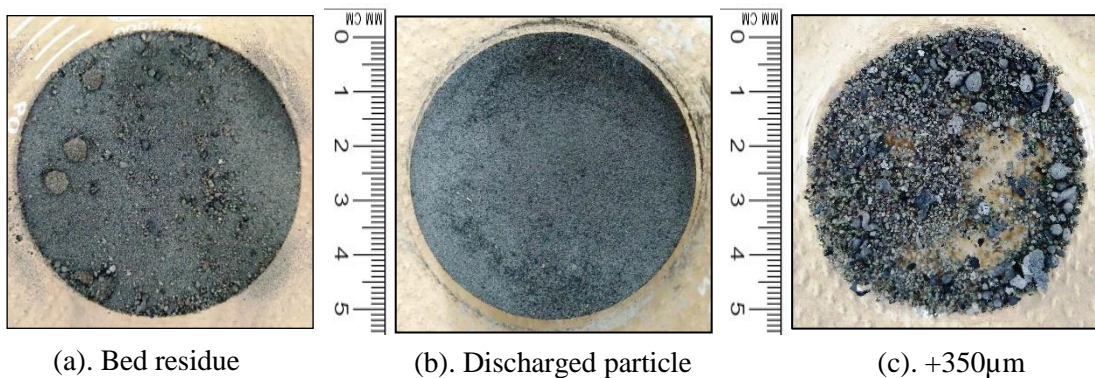
Figure 2-25. Bentonite bed residue, discharged particles, and sieved bed residue at T= 750°C, 4.3 U$_{mf}$

Figure 2-25 showed the status of bed residue and discharged particles after the operation. A few agglomerates in the bed residue might be primary agglomerates of encapsulated samples. Except for the primary agglomerates, only a few numbers of small agglomerates could be observed. From the above results, bentonite bed could be stably fluidized up to 4.66 wt.% of ash in the bed at 750°C. Referring to XRF measurement in **Table 2-15** and **Figure 2-26**, calculation of agglomeration indicator in **Table 2-16** showed low indicator values of I_1 and I_2 in comparison with silica sand in the same condition, but agglomeration was still possible to be produced.

Table 2-15 Composition of wt.% mixture of bentonite materials based on XRF measurement under treatment and ashing processes temperature at 750°C

Elements	Bed residue particles								Bentonite	EFB ash
	+350μm	+297-350μm	+250-297μm	+177-250μm	+125-177μm	+88-125μm	-88μm	Discharge		
	T =750°C									T = 700°C
K	8.45%	6.81%	5.97%	5.63%	4.78%	6.49%	7.08%	4.79%	1.54%	48.64%
Ca	10.94%	14.19%	13.61%	15.43%	16.45%	4.14%	6.30%	6.09%	4.01%	18.95%
Si	52.26%	49.84%	51.64%	48.34%	48.04%	66.85%	62.32%	62.43%	71.63%	13.26%
Mg	1.59%	1.65%	1.69%	1.65%	2.08%	2.53%	2.59%	2.40%	2.31%	2.56%
Al	3.62%	3.80%	3.61%	3.31%	4.98%	10.03%	9.66%	9.30%	11.30%	1.17%
Cl	0.47%	0.36%	0.46%	0.35%	0.35%	0.00%	0.54%	0.96%	0.00%	3.99%
S	1.53%	1.43%	1.59%	1.47%	1.32%	0.55%	0.85%	0.94%	1.30%	2.29%
P	2.08%	2.61%	2.78%	2.72%	2.54%	0.00%	0.74%	0.99%	0.00%	1.92%
Fe	14.91%	15.67%	14.83%	16.74%	15.39%	7.63%	8.09%	9.33%	6.83%	4.71%
Na	0.00%	0.00%	0.00%	0.00%	0.00%	0.00%	0.00%	0.00%	0.00%	1.30%
Ti	1.93%	0.94%	0.86%	1.01%	1.06%	1.27%	1.20%	1.99%	0.61%	0.32%
Others	2.20%	2.71%	2.97%	3.35%	3.01%	0.51%	0.62%	0.78%	0.46%	0.89%
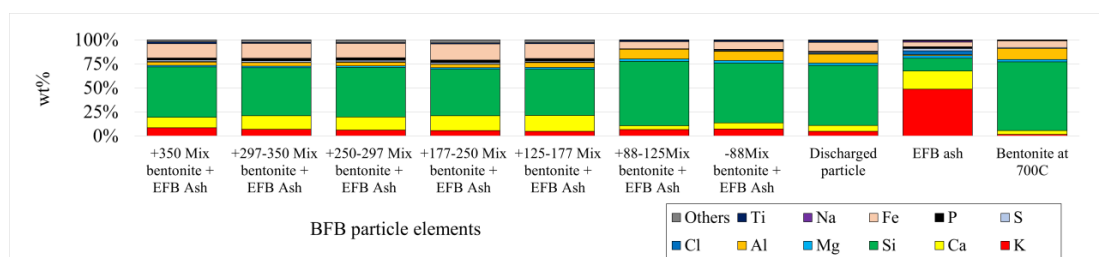
Figure 2-26 Comparison of alkaline and dominant elements in a mixture of bentonite at 750°C, thermal bentonite, and EFB ash

However low values of indicator I_1 showed that bentonite particle was more difficult to build up sticky agglomeration than silica sand, and slight coating layer would be formed in small amount based on I_2. Meanwhile, agglomeration formation based on indicator I_3 was also insignificant the same as silica sand.

Table 2-16 Summary of agglomeration indicator (I_1-I_4) from a mixture of BFB material with bentonite utilization at 750°C, 4.3 U_{mf}

Indicator agglomeration	Bed residue particles							Discharged particles
	+350µm	+297-350µm	+250-297µm	+177-250µm	+125-177µm	+88-125µm	-88µm	
	$T_{pyrolysis} = 750°C$							
I_1	2.39	2.11	1.65	1.71	1.60	5.91	3.15	1.68
I_2	4.16	3.07	3.19	2.73	2.51	11.00	7.21	7.09
I_3	0.16	0.14	0.12	0.12	0.10	0.10	0.11	0.08
I_4	0.07	0.08	0.07	0.07	0.10	0.15	0.15	0.15

2.4.6 Agglomeration and defluidization behavior of bentonite particles against EFB ash added at 800°C

According to mass balance measurement in **Table 2-17**, total bed particle after the operation was 61.40 g, and there was 13.87 g emitted particle leaving the bed, 0.30 g settle in discharge line indicating 13.57 g total bed particle had been lost.

Table 2-17 Mass balance of thermal BFB treatment involving bentonite at 800°C, 4.3 U_{mf}

	Parameter	Value
Bed residue particle		
1.	1. Bentonite input mass ($m_{1.1}$)	65.10 g
	2. Total ash EFB addition mass ($m_{1.2}$)	3.04 g
	3. Total cellulose capsule mass ($m_{1.3}$)	7.13 g
	4. Total accumulated bed particle ($m_{1.4}=m_{1.5}+ m_{1.2}+m_{1.3}$)	75.27 g
	5. Total bed particle mass after pyrolysis ($m_{1.5}$)	61.40 g
	5.1. +350µm particle size	1.71 g
	5.2. +297-350µm particle size	0.12 g
	5.3. +250-297µm particle size	0.03 g
	5.4. +177-250µm particle size	0.33 g
	5.5. +125-177µm particle size	0.76 g
	5.6. +88-125µm particle size	51.65 g
	5.7. -88µm particle size	6.81 g
	6. Total emitted bed particle mass ($m_{1.6}=m_{1.5}-m_{1.4}$)	13.87 g
Discharged particle		
2.	1. Discharge line before operation ($m_{2.1}$)	699.50 g
	2. Discharge line after operation ($m_{2.2}$)	699.80 g
	3. Total discharged filter particle mass ($m_{2.3}=m_{2.2}-m_{2.1}$)	0.30 g
Total mass loss		
	The difference of entrained bed and discharged particles mass ($m_{loss}=m_{1.6}-m_{2.3}$)	13.57 g

From the time history of pressures as shown in **Figure 2-27**, fixed bed stages I-III was started from $\overline{\Delta P}$ deviation = 3 Pa, followed by starting N_2 supply to reach bubbling fluidization stage V with $\overline{\Delta P}$ deviation = 182 Pa and $\overline{\Delta P}$ = 338 Pa. Significant agglomerates were predicted to form according to the decrease of $\overline{\Delta P}$ after the first feeding of capsulated ash by 0.04 wt.% of initial bed material mass ($m_{1.1}$) as listed in Table 2-17, with $\overline{\Delta P}$ = 291 Pa in contrast with $\overline{\Delta P}_{FB}$ = 338 Pa. Accumulation of larger agglomerates were already formed by 3.5 wt.% over capsulated ashes addition including significant $\overline{\Delta P}$ decrement. $\overline{\Delta P}$ decreased by addition of ash to be reached to 115 Pa at 0.62 wt.% of EFB ash in the bed. After 0.62 wt.% of ash addition, $\overline{\Delta P}$ slightly increased to 216 Pa at the end of ash addition. Although $\overline{\Delta P}$ was below $\overline{\Delta P}_{FB}$, during fluidization, $\overline{\Delta P}$ deviation was around 90 Pa which was relatively high. Therefore, smooth fluidization was taking place throughout the fluidization operation.
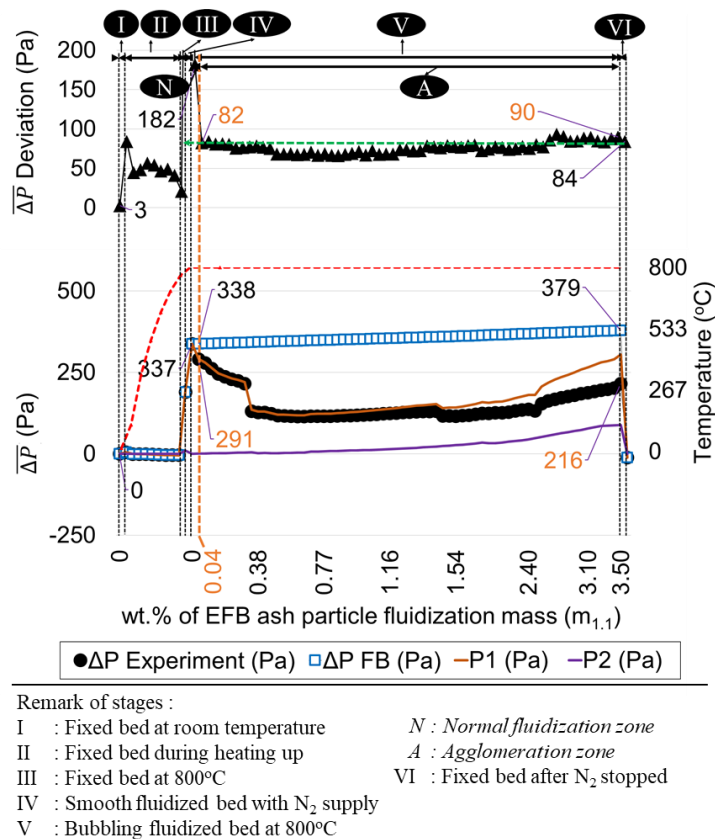
Figure 2-27. Agglomeration and defluidization analysis on bentonite at 800°C, 4.3 U_{mf}

This behavior could be explained by the formation of weak agglomerates. When a weak agglomerate was formed in a column, a large agglomerate might be easily broken or ground by collision with other agglomerates to regenerate particles which had a similar size to primary particles. This phenomenon might reach equilibrium size distribution. Therefore, a portion of particles kept fluidizing.

| (a). Bed residue | (b). Discharged particle | (c). +350μm |
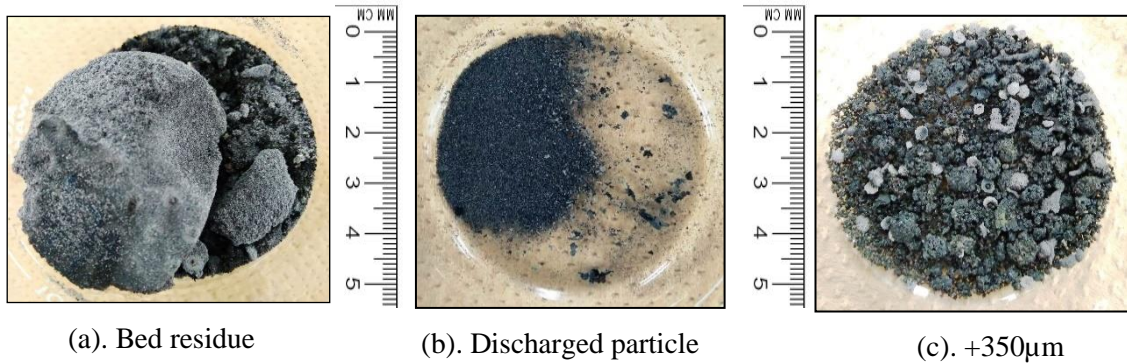
Figure 2-28. Bentonite bed residue, discharged, and sieved bed residue at T= 800°C, 4.3 U_{mf}

The condition of particles remained in the BFB column after the treatment was shown in **Figure 2-28**. Huge size but very weak agglomerates were observed in mixture bed residue particle (a), and +350 µm sieved bed particle (c) where bulk agglomerates could be degraded easily during mechanical sieving treatment and back to be smaller size again.

Table 2-18 Composition of wt.% mixture of bentonite materials based on XRF measurement under treatment and ashing processes temperature at 800°C

| Elements | Bed residue particles | | | | | | | Discharge | Bentonite | EFB ash |
	+350μm	+297-350μm	+250-297μm	+177-250μm	+125-177μm	+88-125μm	-88μm			
	T =800°C									T = 700°C
K	31.84%	31.57%	28.61%	28.56%	21.79%	3.60%	4.86%	20.58%	1.34%	48.64%
Ca	12.42%	11.45%	10.21%	9.73%	8.30%	3.97%	4.49%	7.87%	3.82%	18.95%
Si	30.90%	25.01%	26.20%	25.74%	37.87%	69.91%	66.93%	30.72%	72.64%	13.26%
Mg	1.64%	1.53%	1.51%	1.68%	1.74%	2.22%	2.26%	1.89%	2.38%	2.56%
Al	2.35%	2.60%	3.15%	3.35%	6.00%	10.35%	9.97%	4.94%	11.44%	1.17%
Cl	0.12%	0.40%	0.29%	0.25%	0.10%	0.29%	0.46%	8.09%	0.00%	3.99%
S	2.46%	2.76%	2.62%	2.81%	2.26%	0.54%	0.82%	3.04%	0.70%	2.29%
P	1.75%	1.22%	0.96%	0.97%	0.73%	0.00%	0.39%	1.04%	6.62%	1.92%
Fe	8.60%	8.61%	9.08%	9.28%	8.70%	7.53%	7.96%	12.17%	0.00%	4.71%
Na	0.00%	0.00%	0.00%	0.00%	0.00%	0.00%	0.00%	5.04%	0.56%	1.30%
Ti	6.42%	13.75%	15.26%	15.96%	11.01%	1.10%	1.30%	3.13%	0.00%	0.32%
Others	1.51%	1.10%	2.11%	1.69%	1.50%	0.50%	0.56%	1.50%	0.50%	0.89%
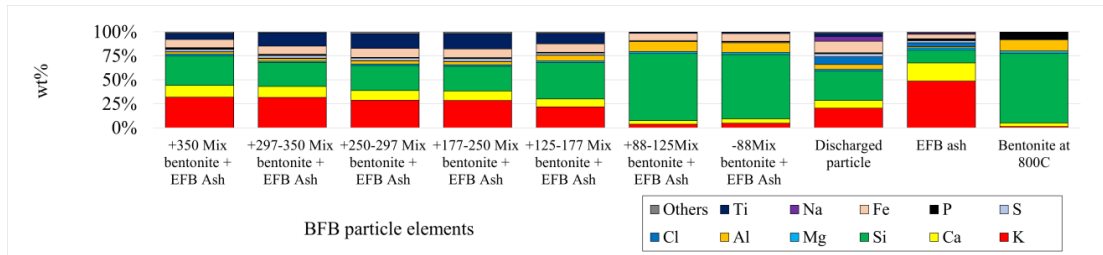
Figure 2-29. Comparison of alkaline and dominant elements in a mixture of bentonite at 800°C, thermal bentonite, and EFB ash

In contrast with silica sand, those agglomerates were separately mixed with small particles. This observation supports the above consideration of agglomeration formation mechanisms.

Elemental data by XRF in **Table 2-18** and **Figure 2-29** and agglomeration indicator measurements in **Table 2-19** showed lower indicator I_1 and I_2 values than silica sand but slightly higher than mixture bentonite from treatment at 700 and 750°C. Those values elucidated that operation at 800°C had a higher stickiness level and a larger coating layer of agglomerates than 700 and 750°C. Meanwhile, melting agglomeration based on the third indicator (I_3) measurement was already formed in a small amount, while potency to avoid agglomeration based on the fourth indicator (I_4) was small too.

Table 2-19 Summary of agglomeration indicator (I_1-I_4) from a mixture of BFB material with bentonite utilization at 800°C, 4.3 U_{mf}

Indicator agglomeration	Bed residue particles							Discharged particles
	+350μm	+297-350μm	+250-297μm	+177-250μm	+125-177μm	+88-125μm	-88μm	
	$T_{pyrolysis} = 800^oC$							
I_1	6.31	5.33	5.17	4.88	4.71	2.63	2.33	1.81
I_2	3.97	3.98	4.32	4.38	5.54	11.88	10.05	5.22
I_3	1.03	1.26	1.09	1.11	0.58	0.05	0.07	0.67
I_4	0.08	0.10	0.12	0.13	0.16	0.15	0.15	0.16

2.5. Agglomeration and defluidization of silica sand and bentonite particles under typical superficial velocity

On treatment at 700°C, in **Figures 2-13** and **2-21**., agglomeration measurement based on pressure differences had run normally both in silica sand and bentonite particles. Temperature increment by 750°C affected agglomerates formation, in which agglomeration process started to be generated after feeding EFB ashes by 0.12 wt.% Meanwhile, the fluidization process on bentonite still kept running well as shown by curves in **Figures 2-15** and **2-24**.

The temperature increasing at 800°C caused a significant increment of agglomerates formation, in which a number of large agglomerates had been formed leading to reach defluidization state as shown in **Figure 2-18**. Different behavior was formed on bentonite utilization, from which the fluidization was still possible to be achieved in the BFB column even though a number of agglomerates had been formed and covered over cross-section area as shown in **Figures 2-27** and **2-28**.
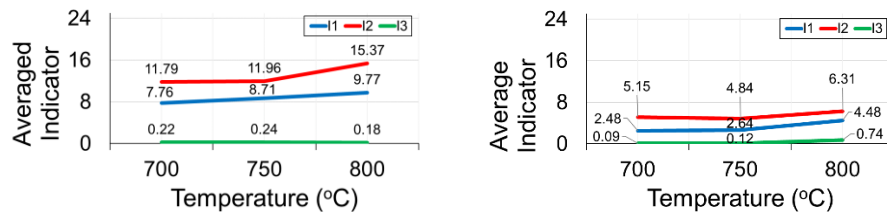
Figure 2-30. Comparison of average indicators values between a mixture of silica sand and bentonite under velocity treatment at 4.3 U$_{mf}$

The effect of temperature increment increased not only bed particle sizes but also the level of stickiness on formed agglomerates. The stickiness level prediction based on elemental measurement showed that agglomerates in silica sand had different stickiness levels to agglomerate in bentonite. The potencies of sticky agglomerates formation on silica sand were higher than bentonite based on I_1-I_2 values as shown in **Tables 2-4, 2-7, 2-10, 2-13, 2-16, 2-19** for each sieved bed particle and **Figure 2-30 was** for the average indicators of sieved bed particles. However, agglomeration based on melting of silicates, I_3, had very small contribution in agglomerates formation. This condition caused large

silica sand agglomerates would remain solid and was not easy to be fragmented into smaller agglomerates size either when fluidization was taking place or sieving process was carried out. Meanwhile, the structure of agglomeration on bentonite formed was absolutely weak and easy to be eroded by 4.3 U_{mf} application during the fluidization process. It could be seen by bed particle shapes after the sieving process which had been mostly degraded as shown in **Figure 2-28**.

2.6. Conclusions

Agglomeration formation and defluidization behavior of silica sand and bentonite particles were compared at 700, 750, and 800°C by introducing EFB ash into the bed up to 6.9 wt.%. Silica sand had higher potency to achieve faster and hard agglomeration than bentonite by interaction with EFB ash at 750°C which was proved by a gradual increase of averaged pressure loss of fluidized bed. Agglomeration formation in silica sand bed was dominated by several mm hard agglomerates formation. However, defluidization of silica sand bed was not observed throughout the operation. Observation of bed residue in bentonite showed that fluidization kept running well even some small agglomerates had been formed.

In fluidization operation at 800°C, both beds of silica sand and bentonite formed agglomerates, but the size and strength were completely different. Lump and hard agglomerates were formed in silica sand beds while huge but weak agglomerates were produced in bentonite beds. Silica sand bed was attained defluidization state after 1.55 wt.% of EFB ash addition on silica sand while no defluidization on bentonite. This difference might be caused by the difference of agglomerate strength based on agglomeration indicator measurement showed that coating formation and sintering behavior on silica sand was much higher than bentonite.

Based on general results, the fluidized bed gasification process involving silica sand for EFB was recommended to be held at operational temperature was less than 750°C, while bentonite was reliable to be carried out by 750°C, even possible by 800°C in a smooth fluidization state. Increasing superficial gas velocity was an option to allow for bentonite application with higher temperatures because weak agglomerates formed in bentonite beds might be easily disintegrated by particle motion.

References

Cuadros, J., Huertas, F., Delgado, A., and Linares, J. (1994). *Determination of Hydration (H₂O−) and Structural (H₂O) Water for Chemical Analysis of Smectites*. Application to Los Trancos Smectites, Spain. Clay Minerals, 29(2), 297

Liu, Huanpeng & Feng, Yujie & Wu, Shaohua & Liu, Dunyu. (2009). *The role of ash particles in the bed agglomeration during the fluidized bed combustion of rice straw. Bioresource technology*. 100. 6511. 10.1016/j.biortech.2009.06.098.

Li, Qinghai & Zhang, Y.G. & Meng, Aihong & Li, L. & Li, G.X.. (2013). *Study on ash fusion temperature using original and simulated biomass ashes*. Fuel Processing Technology. 107. 110. 10.1016/j.fuproc.2012.08.012.

Mu, L., Zhao, L., Liu, L., and Yin, H. (2012). *Elemental Distribution and Mineralogical Composition of Ash Deposits in a Large-Scale Wastewater Incineration Plant: A Case Study*. Industrial and Engineering Chemistry Research. 51. 8684–8694. 10.1021/ie301074m.

Niu, Yanqing & Zhu, Yiming & Tan, Houzhang & Wang, Xuebin & Hui, Shi'en & Du, Wenzhi. (2014). *Experimental study on the coexistent dual slagging in biomass-fired furnaces: Alkali- and silicate melt-induced slagging*. Proceedings of the Combustion Institute. 35. 10.1016/j.proci.2014.06.120. Pages 2406

Visser, H.. (2004). *The influence of fuel composition on agglomeration behaviour in fluidised bed combustion*.

Visser, H. & Hofmans, H. & Huijnen, H. & Kastelein, R. & Kiel, J.. (2008). *Biomass Ash – Bed Material Interactions Leading to Agglomeration in Fluidised Bed Combustion and Gasification*. 10.1002/9780470694954.ch20.

CHAPTER III

Agglomeration and Defluidization of Silica Sand and Bentonite Particles Processes influenced by superficial velocity intensity (1.5 U$_{mf}$) with thermal treatment temperature at 700, 750 and 800°C

3.1 Introduction

The thermal fluidized bed in this process needed some velocity to achieve a complete reaction. In the previous chapter, analysis with typical intensity (4.3 U$_{mf}$) had been carried out to show bentonite gave high potency to maintain fluidization from 700°C even at 800°C. In this chapter, analysis agglomeration and defluidization with lower velocity would be carried out with intensity velocity by 1.5 of U$_{mf}$. One of the considerations in applying the lower intensity is to reduce fluidization gas flow. Imagining an actual process, fluidized bed gasifiers will be operated by steam. Steam consumption in those processes leads to low energy efficiency, so that low steam consumption, that is operation with low gas velocity is preferable.

However, low-velocity applications that might change agglomeration and defluidization phenomena related to the capability of bed particles to keep maintaining fluidization state under low superficial velocity conditions could not be found out. The agglomeration formation was closely relevant with elements contained in bed material. If bed material was dominated by elements leading to form sticky agglomerates, then that agglomerates might be faster and easier to grow up with the assumption that complete reaction had been taken place over the cross-bed area. Furthermore, the decrease of velocity should lower momentum particle in making a number of agglomerates formed which could be more difficult to be eroded each other. According to that consideration, analysis of agglomeration and defludization at low-intensity velocity was important to be known too.

3.2 Experimental

Analysis was carried out with the same materials consisted of bed particle as silica sand, bentonite, and encapsulated EFB ash with the mass of 0.025, 0.05, 0.25, and 0.5 g

with 30 times total addition. Bubbling Fluidized Bed system was used as apparatus for this study.

3.3. Method

3.3.1 Determination of agglomeration and defluidization stages

The method used in this chapter was the same as Chapter II by involving the measurement of mass balance and determination of agglomeration and defluidization state based on the pressure difference and elemental measurement analysis. The pressure difference data were obtained only from a single pressure sensor in the range of operational pressure 0-5000 Pa instead of $\pm$ 12000 Pa. The change of pressure sensor installation was relevant to increase the precision measurement of ΔP against ΔP theoretical data value around 300 Pa at around 65 g initial bed material mass.

3.3.2 Identification of channeling formation caused by agglomeration

In this chapter, channeling formation caused by agglomeration was investigated too. Channeling formation behaviors of sample beds were directory observed by changing the superficial velocity from 0 to 0.018 m/s that equaled to 1.5 U_{mf} superficial velocity application. Channeling formation is a blockage on the cross-section area making gas supply decrease because it will be more difficult to introduce from the distributor into the reactor. The phenomenon was first formed on deposition on the wall, agglomerate formation in the bed leading to reach defluidization state. The complete channeling formation was formed when agglomeration had been formed on the bed, so the $\overline{\Delta P}$ should be zero. Some conditions showed the incomplete channeling process referring to a temporary slagging formation which still could be shattered by adjusted velocity. When complete and incomplete channeling were taking place, minimum fluidization velocity called U_{mf} was difficult and would take longer time to be attained than the normal state. It would need velocity adjustment to shatter agglomerated bed particles. The minimum velocity needed to shatter the channeling is called by U_{sc}. Typical channeling conditions were described by the diagram in **Figure 3-1.** The normal fluidization was described in number 1. When small agglomeration had been first formed, the minimum velocity that was needed to create fluidization would increase too. The channeling formation had been

formed even though in incomplete formation only as shown in numbers 3 and 4, while the complete channeling followed by stuck-up bed particles were figured by number 5.
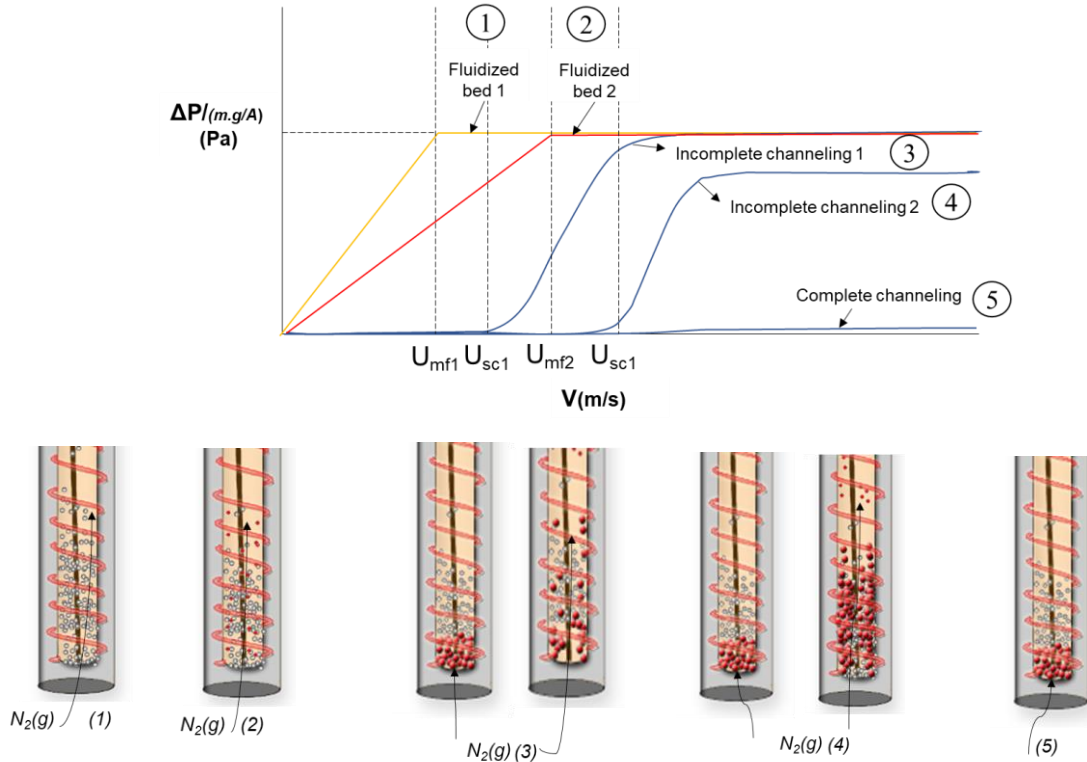
Fig. 3-1 Typical channeling formations based on U_{mf} measurements

3.4. Result and discussion

3.4.1 Agglomeration and defluidization behavior of silica sand particles against EFB ash added at 700ºC

Total bed particles in condition before and after operation were 73.89 and 67.05 g. As shown in **Table 3-2**, there was 6.84 g bed particle leaving bed reaction towards the discharge line. Since the total accumulated discharge particle was 1.6 g, so total loss particle mass was 5.24 g. Meanwhile, fluidization activity measurement according to pressure difference in **Figure 3-2** showed the fluidization kept running well. $\overline{\Delta P}$ deviation and $\overline{\Delta P}$ showed value 5.26 and 0 Pa at condition before the operation started. When thermal treatment was started and fluidization condition had been achieved, $\overline{\Delta P}$ deviation increased into 30.27 and $\overline{\Delta P}$ became 273.97 Pa.

Table 3-1 Mass balance of thermal BFB treatment involving silica sand at 700°C, 1.5U$_{mf}$

Parameter	Value
Bed residue particle	
1. Silica sand input mass (m$_{1.1}$)	65.09 g
2. Total EFB ash addition mass (m$_{1.2}$)	4.53 g
3. Total cellulose capsule mass (m$_{1.3}$)	4.28 g
4. Total accumulated bed particle (m$_{1.4}$= m$_{1.1}$+m$_{1.2}$+m$_{1.3}$)	73.89 g
5. Total bed particle mass after operation (m$_{1.5}$)	67.05 g
5.1. +350µm particle size	0.87 g
5.2. +297-350µm particle size	0.10 g
5.3. +250-297µm particle size	0.05 g
5.4. +177-250µm particle size	2.39 g
5.5. +125-177µm particle size	2.69 g
5.6. +88-125µm particle size	23.49 g
5.7. -88µm particle size	37.47 g
6. Total emitted bed particle mass (m$_{1.6}$ = m$_{1.5}$-m$_{1.4}$)	6.84 g
Discharged particle	
1. Discharge line before pyrolysis (m$_{2.1}$)	699.60 g
2. Discharge line after operation (m$_{2.2}$)	701.20 g
3. Total discharged filter particle mass (m$_{2.3}$=m$_{2.2}$-m$_{2.1}$)	1.60 g
Total mass loss	
The difference of entrained bed particle and discharged particles mass (m$_{loss}$=m$_{1.6}$-m$_{2.3}$)	5.24 g

Those results showed that the fluidization kept running well from which $\overline{\Delta P}$ deviation and $\overline{\Delta P}$ kept stable without getting significant decrement as shown in last addition of ash, $\overline{\Delta P}$ deviation achieved 26.3 Pa and $\overline{\Delta P}$ was 259.97 Pa.

Remark of stages :
I   : Fixed bed at room temperature
II   : Fixed bed during heating up
III : Fixed bed at 700°C
IV   : Smooth fluidized bed with N$_2$ supply
V   : Bubbling fluidized bed at 700°C

N : Normal fluidization zone
VI : Fixed bed after N$_2$ stopped
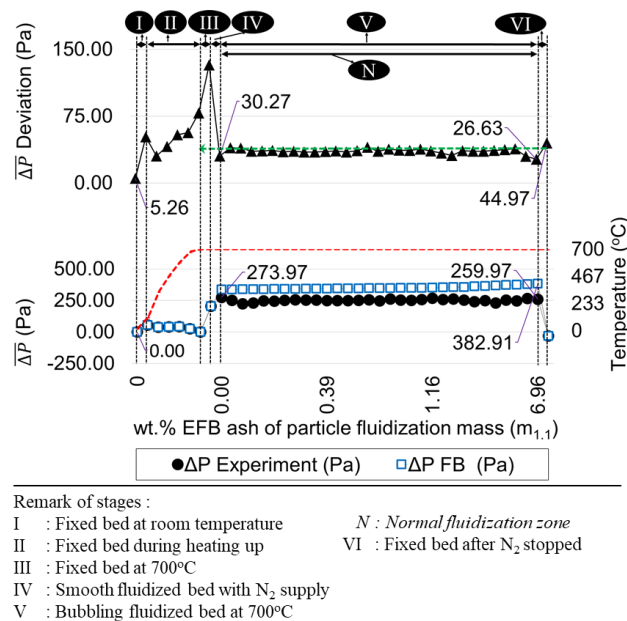
Fig. 3-2 Agglomeration and defluidization analysis on silica sand at 700°C, 1.5 U$_{mf}$

Related to the analysis of pressure differences, U_{mf} measurement as shown in **Figure 3-3** relatively showed that the fluidization state kept being achieved in velocity range 0-0.018 m/s. U_{mf} of silica sand at room temperature before the operation was 0.009 m/s and the adjusted velocity of operation was 1.5 U_{mf} or 0.014 m/s. U_{mf} measurement at preset temperature 700°C, after both 0.025 and 0.05 g for 10 times addition, after both 0.25 and 0.5 g for 5 times addition, and after cooling process were 0.034, 0.0039, 0.0068, 0.0098, 0.0138, and 0.0149 respectively which gradually increased by the density of bed particle increment. The capsulated ash was mostly incomplete degraded by fluidization between 0.025 g for 10 times and 0.25 g for 5 times of EFB ash addition range, so the alkali-silicate reaction that led to reaching agglomeration was not formed completely. In U_{mf} measurement after 0.5 g and cooling process, initial fluidization was achieved when those $\overline{\Delta P}$ were lower than theoretical $\overline{\Delta P}$ value. Those U_{mf} values might be relevant to the decrease of bed material mass caused by the small formation of agglomerates because the number of capsulated ashes had been degraded to react with silica sand as channeling on the wall reactor. The decrement was caused by entrainment few number fine particles towards the discharge line that made the decrease of $\overline{\Delta P}$. So, the fluidization of both conditions was slowly achieved. The schematic of the channeling process was figured in **Figure 3-1** for phenomenon no.2.
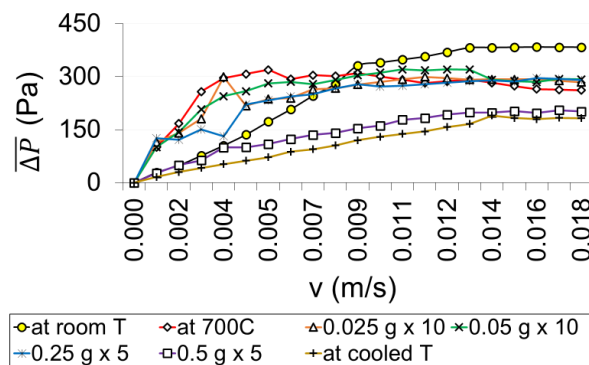
Fig. 3-3 Channelling formation behaviors of silica sand bed particle before and after treatment at 700°C,

Some agglomerates in the discussion above could be seen in real bed particle pictures after operation in **Figure 3-4**. Based on that figure, there was an amount of agglomeration in bed residue.

|(Bed residue).|(Disharged particle).|(+350µm).|
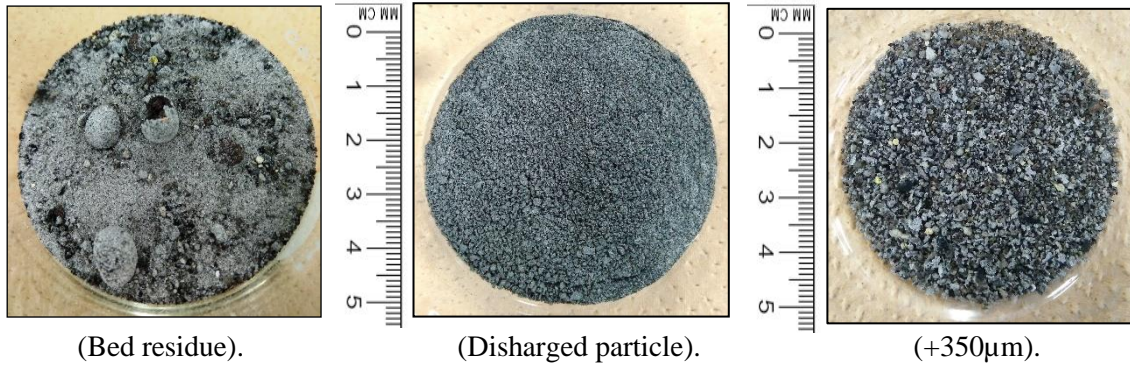
Fig. 3-4 Silica sand bed residue, discharged particles, and sieved bed residue at T= 700ºC, 1.5U$_{mf}$

The agglomerates were dominated by ashes which were incompletely degraded during the fluidization process. Therefore, the agglomeration caused by the alkali-silicate reaction was not much formed yet. According to mass balance measurement in **Table 3-1**, bed material was still dominated by +88-125 and -88µm, but still not much for bigger particle size yet.

Related to measurement in agglomeration content based on measurement in **Table 3-2** and **Figure 3-5**, some agglomerated particles had been formed in the whole of sieved particles as the result of alkali-silicate reaction based on indicator (I$_1$) measurement in **Table 3-3**.

Table 3-2 Composition of wt.% mixture of silica sand bed particles based on XRF measurement under treatment and ashing processes temperature at 700ºC

Elements	Bed residue particles							Discharged particles	Silica sand	EFB ash
	+350µm	+297-350µm	+250-297µm	+177-250µm	+125-177µm	+88-125µm	-88µm			
	T =700ºC									T = 700ºC
K	25.79%	21.30%	21.45%	17.53%	13.45%	11.93%	13.12%	21.55%	6.98%	48.64%
Ca	15.73%	12.31%	14.92%	9.50%	7.47%	4.59%	5.55%	14.68%	3.66%	18.95%
Si	34.36%	42.93%	38.29%	58.27%	62.61%	70.87%	67.26%	30.41%	80.21%	13.26%
Mg	1.39%	1.20%	1.50%	0.28%	0.00%	0.00%	0.00%	1.33%	0.00%	2.56%
Al	2.65%	2.70%	2.85%	4.98%	6.34%	8.30%	8.07%	5.03%	6.89%	1.17%
Cl	0.59%	0.92%	0.92%	0.65%	0.47%	0.35%	0.81%	8.58%	0.00%	3.99%
S	2.34%	1.61%	2.03%	1.32%	1.04%	0.45%	0.59%	1.60%	0.26%	2.29%
P	1.81%	1.79%	1.85%	1.05%	0.65%	0.00%	0.26%	1.69%	0.00%	1.92%
Fe	8.98%	10.86%	11.13%	4.38%	5.43%	2.07%	2.88%	8.29%	1.16%	4.71%
Na	0.00%	0.00%	0.00%	0.00%	0.00%	0.00%	0.00%	0.00%	0.00%	1.30%
Ti	1.11%	0.83%	0.85%	0.63%	0.90%	0.76%	0.66%	4.86%	0.50%	0.32%
Others	5.26%	3.56%	4.22%	1.42%	1.66%	0.64%	0.79%	1.98%	0.33%	0.89%
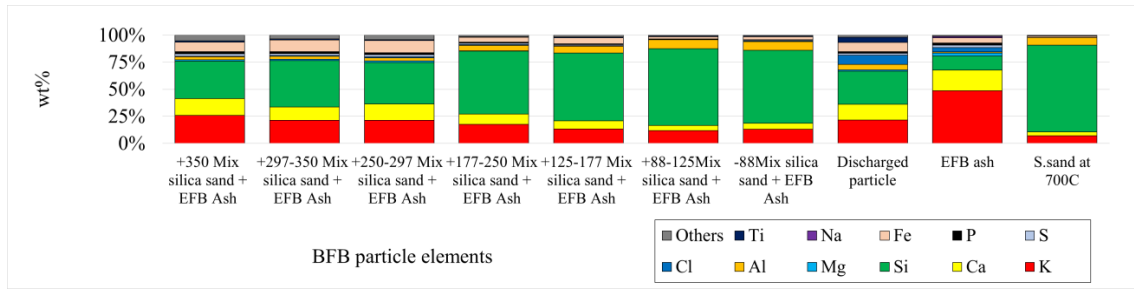
Figure 3-5. Comparison of alkaline and dominant elements in a mixture of silica sand bed particle at 700°C with 1.5U_{mf}, thermal silica sand, and EFB ash

Similar agglomeration also had been carried out based on the second indicator (I_2), from which the number of agglomerates caused by coating outer particles had been formed as well. When compared to agglomeration discussion in operation at 700°C in high fluidization velocity (4.3U_{mf}), then the low velocity produced lower sticky particle with lower accumulated agglomeration mass too. Regarding the measurement of indicators I_3 and I_4, these results were still so small that supported agglomeration state.

Table 3-3 Summary of agglomeration indicator (I_1-I_4) from mixture BFB material with silica sand utilization at 700°C

Indicator agglomeration	Bed residue particles							Discharged particles
	+350μm	+297-350μm	+250-297μm	+177-250μm	+125-177μm	+88-125μm	-88μm	
	$T_{pyrolysis} = 700^oC$							
I_1	4.89	5.15	4.31	5.33	5.28	9.52	6.57	1.83
I_2	3.18	4.20	3.27	7.00	9.38	18.03	13.82	2.94
I_3	0.75	0.50	0.56	0.30	0.21	0.17	0.20	0.71
I_4	0.08	0.06	0.07	0.09	0.10	0.12	0.12	0.17

3.4.2 Agglomeration and defluidization behavior of silica sand particles against EFB ash added at 750°C

The total mass loss resulted from the difference between the total entrained particle (6.55 g) and total discharged particle (1.5 g) was 5.05 g as shown in **Table 3-4**. Based on **Figure 3-6** fluidization condition was still achieved during EFB ash addition with $\overline{\Delta P}$ deviation increment from 35 until 62 Pa.

Table 3-4 Mass balance of thermal BFB treatment involving silica sand at 750°C, 1.5 U$_{mf}$

Parameter	Value
Bed residue particle	
1. Silica sand input mass (m$_{1.1}$)	65.09 g
2. Total ash EFB addition mass (m$_{1.2}$)	4.53 g
3. Total cellulose capsule mass (m$_{1.3}$)	3.35 g
4. Total accumulated bed particle (m$_{1.4}$= m$_{1.1}$+m$_{1.2}$+m$_{1.3}$)	72.97 g
5. Total bed particle mass after operation (m$_{1.5}$)	66.42 g
5.1. +350µm particle size	1.39 g
5.2. +297-350µm particle size	0.19 g
5.3. +250-297µm particle size	0.09 g
5.4. +177-250µm particle size	2.22 g
5.5. +125-177µm particle size	2.70 g
5.6. +88-125µm particle size	35.75 g
5.7. -88µm particle size	24.09 g
6. Total emitted bed particle mass (m$_{1.6}$ = m$_{1.5}$-m$_{1.4}$)	6.55 g
Discharged particle	
1. Discharge line before operation (m$_{2.1}$)	699.60 g
2. Discharge line after operation (m$_{2.2}$)	701.10 g
3. Total discharged filter particle mass (m$_{2.3}$=m$_{2.2}$-m$_{2.1}$)	1.50 g
Total mass loss	
The difference of entrained bed and discharged particle mass (m$_{loss}$=m$_{1.6}$-m$_{2.3}$)	5.05 g

The movement of $\overline{\Delta P}$ was still running normally, even though several decrements of $\overline{\Delta P}$ were taking place which indicated some agglomerates shapes had been formed.

Fig. 3-6 Agglomeration and defluidization analysis on silica sand at 750°C, 1.5 U$_{mf}$

However, those agglomerated particles were still eroded in that fluidization state. Normal fluidization condition could be seen in that curve from which the $\overline{\Delta P}$ kept increasing from the beginning (322 Pa) until the last of ash addition (368 Pa).

U_{mf} analysis showed that the sintering phenomenon at 750°C had been formed in a small amount, and some incomplete channeling formations also had been formed in the range adjusted velocity from 0-0.018 m/s for several conditions after starting operation. The U_{mf} values in **Figure 3-7** started from condition after heating up at 750°C, after 0.25 g for 5 times, and 0.5 g for 5 times were 0.0154, 0.0127, 0.045 and 0.0107 m/s. While U_{mf} measurement on 0.025 g for 10 times and 0.05 g for 10 times could not be determined that was caused by incomplete channeling formation. The measurement with velocity adjustment was carried out to determine U_{sc}. The minimum velocity to shatter the channeling was 0.010 and 0.011 m/s for 0.025 and 0.05 g for 10 times, respectively. Application of lower velocity made the alkali-silicate reaction might be not formed completely, so incomplete channeling would be easier to be degraded into original size again by adjusted velocity. Therefore, the bed particle reverted to fluidize again and reached similar even faster to reach the U_{mf} caused by high temperature than U_{mf} at normal temperature. The phenomena were shown in the curve for U_{mf} measurement after addition 0.25 g for 5 times, 0.5 g for 5 times of ashes, and after cooling down.
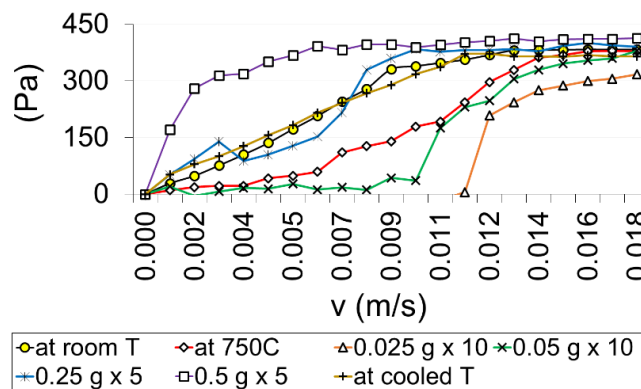
Fig. 3-7 Channelling formation behaviors of silica sand bed particle before and after treatment at 750°C

In **Figure 3-8**, there was a similar appearance with treatment condition at 700°C, in which some encapsulated ashes could not degrade completely in fluidization state with

low velocity. However, those particles could be degraded when bed residue particles after being taken out and then sieved by mechanical sieving.

(Bed residue). (Discharged particle). (+350μm).
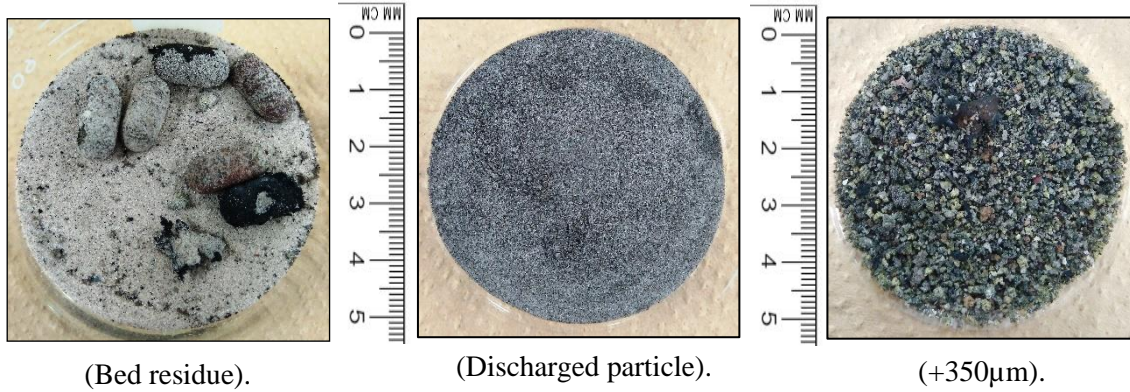
Figure 3-8. Silica sand bed residue, discharged particles, and sieved bed residue at T= 750°C, 1.5 U$_{mf}$

The phenomenon showed that big particles had a low sticky level to maintain that initial agglomerate shapes. Total +350μm particle size mass at 750°C was higher than 700°C as shown in **Table 3-4**, but bed residue was the same that mainly dominated by +88-125 μm and -88 μm.

Table 3-5 Composition of wt.% mixture of silica sand materials based on XRF measurement under treatment and ashing processes temperature at 750°C

Elements	Bed residue particles							Discharged particles	Silica sand	EFB ash
	+350μm	+297-350μm	+250-297μm	+177-250μm	+125-177μm	+88-125μm	-88μm			
	T =750°C									T = 700°C
K	35.14%	29.97%	28.36%	16.12%	15.41%	11.04%	12.95%	11.51%	6.59%	48.64%
Ca	17.71%	14.50%	13.97%	8.80%	7.92%	4.62%	4.91%	9.76%	3.28%	18.95%
Si	24.06%	27.52%	32.79%	57.13%	60.61%	72.22%	69.26%	55.21%	81.80%	13.26%
Mg	1.54%	1.41%	1.16%	0.00%	0.00%	0.00%	0.00%	0.68%	0.00%	2.56%
Al	1.23%	2.29%	2.34%	5.28%	6.20%	8.67%	8.13%	6.97%	6.34%	1.17%
Cl	1.35%	1.57%	1.32%	0.67%	0.54%	0.16%	0.44%	3.89%	0.00%	3.99%
S	1.83%	1.74%	1.88%	1.42%	1.08%	0.33%	0.41%	1.31%	0.21%	2.29%
P	1.83%	1.68%	1.65%	0.87%	0.68%	0.00%	0.13%	1.61%	0.00%	1.92%
Fe	10.68%	12.97%	11.24%	5.99%	4.64%	1.64%	2.05%	5.61%	0.98%	4.71%
Na	0.00%	0.00%	0.00%	0.00%	0.00%	0.00%	0.00%	0.00%	0.00%	1.30%
Ti	0.87%	0.91%	0.75%	1.02%	1.18%	0.76%	1.11%	2.15%	0.37%	0.32%
Others	3.78%	5.46%	4.55%	2.70%	1.74%	0.56%	0.63%	1.31%	0.43%	0.89%

According to agglomeration measurement based on XRF measurement data in **Table 3-5** and **Figure 3-9**, some sticky agglomerates from indicator (I$_1$) had been formed whose value was higher than 700°C in low velocity, but lower than treatment with the typical velocity at the same temperature.
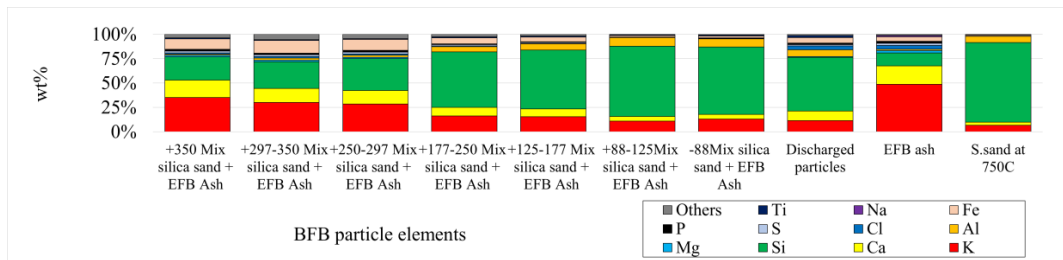
Figure 3-9. Comparison of alkaline and dominant elements in a mixture of silica sand bed particles at 750°C, thermal silica sand, and EFB ash

Outer coating formation as a non-sticky layer was formed and adhere together with sticky layer to form a bigger size according to those results in indicator (I_2). Meanwhile, the alkali melting process based on indicator (I_3) had been formed during that treatment supporting to achieve another typical agglomerate which had been formed in +350 and +297-350µm bed residue particle size. Indicator (I_4) resulted in a small amount which might predict that the agglomeration had been formed in bed material too.

Table 3-6 Summary of agglomeration indicator (I_1-I_4) from a mixture of BFB material with silica sand utilization at 750°C

Indicator agglomeration	Bed residue particles							Discharged particles
	+350µm	+297-350µm	+250-297µm	+177-250µm	+125-177µm	+88-125µm	-88µm	
	$T_{pyrolysis}$ = 750°C							
I_1	7.00	5.95	5.59	4.61	5.68	13.44	10.36	1.77
I_2	2.81	3.27	3.64	7.57	8.84	18.04	16.32	5.54
I_3	1.46	1.09	0.86	0.28	0.25	0.15	0.19	0.21
I_4	0.05	0.08	0.07	0.09	0.10	0.12	0.12	0.13

3.4.3 Agglomeration and defluidization behavior of silica sand particles against EFB ash added at 800°C

Thermal treatment at 800°C had produced bed particles with a total mass of 67.20 g. As shown in **Table 3-7**, there were 5.65 g and 0.5 g of entrained bed and discharged particles with total mass loss was 5.15 g. Total mass loss at 800°C was not different from thermal treatment at below temperature, from which the mass loss mainly came from the degradation of cellulose capsule.

Table. 3-7 Mass balance of thermal BFB treatment involving silica sand utilization at 800°C, 1.5 U_{mf}

Parameter	Value
Bed residue particle	
1. Silica sand input mass ($m_{1.1}$)	65.09 g
2. Total EFB ash addition mass ($m_{1.2}$)	4.52 g
3. Total cellulose capsule mass ($m_{1.3}$)	3.24 g
4. Total accumulated bed particle ($m_{1.4}= m_{1.1}+m_{1.2}+m_{1.3}$)	72.85 g
5. Total bed particle mass after operation ($m_{1.5}$)	67.20 g
5.1. +350µm particle size	3.12 g
5.2. +297-350µm particle size	0.99 g
5.3. +250-297µm particle size	0.31 g
5.4. +177-250µm particle size	5.98 g
5.5. +125-177µm particle size	20.26 g
5.6. +88-125µm particle size	34.57 g
5.7. -88µm particle size	1.96 g
6. Total emitted bed particle mass ($m_{1.6} = m_{1.5}-m_{1.4}$)	5.65 g
Sintering Filter	
1. Discharge line before operation ($m_{2.1}$)	699.80 g
2. Discharge line after operation ($m_{2.2}$)	700.30 g
3. Total discharged filter particle mass ($m_{2.3}=m_{2.2}-m_{2.1}$)	0.50 g
Total mass loss	
The difference of entrained bed and discharged partcle mass ($m_{loss}=m_{1.6}-m_{2.3}$)	5.15 g

Analysis of fluidization perform in **Figure 3-10** showed that the normal fluidization was taking place from initial fluidization with $\overline{\Delta P}$ deviation = 38 Pa, $\overline{\Delta P}$ = 142 Pa until 0.04 wt.% ash had been fed into the BFB system, and after that, the agglomeration formation was started. During agglomeration state, bed particle returned to be fluidized again for several times after 0.7 wt.% ash addition with $\overline{\Delta P}$ deviation =32 Pa, $\overline{\Delta P}$ = 283 Pa. However, gradual agglomerates had been formed again in a stable state leading to achieve a defluidization state when $\overline{\Delta P}$ =20 Pa, $\overline{\Delta P}$ = 3 Pa after 3.87 wt.% of EFB ashes addition.
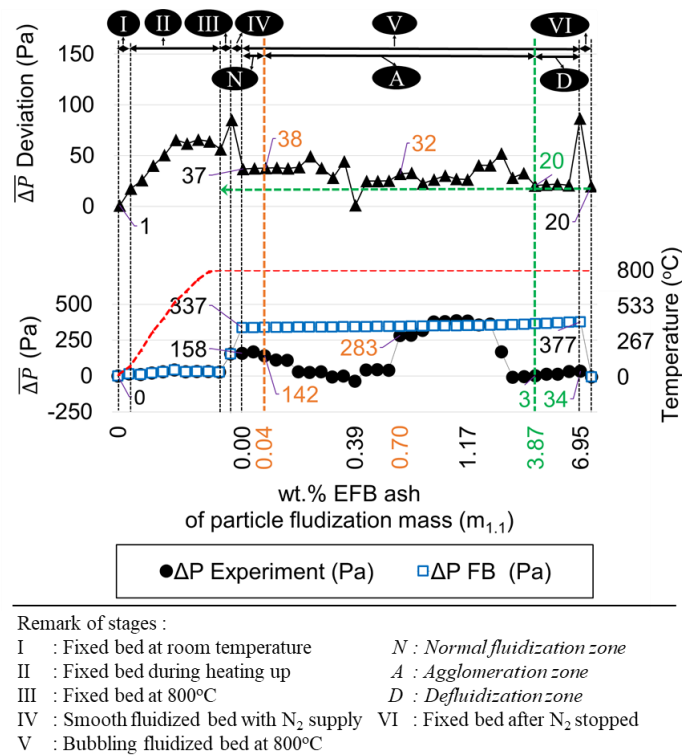
Figure 3-10. Agglomeration and defluidization analysis on silica sand at 800°C, 1.5 U_{mf}

Analysis U_{mf} shown in **Figure 3-11** showed fluidization performance started decreasing until reaching smooth fluidization state in which fluidization state almost stopped after EFB ash several mass additions, namely 0.025 and 0.05 g.
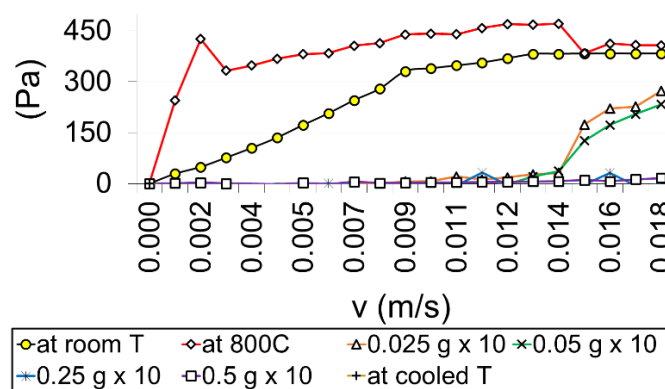
Figure 3-11. Channeling formation behaviors of silica sand bed particle before and after treatment at 800°C

Additions of ashes with higher mass were 0.025 and 0.05 g made the defluidization state achieved. The U_{mf} of bed particle which ran in the normal state was only achieved in condition after heating process up to 800°C of 0.0015 m/s. The U_{ms} was only can be measured on an incomplete channeling state, namely after 0.025 g for 10 times and 0.05 g for 10 times too. While the Ums after interval 0.25 and 0.5 g, and after cooling down could not be determined caused by the complete channeling as described in **Figure 3.1** for No.5 had been formed.

(Before taking out).   (Bed residue).   (Discharged particle).   (+350µm)
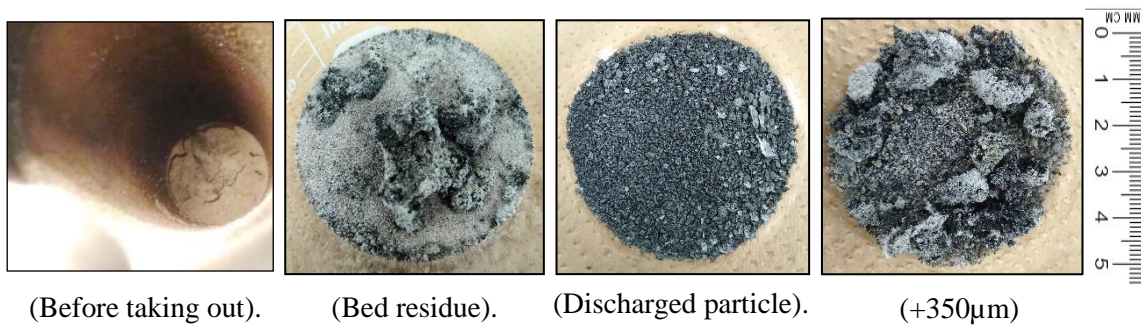
Figure 3-12. Silica sand bed residue before and after taking out, discharged particles, and sieved bed residue particles at T= 800°C, 1.5 U_{mf}

Bed residue condition after thermal treatment could be seen in **Figure 3-12**. In which the bulk agglomerates had been formed covering all of cross bed area (a).1. Similar conditions were shown in figure (a).2 and figure (c), in which the lump agglomerates had been formed. Total +350µm bed particle had been much formed with the amount of 3.12 g when compared to the temperature at 700 and 750°C, while bed material was dominated by +125-177 and +88-125 µm bed particles.

Mechanism of agglomeration formation based on XRF data in **Table 3-8** and **Figure 3-13** showed that the sticky agglomerates had been formed according to prediction with the indicator (I_1) in **Table 3-9**. Furthermore, a lot of coating formation according to the prediction of indicator (I_2) had built up bulk agglomerates. However, there was a difference of strength agglomeration level in high and low velocity at the same temperature, from which the lower velocity would result in lower strength agglomeration than agglomeration resulted from the typical superficial velocity.

Table 3-8 Composition of wt.% mixture of silica sand materials based on XRF measurement under treatment and ashing processes temperature at 800°C

Elements	Bed residue particles							Discharged particles	Silica sand	EFB ash
	+350μm	+297-350μm	+250-297μm	+177-250μm	+125-177μm	+88-125μm	-88μm			
	T =800°C									T = 700°C
K	20.16%	12.85%	11.21%	9.24%	10.98%	9.89%	12.59%	20.23%	6.84%	48.64%
Ca	8.44%	7.71%	6.80%	6.22%	4.90%	4.39%	5.99%	12.72%	3.42%	18.95%
Si	52.36%	64.16%	68.15%	73.51%	71.42%	74.43%	65.71%	24.25%	80.94%	13.26%
Mg	0.56%	0.00%	0.00%	0.00%	0.00%	0.00%	0.00%	1.24%	0.00%	2.56%
Al	4.52%	5.57%	5.57%	6.26%	8.32%	7.62%	8.86%	4.21%	6.71%	1.17%
Cl	0.74%	0.00%	0.27%	0.51%	0.43%	0.41%	1.22%	15.18%	0.00%	3.99%
S	1.65%	0.69%	0.68%	0.41%	0.34%	0.25%	0.50%	1.27%	0.30%	2.29%
P	1.18%	0.93%	0.70%	0.31%	0.14%	0.00%	0.46%	1.73%	0.00%	1.92%
Fe	7.72%	6.05%	4.60%	2.41%	1.79%	1.53%	2.61%	8.93%	1.07%	4.71%
Na	0.00%	0.00%	0.00%	0.00%	0.00%	0.00%	0.00%	4.75%	0.00%	1.30%
Ti	1.17%	1.05%	1.21%	0.64%	1.20%	1.04%	1.48%	3.56%	0.45%	0.32%
Others	1.51%	0.99%	0.83%	0.50%	0.47%	0.45%	0.57%	1.93%	0.26%	0.89%
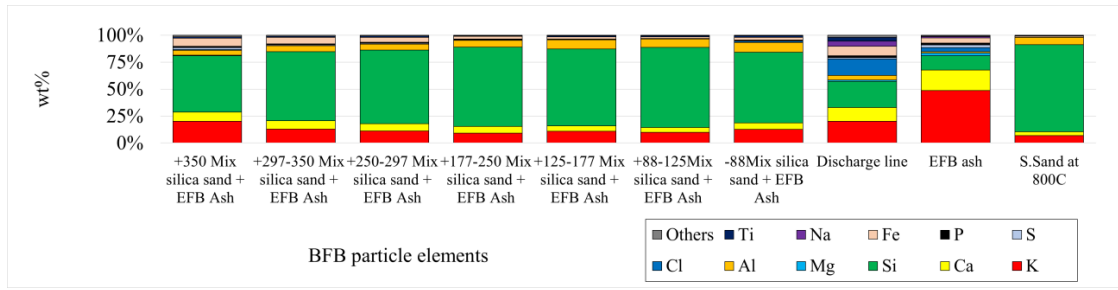
Figure 3-13. Comparison of alkaline and dominant elements in a mixture of silica sand at 800°C, thermal silica sand, and EFB ash

While prediction of agglomeration formation based on measurement of indicator (I_3) was not formed. Prediction of (I_4) showed that the potency to avoid agglomeration was insignificant.

Table 3-9 Summary of agglomeration indicator (I_1-I_4) from a mixture of BFB material with silica sand utilization at 800°C

Indicator agglomeration	Bed residue particles							Discharged particles
	+350μm	+297-350μm	+250-297μm	+177-250μm	+125-177μm	+88-125μm	-88μm	
	$T_{pyrolysis}$ = 800°C							
I_1	5.00	9.37	6.90	6.94	9.89	10.99	5.68	1.41
I_2	7.12	8.91	10.59	12.67	16.33	19.23	12.13	3.14
I_3	0.39	0.20	0.16	0.13	0.15	0.13	0.19	0.83
I_4	0.09	0.09	0.08	0.09	0.12	0.10	0.13	0.17

3.4.4 Agglomeration and defluidization behavior of bentonite particles against EFB ash added at 700ºC

The study of agglomeration involving utilization of bentonite was shown in **Table 3-10**, the total of bed particles after the operation was 62.35 g. There were 10.65 g entrained particles from the bed, and 1 g accumulated fine particle in the discharge line. So, the total amount of mass loss during the operation was 9.56 g.

Table 3-10 Mass balance of thermal BFB treatment involving bentonite at 700ºC, 1.5 U_{mf}

	Parameter	Value
	Bed residue particle	
1.	1. Bentonite input mass ($m_{1.1}$)	65.10 g
	2. Total EFB ash addition mass ($m_{1.2}$)	4.53 g
	3. Total cellulose capsule mass ($m_{1.3}$)	3.28 g
	4. Total accumulated bed particle ($m_{1.4}= m_{1.1}+m_{1.2}+m_{1.3}$)	72.91 g
	5. Total bed particle mass after operation ($m_{1.5}$)	62.35 g
	5.1. +350µm particle size	1.74 g
	5.2. +297-350µm particle size	0.27 g
	5.3. +250-297µm particle size	0.38 g
	5.4. +177-250µm particle size	0.12 g
	5.5. +125-177µm particle size	34.92 g
	5.6. +88-125µm particle size	24.23 g
	5.7. -88µm particle size	0.69 g
	6. Total emitted bed particle mass ($m_{1.6} = m_{1.5}-m_{1.4}$)	10.56 g
	Discharged particle	
2.	1. Discharge line before operation ($m_{2.1}$)	699.60 g
	2. Discharge line after operation ($m_{2.2}$)	700.60 g
	3. Total discharged filter particle mass ($m_{2.3}=m_{2.2}-m_{2.1}$)	1.00 g
	Total mass loss	
	The difference of entrained bed and discharged particle mass ($m_{loss}=m_{1.6}-m_{2.3}$)	9.56 g

The fluidization was running in normal condition at temperature 700ºC. However, the difference of $\overline{\Delta P}$ between experimental and theoretical measurement was caused by a reduced amount of moisture in bentonite mass during heating up stage (II), in **Figure 3-14**. $\overline{\Delta P}$ deviation showed that particle fluctuation kept running normally from 45 until 42 Pa which meant the fluidization behavior was still good.

Figure 3-14. Agglomeration and defluidization analysis on bentonite at 700°C, 1.5 U_{mf}

U_{mf} measurement in **Figure 3-15** showed that the fluidization state was still achieved in all of the measurements started from after heating at 700°C until after cooling treatment with similar U_{mf} values were 0.016, 0.002, 0.011, 0.012, 0.011, and 0.014 m/s respectively.
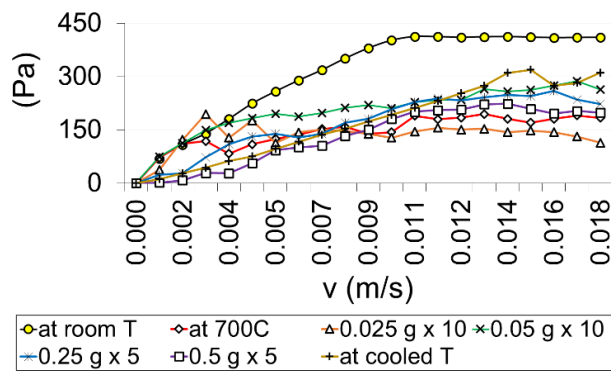
Figure 3-15 Channelling formation behaviors of bentonite bed particle before and after treatment at 700°C

The real condition of bed residue in **Figure 3-16** showed that the interaction between ash and bentonite particles was not reacted completely. The small number of unmixed agglomerates might be caused by the low-velocity application, making particles' contact small.

(Bed residue).   (Discharged particle).   (+350 µm).
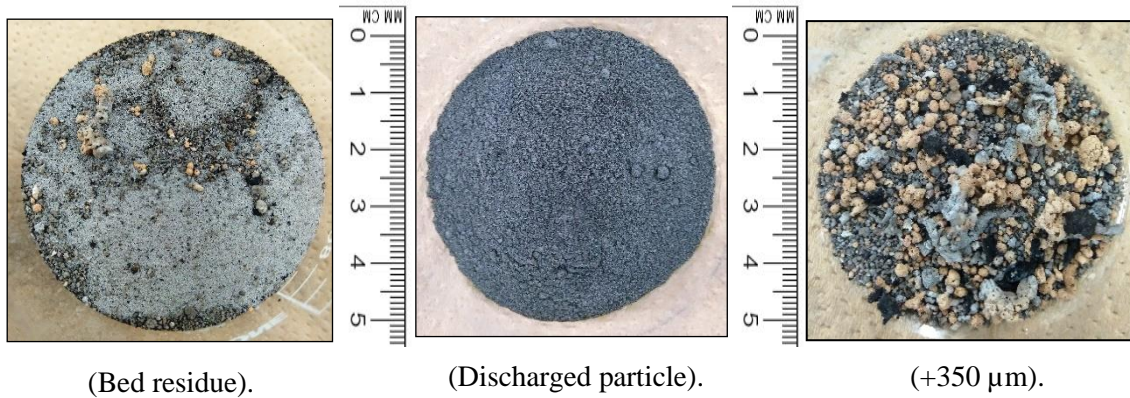
Figure 3-16. Bentonite bed residue, discharged, and sieved bed residue at T= 700°C, 1.5 U$_{mf}$

XRF measurement showed that alkaline content in mixture bentonite was lower than mixture silica sand in bed residue particle at the same condition. It caused the sticky agglomeration (I$_1$) was only formed in a small amount.

Table 3-11 Composition of wt.% mixture of bentonite materials based on XRF measurement under treatment and ashing processes temperature at 700°C

Elements	Bed residue particles							Discharged particle	Bentonite	EFB ash
	+350µm	+297-350µm	+250-297µm	+177-250µm	+125-177µm	+88-125µm	-88µm			
	T =700°C									T = 700°C
K	11.19%	9.13%	7.01%	8.63%	7.34%	7.30%	8.61%	13.59%	1.57%	48.64%
Ca	18.35%	20.56%	18.03%	23.36%	4.59%	4.76%	7.12%	22.37%	3.86%	18.95%
Si	42.46%	38.08%	45.71%	37.04%	65.84%	65.58%	60.16%	32.44%	71.51%	13.26%
Mg	2.80%	2.84%	2.95%	2.91%	2.28%	2.29%	2.39%	3.22%	2.35%	2.56%
Al	3.35%	3.15%	6.09%	2.68%	10.26%	10.28%	9.29%	4.45%	11.25%	1.17%
Cl	1.28%	1.51%	1.29%	1.75%	0.55%	0.53%	1.25%	4.58%	0.05%	3.99%
S	1.55%	1.60%	1.39%	1.52%	0.54%	0.59%	1.04%	2.26%	1.35%	2.29%
P	3.30%	3.19%	2.58%	3.61%	0.31%	0.32%	0.91%	2.86%	0.00%	1.92%
Fe	13.26%	15.31%	12.37%	14.78%	6.81%	6.85%	7.42%	10.33%	6.94%	4.71%
Na	0.00%	0.00%	0.00%	0.00%	0.00%	0.00%	0.00%	0.00%	0.00%	1.30%
Ti	0.61%	0.65%	1.04%	0.78%	0.91%	0.95%	1.12%	2.47%	0.60%	0.32%
Others	1.84%	3.98%	1.56%	2.93%	0.57%	0.55%	0.70%	1.42%	0.51%	0.89%

Figure 3-17. Comparison of alkaline and dominant elements in a mixture of bentonite at 700°C, thermal bentonite, and EFB ash

The coating process was only formed in a small amount too. Meanwhile, prediction of agglomeration formation based on indicators (I_3) and (I_4) was not much contributed to maintaining fluidization state.

Table 3-12 Summary of agglomeration indicator (I_1-I_4) from mixture BFB material with bentonite utilization at 700°C

Indicator agglomeration	Mixture particles							Discharged particle
	+350μm	+297-350μm	+250-297μm	+177-250μm	+125-177μm	+88-125μm	-88μm	
	$T_{pyrolysis} = 700^{o}C$							
I_1	2.56	1.94	1.72	1.80	4.50	4.28	2.59	1.49
I_2	2.19	1.78	2.24	1.53	10.20	9.88	6.60	1.62
I_3	0.26	0.24	0.15	0.23	0.11	0.11	0.14	0.42
I_4	0.08	0.08	0.13	0.07	0.16	0.16	0.15	0.14

3.4.5 Agglomeration and defluidization behavior of bentonite particles against EFB ash added at 750°C

Mass balance measurement in **Table 3-13** showed that 10.92 g fine particles were leaving the bed chamber into the discharge line. The total accumulated particles in the discharge line were 0.2 g, while the difference values between both masses were 10.72 g as total mass loss during thermal treatment at 750°C which might be dominated by cellulose capsules and evaporated moisture.

Analysis of agglomeration and defluidization in **Figure 3-18** showed that fluidization in stage (V) was running in a normal state until EFB ash addition was 0.39wt%. In that condition, $\overline{\Delta P}$ deviation increased from 31 until 43 Pa.

Table 3-13 Mass balance of thermal BFB treatment involving bentonite at 750°C, 1.5 U_{mf}

Parameter	Value
Bed residue particle	
1. Bentonite input mass ($m_{1.1}$)	65.08 g
2. Total EFB ash addition mass ($m_{1.2}$)	4.53 g
3. Total cellulose capsule mass ($m_{1.3}$)	3.33 g
4. Total accumulated bed particle ($m_{1.4} = m_{1.1} + m_{1.2} + m_{1.3}$)	72.94 g
5. Total bed particle mass after pyrolysis ($m_{1.5}$)	62.02 g
5.1. +350µm particle size	0.76 g
5.2. +297-350µm particle size	0.20 g
5.3. +250-297µm particle size	0.02 g
5.4. +177-250µm particle size	0.57 g
5.5. +125-177µm particle size	1.78 g
5.6. +88-125µm particle size	53.09 g
5.7. -88µm particle size	5.60 g
6. Total emitted bed particle mass ($m_{1.6} = m_{1.5} - m_{1.4}$)	10.92 g
Discharge particle	
1. Discharge line before operation ($m_{2.1}$)	700.40 g
2. Discharge line after operation ($m_{2.2}$)	700.60 g
3. Total discharged filter particle mass ($m_{2.3} = m_{2.2} - m_{2.1}$)	0.20 g
Total mass loss	
The difference of entrained bed and discharged particle mass ($m_{loss} = m_{1.6} - m_{2.3}$)	10.72 g

The agglomeration state was formed with stable deviation at 43-46 Pa and $\overline{\Delta P}$ fluctuation from 185 to 196 Pa. However, during feeding ashes, there were agglomerates formation making fluidization stopped but could return to be fluidized again for several times after that.
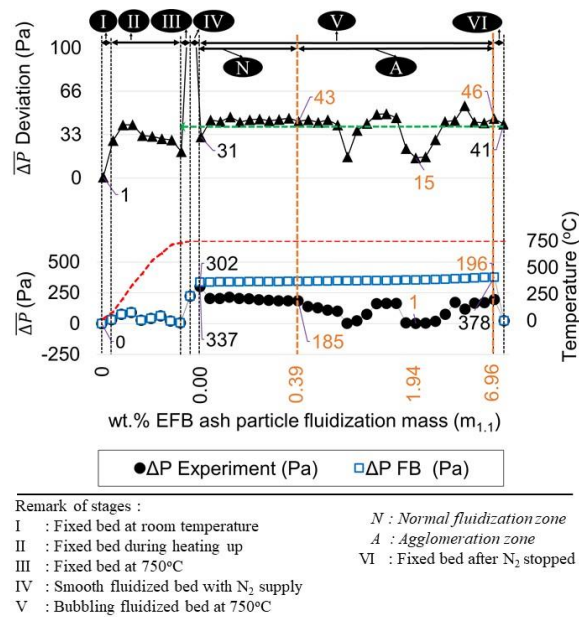
Figure 3-18. Agglomeration and defluidization analysis on bentonite at 750°C, 1.5 U_{mf}

That condition was closely relevant to velocity measurement results started from the condition after heating treatment until cooling treatment as shown in **Figure 3-19**. The result of U_{mf} measurement could not be determined, but the U_{ms} for the condition at 800°C and all of the intervals of ashes addition could be measured, as 0.010, 0.011, 0.012, 0.012, 0.008, and 0.005 m/s for the condition after heating at 750°C because of the sintering process, after feeding ashes feeding with interval 0.025, 0.05, 0.25, 0.5 g, and after cooling treatments, respectively.
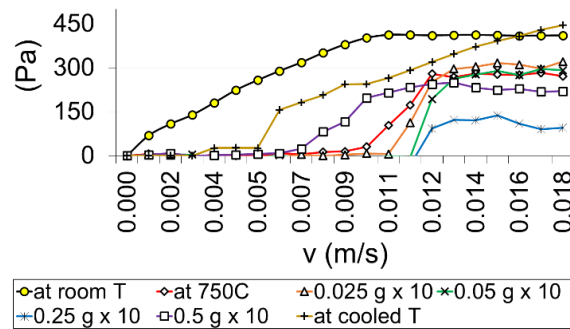
Fig. 3-19 Channelling formation behaviors of bentonite bed particle before and after thermal treatment at 750°C

That phenomenon was caused by the agglomeration effect as shown in **Figure 3-20**, in which that agglomerates made segregation of bed particle caused by the drag force of N_2 stopped until increment at certain velocity enabled the drag force to segregate bed particle again and then bed particle could start to move up and achieve fluidization state.

(Bed residue). (Discharged particle). (+350 μm).
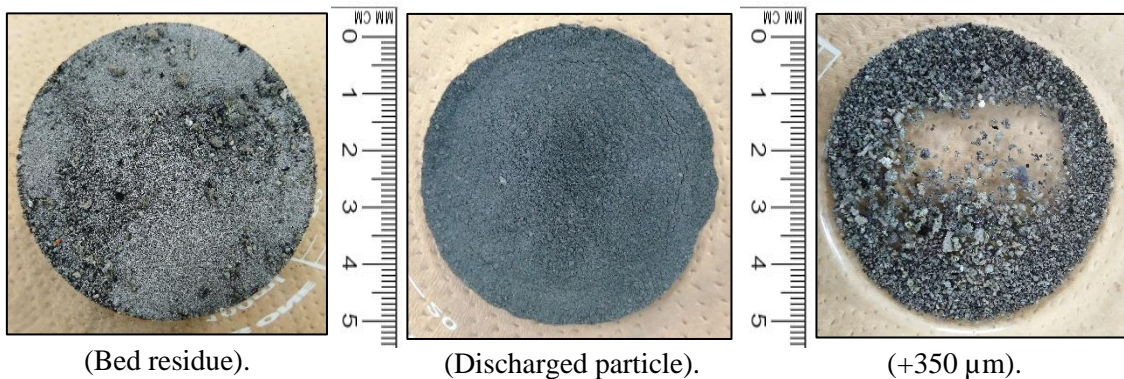
Fig. 3-20 Bentonite bed residue, discharged, and sieved bed residue particles at T= 750°C, 1.5 U_{mf}

Condition of bed residue showed some small agglomerates had been clearly formed in a small amount. The distribution of sieved bed residue showed that the total of +350µm particle size agglomerates was still low. The bed residue particle was dominated by a +88-125µm particle size of 53.09 g.

According to XRF measurement in **Table 3-14** and **Figure 3-21**, predicting of sticky agglomerates by measurement of indicator (I_1) showed sticky agglomerates had been formed in the low amount of big mass (+350µm), even it was lower than condition at temperature 700°C in certain sieved particle size, Table 3-15. The coating process had been formed in a small amount during thermal treatment too.

Table 3-14 Composition of wt.% mixture of bentonite materials based on XRF measurement under treatment and ashing processes temperature at 750°C

Elements	Bed residue particles								Bentonite	EFB ash
	+350µm	+297-350µm	+250-297µm	+177-250µm	+125-177µm	+88-125µm	-88µm	Discharge		
	T =750°C									T = 700°C
K	5.61%	3.37%	4.11%	3.93%	6.11%	7.19%	8.76%	13.12%	1.54%	48.64%
Ca	16.43%	20.43%	16.07%	17.59%	9.19%	4.15%	7.79%	19.84%	4.01%	18.95%
Si	44.62%	39.20%	46.07%	43.73%	60.05%	66.62%	57.60%	33.01%	71.63%	13.26%
Mg	2.40%	3.14%	2.37%	2.90%	2.34%	2.43%	2.70%	2.95%	2.31%	2.56%
Al	1.93%	2.17%	3.47%	4.82%	8.68%	9.93%	8.67%	4.44%	11.30%	1.17%
Cl	0.40%	0.44%	0.44%	0.50%	0.41%	0.27%	1.81%	6.39%	0.00%	3.99%
S	1.50%	1.91%	1.38%	1.51%	0.87%	0.51%	1.24%	1.96%	1.30%	2.29%
P	3.64%	3.90%	2.94%	2.91%	1.21%	0.21%	1.45%	2.57%	0.00%	1.92%
Fe	20.01%	22.00%	17.86%	17.97%	9.35%	7.16%	8.13%	11.48%	6.83%	4.71%
Na	0.00%	0.00%	0.00%	0.00%	0.00%	0.00%	0.00%	0.00%	0.00%	1.30%
Ti	0.83%	0.94%	0.78%	0.92%	0.93%	0.96%	1.09%	2.02%	0.61%	0.32%
Others	2.63%	2.51%	4.52%	3.23%	0.86%	0.58%	0.75%	2.22%	0.46%	0.89%

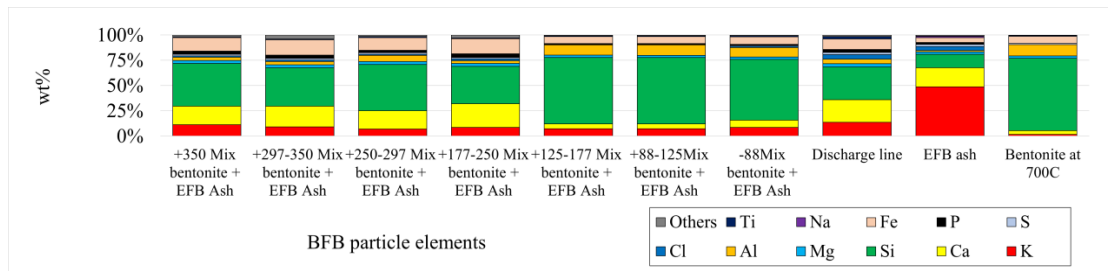**Figure 3-21.** Comparison of alkaline and dominant elements in a mixture of bentonite at 750°C, thermal bentonite, and EFB ash

Meanwhile, agglomeration prediction caused by indicators (I_3) and (I_4) was insignificant. It made these supports to maintain fluidization was low too. Analysis at temperature 700 and until 750°C showed that the application of bentonite was still ideal to maintain fluidization with low-velocity intensity.

Table 3-15 Summary of agglomeration indicator (I_1-I_4) from a mixture of BFB material with bentonite utilization at 750°C

Indicator agglomeration	Bed residue particles							Discharged particles
	+350μm	+297-350μm	+250-297μm	+177-250μm	+125-177μm	+88-125μm	-88μm	
	$T_{pyrolysis}$ = 750°C							
I_1	1.65	0.79	1.29	1.12	2.84	5.60	2.04	1.27
I_2	2.24	1.55	2.35	2.04	5.19	10.88	5.56	1.82
I_3	0.13	0.09	0.09	0.09	0.10	0.11	0.15	0.40
I_4	0.04	0.06	0.08	0.11	0.14	0.15	0.15	0.13

3.4.6 Agglomeration and defluidization behavior of bentonite particles against EFB ash added at 800°C

Treatment bentonite at 800°C was started by placing and heating 65.07 gr initial bentonite mass into BFB chamber where alkali silicate reaction after EFB ash addition was started taking place until 61.78 g bed particle had been produced during that reaction. There was 11 g bed particle left bed-chamber towards discharge line and had been accumulated over there with the mass of 0.71 g. Therefore, total mass loss during the operation was 10.9 g as shown in mass balance measurement data, **Table 3-16**.

Table 3-16 Mass balance of thermal BFB treatment involving bentonite at 800°C, 1.5 U_{mf}

	Parameter	Value
Bed residue particle		
	1. Bentonite input mass ($m_{1.1}$)	65.07 g
	2. Total EFB ash addition mass ($m_{1.2}$)	4.53 g
	3. Total cellulose capsule mass ($m_{1.3}$)	3.19 g
	4. Total accumulated bed particle ($m_{1.4}$= $m_{1.1}$+$m_{1.2}$+$m_{1.3}$)	72.78 g
	5. Total bed particle mass after operation ($m_{1.5}$)	61.78 g
1.	5.1. +350μm particle size	2.43 g
	5.2. +297-350μm particle size	0.20 g
	5.3. +250-297μm particle size	0.05 g
	5.4. +177-250μm particle size	0.71 g
	5.5. +125-177μm particle size	3.76 g
	5.6. +88-125μm particle size	48.56 g
	5.7. -88μm particle size	6.08 g
	6. Total emitted bed particle mass ($m_{1.6}$ = $m_{1.5}$-$m_{1.4}$)	11.00 g
Discharged particle		
	1. Discharged line before operation ($m_{2.1}$)	700.00 g
2.	2. Discharge line after operation ($m_{2.2}$)	700.10 g
	3. Total discharged filter particle mass ($m_{2.3}$=$m_{2.2}$-$m_{2.1}$)	0.10 g
Total mass loss		
	The difference of entrained bed particle and discharged particle mass (m_{loss}=$m_{1.6}$-$m_{2.3}$)	10.90 g

Analysis of agglomeration according to the discussion in **Figure 3-22** showed fluidization was running normally from $\overline{\Delta P}$ deviation was 82 Pa until 81 Pa and $\overline{\Delta P}$ fluctuation was from 208 until 204 Pa after the first addition of ash was 0.04wt%. The agglomeration state had started to be formed, then, according to significant decrement, $\overline{\Delta P}$ deviation was 25 Pa and $\overline{\Delta P}$ fluctuation was 32 Pa. In that state, small until lump agglomerates might be built up and smooth fluidization condition was taken place. After that, the 0.46 wt.% addition had stopped the fluidization. It was shown by $\overline{\Delta P}$ deviation movement which was permanently stopped at 26 Pa and $\overline{\Delta P}$ fluctuation which had been permanently stopped at 37 Pa.
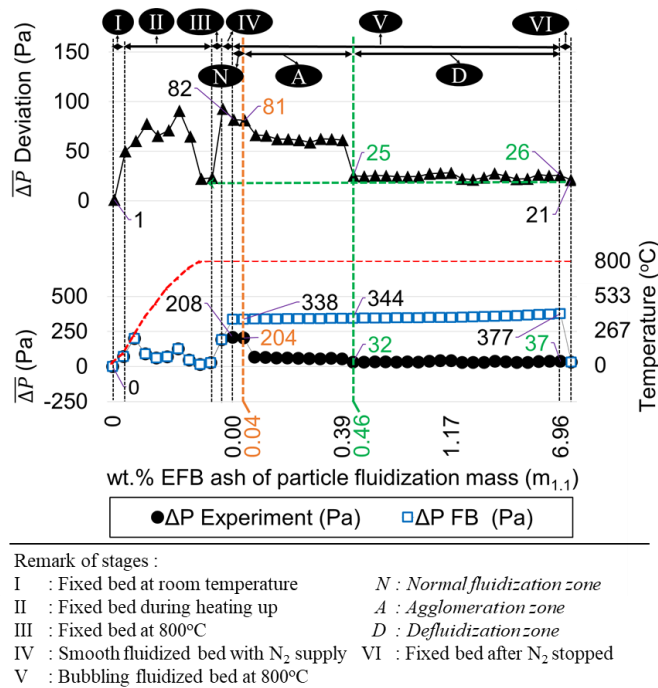
Figure 3-22. Agglomeration and defluidization analysis on bentonite at 800°C, 1.5 U$_{mf}$

That defluidization mechanism was relevant to channeling analysis for several stages, as shown in **Figure 3-23** curve. Thermal treatment at 800°C had high potency to create agglomeration phase even in the low-velocity intensity of fluidization condition which only involved pure bentonite as bed particle. At 800°C, the bentonite was easier to sinter and form solid and strength agglomerates and channeling than treatment at 750°C. Therefore, during initial heating up treatment, that process should be followed by a fluidization treatment to avoid sintered particles causing agglomeration. Meanwhile, the

U_{mf} could not be achieved over velocity adjustment because large and sticky agglomerates leading to reach extensive channeling formation had been formed. Therefore, U_{mf} measurement was not achieved during adjusted velocity from 0 - 0.018 m/s. U_{sc} measurement showed that the shattering of incomplete channeling was only formed on condition after heating treatment at 800°C, namely 0.008 m/s.
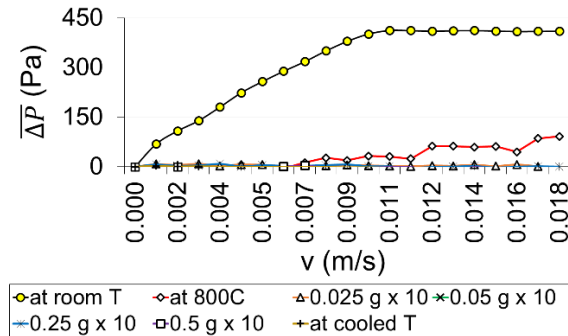
Figure 3-23 Channelling formation behaviors of bentonite bed material before and after thermal treatment at 800°C

When compared to the study by using typical velocity intensity (4.3 U_{mf}), then potential sintering was low and potency agglomeration caused by sintering was insignificant.

(a). Before taking out   (b). Bed residue   (c). Discharged particle).   (d). +350 µm.
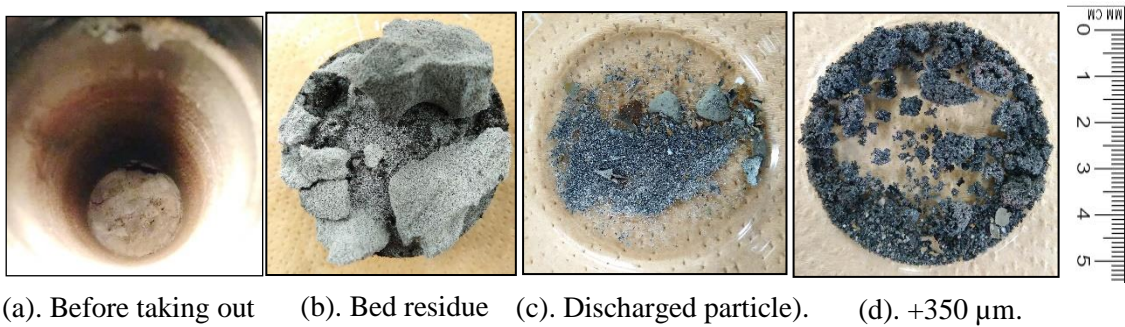
Figure 3-24. Bentonite bed residue before and after taking out, discharged particles, and sieved bed residue particles at T=800°C, 1.5 U_{mf}

The real condition of defluidization could be seen in **Figure 3-24**, in which extensive bulk agglomeration had been formed as shown in (a). Lump agglomerates had

been obtained after taking out bed residue as shown in (b), discharged particle in (c), and (d) was for the appearance of the biggest of sieved bed particle (+350µm).

Table 3-17 Composition of wt.% mixture bentonite materials based on XRF measurement under treatment and ashing processes temperature at 800°C

Elements	Bed residue particles							Discharged particles	Bentonite	EFB ash
	+350µm	+297-350µm	+250-297µm	+177-250µm	+125-177µm	+88-125µm	-88µm			
	T =800°C									T = 700°C
K	24.06%	18.60%	17.74%	11.47%	4.64%	5.16%	6.56%	9.85%	1.34%	48.64%
Ca	13.02%	15.21%	11.18%	10.51%	5.08%	4.21%	5.26%	5.68%	3.82%	18.95%
Si	37.21%	33.36%	40.74%	45.41%	66.41%	68.33%	63.92%	52.24%	72.64%	13.26%
Mg	1.73%	2.16%	1.92%	2.20%	2.28%	2.29%	2.35%	2.04%	2.38%	2.56%
Al	3.18%	3.45%	4.06%	6.80%	9.86%	10.27%	9.58%	7.99%	11.44%	1.17%
Cl	1.93%	0.67%	0.53%	0.59%	0.23%	0.36%	1.04%	10.06%	0.00%	3.99%
S	1.89%	2.31%	2.26%	1.80%	0.53%	0.42%	0.75%	1.04%	0.70%	2.29%
P	2.01%	2.23%	1.73%	1.37%	0.38%	0.00%	0.68%	0.61%	6.62%	1.92%
Fe	11.67%	14.67%	14.01%	12.52%	8.64%	7.44%	7.87%	8.72%	0.00%	4.71%
Na	0.00%	0.00%	0.00%	0.00%	0.00%	0.00%	0.00%	0.00%	0.56%	1.30%
Ti	1.82%	5.43%	3.67%	6.26%	1.34%	0.89%	1.33%	0.71%	0.00%	0.32%
Others	1.47%	1.92%	2.16%	1.08%	0.61%	0.64%	0.67%	1.06%	0.50%	0.89%

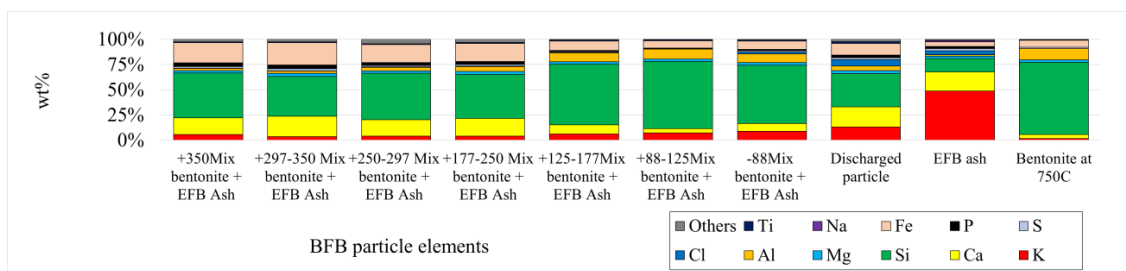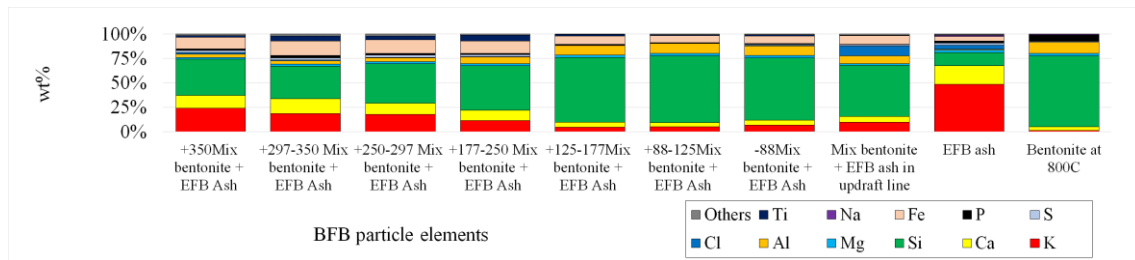**Figure 3-25.** Comparison of alkaline and dominant elements in a mixture of bentonite at 800°C, thermal bentonite, and EFB ash

Prediction of agglomeration based on XRD measurement data in **Table 3-17** and **Figure 3-25** explained that sticky agglomerates formation based on (I_1) and coating process based on (I_2) was mostly higher than treatment of bentonite at 700 and 750°C in the same low-velocity intensity. It showed that utilization of bentonite at low intensity was only possible to be carried out at temperature by 750°C.

Table 3-18 Summary of (I_1-I_4) from a mixture of BFB material with bentonite at 800°C

Indicator agglomeration	Bed residue particles							Discharged particles
	+350µm	+297-350µm	+250-297µm	+177-250µm	+125-177µm	+88-125µm	-88µm	
	$T_{pyrolysis}$ = 800°C							
I_1	4.21	3.52	3.51	2.74	3.57	4.32	2.59	0.81
I_2	3.65	2.65	3.95	4.04	9.17	11.31	8.50	7.46
I_3	0.65	0.56	0.44	0.25	0.07	0.08	0.10	0.19
I_4	0.09	0.10	0.10	0.15	0.15	0.15	0.15	0.15

3.5. Influence of superficial gas velocity on channeling formation behavior

A superficial velocity application, 1.5 U_{mf}, would reduce contact area among bed particles making the alkali-silicate reaction could not run completely. Furthermore, some encapsulated ashes could not disintegrate perfectly and degrade completely which also made a number of fed ashes was not reacted to silica sand or bentonite bed particles. This phenomenon was relevant to the bed residue condition as shown in **Figures 3-4, 3-8,** and **3-16.**

The 1.5 U_{mf} application could form channeling formation easily because during the increasing agglomeration, bed particles would be difficult to fluidize as the normal state but have tendency to attach on the wall and bottom of column. The capability of shattering agglomerates was depended on velocity adjustment. Therefore, the increase of superficial velocity could ease the shattering of chaneling formation. The increment of temperature also significantly increased agglomerates formation stimulating incomplete and complete chanelings that would take place at 750° and 800°C on both mixtures of bed particles as shown in **Figures 3-7, 3-11, 3-19** and **3-23**.

3.6. Agglomeration and defluidization of silica sand and bentonite particles under lower superficial velocity

During treatment at 700°C, fluidization performance in **Figures 3.2** and **3.14** on silica sand and bentonite kept running well over ashes addition, namely 6.96 wt.%. On the treatment at 750°C in **Figure 3.6**, fluidization of silica sand kept running well but agglomeration process had been formed as shown by the decrease of $\overline{\Delta P}$ or the increase of $\overline{\Delta P}$ loss disparity after ashes addition by 0.39 wt.%. Defluidization process at 800°C in **Figure 3.10** and **3.22** had been formed both on silica sand and bentonite which had been initiated by agglomerate formation by 0.04 wt.%. The increase of agglomeration kept continuing until reached defluidization state by 3.87 and 0.46 wt.% for silica sand and bentonite, respectively. The fluidization process on low-velocity application caused the mixing process among bed particles was not formed completely. Some capsules here that supplied ashes could not react completely with bed particles because most of the

alkaline in the ashes could not be volatilized completely, making the fluidization state became stable at treatment 700°C.

Temperature increment at 750°C caused degradation of capsule becoming more complete and resulting in an optimal reaction. It could be seen by incomplete channeling formation both on silica sand and bentonite indicating some higher agglomerates had been formed than treatment at 700°C as shown in **Figure 3.7**. Channeling formation on bentonite, **Figure 3.19**, was higher, but agglomeration structures in bentonite consisted of alkali-alumina silicate compounds was weaker than those of silica sand.

On the treatment at 800°C, complete channeling formation had been formed on bentonite and silica sand particles which showed that a number of large agglomerates had been generated to cover all cross-section areas as shown in **Figure 3.11** and **3.23**. That indicated fluidization of bed particles had stopped. The low-velocity application significantly decreased to degrade formed large agglomerates. It was proven by comparing 4.3 and 1.5 U_{mf} application, from which degradation of alkali-alumina silicate on higher velocity would be easier to reduce the agglomerated size into primary size by the remaining number of alkali silicates that had stronger structure to keep tightening up even though the velocity increased. It caused the structure of the bentonite surface to become weak due to incomplete coating and sintering processes.
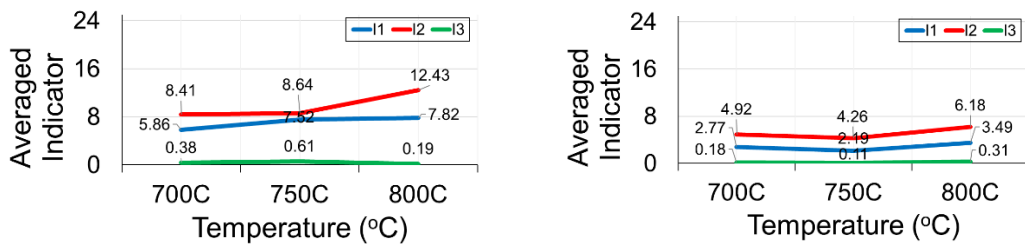
Figure 3-26. Comparison of average indicators values between a mixture of silica sand and bentonite under velocity treatment at 1.5 U_{mf}

Defluidization at 800°C showed that the higher temperature made, the more significant increment on the strength or stickiness level. The indicators of agglomeration measurements on various sieved bed particles as shown in **Tables 3-6, 3-9, 3-12, 3-15, 3-**

18 and in the mixture of bed particles as shown in **Figure 3-26** showed that the silica sand had a higher propensity to form stickier agglomerates. Furthermore, when comparing those indicator values to the results from analysis with $4.3U_{mf}$ superficial velocity application, it showed that the decrease of velocity would decrease the potential of sticky agglomerates formation. It resulted in a stronger agglomeration structure on the $4.3\ U_{mf}$ application.

3.7. Conclusion

Analysis of agglomeration and defluidization formation using silica sand and bentonite as particle fluidization at temperatures $700^{\circ}C$ and $750^{\circ}C$ showed good performance, in which fluidization state was still achieved even though some agglomerates and incomplete channeling states had been formed. However, silica sand gave better performance than bentonite bed particles since fluidization was still running well without significant fluctuation caused by a small number of agglomeration formations during thermal treatment at $750^{\circ}C$. Silica sand also had a higher propensity to maintain fluidization state than bentonite at treatment in temperature $800^{\circ}C$ caused by the change of agglomeration state, so fluidization state could be stable again after 0.70 wt.% of EFB ash addition taken place. Furthermore, the capability of silica sand to inhibit defluidization formation was longer than bentonite, in which the percentage mass of ash on silica sand and bentonite to reach defluidization state were 3.87% and 0.46%, respectively.

CHAPTER IV

Identification of agglomeration mechanism based on reaction and distribution particle pores

4.1 Introduction

4.1.1 Identification of silica sand and clay minerals

Silicon Oxide (SiO_2) is already known well as silica which presence in nature is in crystalline form. Generally, silica sand is used in very high purity for a solar cell application, glassmaking company, and soda-lime glass production (Sabina, *et.al.*, 2016; Valchev, *et.al.*, 2011; Mandaoui, *et.al.*, 2007); as an abrasive in blasting, grinding and polishing material; as hydraulic fracturing material of oil reservoirs; and as a refractory agent in foundry and manufacture of refractory brick (Mc Laws, 1971). Some chemical specifications in silica sand consist of silica (SiO_2), Iron Oxide (Fe_2O_3), Lime (CaO), Magnesia (MgO), Titanium dioxide (TiO_2), and Alumina (Al_2O_3) including heavy minerals. The presence of alumina in the sand should be uniform but not as uniform as in clay. The high alumina affects the particle to melt more difficultly (Bowdish,1967). Silica sand for industry should deal with some properties, such as cleanness, no color, grain size, refractoriness, or durability to withstand at high temperature, shape, and sorting which refers to the range of particle size. Quartz (SiO_2) is the principal constituent of silica sand having high refractory temperature and it will decrease in the alkali-bearing mineral state between 1200-1300°C. Refractoriness is influenced by grain particle size which determines the surface area against heat and fluxing ingredients. Therefore, the increase of fine or small size will be highly affected the durability of refractoriness. Permeability becomes an important factor to determine the capability of gas flow into particle pores. The finer size will be more difficult to be flowed by air than coarse size into particle. Therefore, the larger size will increase the permeability level of silica sand. Silica sand has a high tendency to be reactive at the high casting temperature to form a silica mineral formation. Therefore, silica sand can be developed by lime addition in some applications (Mc Laws, 1971).

Clay is a deposit that is extensively distributed over the earth with high impurities (Weems, 1903). Clay is mainly composed of fine-grained minerals. It generally plastic at appropriate water contents and will harden when dried or fired. The structure consists of phyllosilicate layer and stable in every weather condition (Al Ani and Sarapaa, 2008). The formation of silicate clay involves weathering process consists of the alteration as the change of particle size process including the loss of potassium part, and silicon addition process from weathering solutions. Another process is recrystallization involving more intense weathering solutions. Kaolinite is a kind of pure clay that resulted from solutions containing soluble aluminum and silicon. However, the clay is normally found in not pure condition resulted from the reaction in original rock and water during the weathering process, from which the clay formation is initiated rock and water contact at near of surface of the earth. The CO_2 gas can dissolve in the water to form a carbonic acid component, consist of Hydrogen ions (H+) and bicarbonate ions making the water slightly acidic. The clay formation is briefly shown in the following reaction (Weems, 1930)

$$2Al_2O_3, 2\,K_2O, 2SiO_3\ (Feldspar) + 4H_2O + 2CO_2 \rightarrow 2Al_2O_3, 3SiO_2, 4H_2O + K_2CO_3 + 9SiO_2\ (clay\ substance) \tag{7}$$
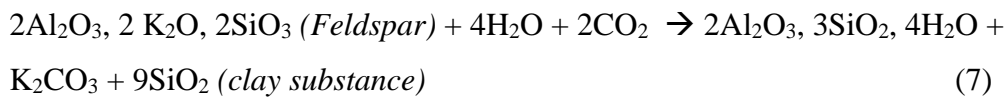
The clays are generally divided into three classes based on purity level. The first is porcelain clay as the purest clay type, one of its physical properties is the color change which will be white or light cream. The second is plastic clay containing some impurities which the color will change becoming yellow-red color. Fire clays as the third type has an almost similar property with porcelain containing higher iron and quartz quantities. (Weems, 1903).

4.1.2 Alumina-silicate structure of clay component

The structure of major clay minerals is different even though they are constructed by octahedral and tetrahedral sheets as the basic building block. The tetrahedron is formed by connecting the centers of four oxygen anions (2-charges) surrounding silicon as the central cation (4+charges). Aluminum, Ferric iron, and other elements are possible to

have functioned as cation too. Octahedron sheet as another geometric form is structured by hydroxyl atoms (OH) anion and Aluminium or Iron, and Magnesium as cations. On a single Al-OH with 3+charge of Al and six OH with -1 charge octahedron, three anions will be directed upwards and connected with a hydroxyl group, while 3 anions left are directed downward to another hydroxyl group (Al Ani and Sarapaa, 2008).

In clay minerals, hydrous aluminum silicate is not always available in pure concentration because Magnesium and other ionic substitutions are possible to change that octahedral form. While Si replacement with lower ion valence is possible in tetrahedral sheets (Al Ani and Sarapaa, 2008). Clay is commonly classified according to layer type, the magnitude of layer charge, type of interlayer material, the character of the tetrahedral sheet, and composition of individual species structure. **Figure 4.1** shows the geometric form of the alumina-silicate structure.
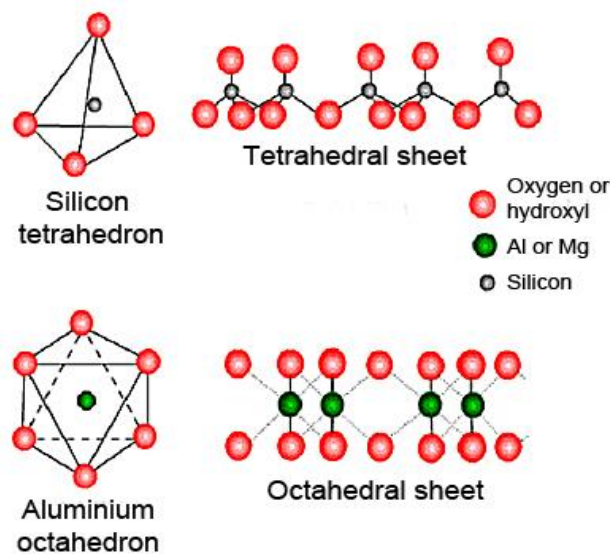
Figure 4-1. Structure of silicate clay

That mineral is similar in chemical and structural composition to primary minerals that originate from the earth's crust (Al Ani and Sarapaa, 2008). The SiO_4 tetrahedron is the composition of all silicate structures consist of four O^{2-} ions and Si^{4+} at the center. The structure is bounded in the same plane by shared oxygen anions forms a hexagonal network as tetrahedral sheet formation. External ions will bond to the tetrahedral sheet to

form one hydroxyl and two oxygen anion groups with aluminum, magnesium, and iron ion are those coordinating cations.

4.1.3 Main properties of smectite (bentonite) as particular of clay minerals

Some researchers (Bailey, 1930; Bailey and Chairman, 1980; Bailey, 1988; Moore and Reynolds, 1997; Murray, 2002; Haydn, 2007) had classified clay minerals based on chemical properties affecting the structure and composition of clay. Clay minerals are a part of a larger class of silicate minerals which are categorized as the phyllosilicate family. Clay classification is shown by the diagram in **Figure 4-2**.
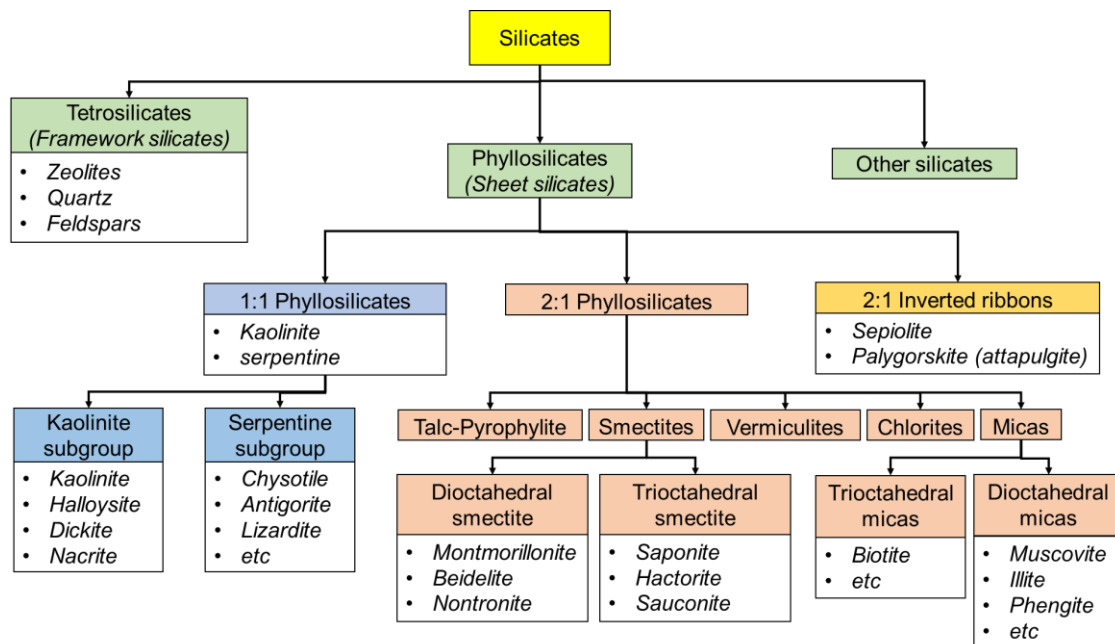
Figure 4-2. Classification of silicates and clay minerals

Bentonite is a dominant compound in a montmorillonite mineral as a part of the smectite group consist of three-layer sheets such as two layers of silica (tetrahedral) and one central layer of alumina (octahedral), while water molecules and cations occupy the space between the 2:1 layer. The major smectite minerals are Na-montmorillonite, Ca-montmorillonite, nontronite (Fe-montmorillonite) and beidellite (Al- montmorillonite). In the geometric structure of smectite, the silicon of the tetrahedral sheet is possible to be substituted by aluminum. The aluminum in octahedral sheet is possible to be substituted

by magnesium and iron too (Haydn, 2007). The smectite has the ability to absorb large amounts of water and to form a water-tight barrier. There are two main varieties of smectite which are classified by their capability to absorb water. The first is sodium smectite having high-swelling properties which can absorb water molecules up to 18 layers between tetrahedral-octahedral sheet layers. Na-smectite is a useful mineral that can be used in the drilling muds process, making protective clay liner for hazardous waste landfills system. The illustration of the geometric structure of Na-bentonite is shown in **Figure 4-3**. The second one is calcium smectite which has lower swelling potency to absorb water molecules. The presence of water within each crystal affects the physical characteristic of bentonite. Water layers can be formed in a uniform or no uniform thickness which will affect the operating temperature in the case of water removal process related to utilization and commercial value purposes. Normally, the loss of absorbed water between silicate sheets takes place between 100-200°C, loss of structural sheet (i.e. hydroxyl) takes place at 450-500°C and complete at 600-750°C.
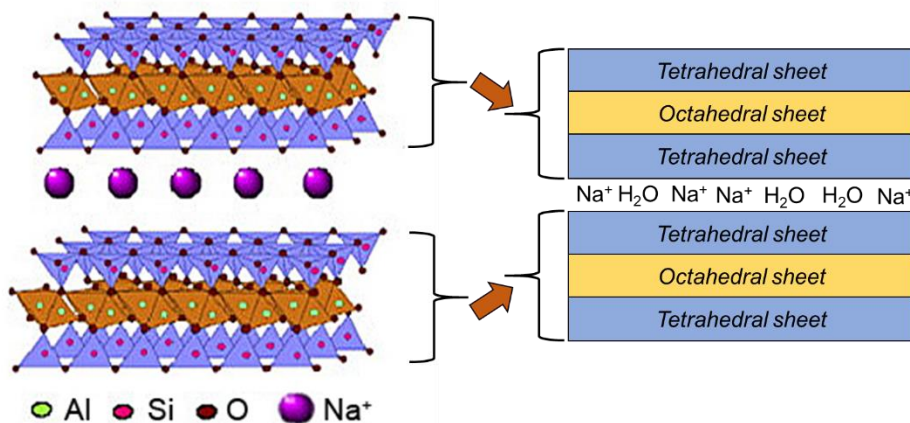
Figure 4-3. Illustration of the geometric structure of Na-bentonite

4.1.4 Alkali silicate reaction for agglomeration formation on bentonite.

In previous chapters, agglomeration of bed material was formed by alkali-silicate reaction, sintering of refractory outer coating, and agglomeration caused by melting alkali-silicate process. The whole agglomeration is caused by the inducing of inorganic EFB components. Defluidization as the worst-case had also been formed by changing of operational temperature at 800°C. Agglomeration is dependent on chemical

characteristics and melting behavior of coating too, which is sensitive to the amount of calcium and potassium in the fuel (Ohman and Nurdin, 2000). The binding between alkali and bentonite compounds from EFB ash could be adapted from the binding process of kaolin based on old works of literature in which the alkaline was denoted with *M* letter (Bostrom, *et.al.*, 2009; Steenari, *et.al.*, 2009). The reaction steps are as follows:

$$Al_2H_2O_{12}Si_4 \text{ (Bentonite)} \rightarrow Al_2Si_4O_{10}(OH)_2 \tag{8}$$

$$Al_2Si_4O_{10}(OH)_2 \rightarrow Al_2O_3.4SiO_2 + H_2O \tag{9}$$

$$2Al_2O_3.4SiO_2 + 4MCl + 2H_2O \rightarrow 4MAlSiO_4 + 4HCl \tag{10}$$

$$2Al_2O_3.4SiO_2 + 2M_2SO_4 \rightarrow 4MAlSiO_4 + 2SO_3 \tag{11}$$

$$2Al2O_3.4SiO_2 + 4MOH \rightarrow 4MAlSiO_4 + 2H_2O \tag{12}$$

$$2Al2O_3.4SiO_2 + 2M_2O \rightarrow 4MAlSiO_4 \tag{13}$$

$$2Al_2O_3.4SiO_2 + 4MCl + 4SiO_2 + 2H_2O \rightarrow 4MAlSi_2O_6 + 4HCl \tag{14}$$

$$2Al_2O_3.4SiO_2 + 2M_2SO_4 + 4SiO_2 \rightarrow 4MASi_2O_6 + 2SO_3 \tag{15}$$

$$2Al_2O_3.4SiO_2 + 4MOH + 4SiO_2 \rightarrow 4MAlSi_2O_6 + 2H_2O \tag{16}$$

$$2Al_2O_3.4SiO_2 + 2M_2O + 4SiO_2 \rightarrow 4MAlSi_2O_6 \tag{17}$$

As the main products of those reactions are $KAlSiO_4$ (Kalsite) and $KAlSi_2O_6$ (leucite) as alkali alumina silicate products having high stickiness levels. Another alkali (i.e. Na) and alkali-earth (i.e. Ca) elements would get a similar reaction to form other alkali-alumina silicates like $NaAlSi_3O_8$ (Albite) and $CaAl_2Si_2O_8$ (Anorthite). Based on the reaction above, the presence of bentonite could reduce the negative impact of alkali chlorides and sulfates resulted from biomass in flue gases and ashes. The performance of bentonite to capture KCl and K_2SO_4 decreased during temperature increment. Based on the discussion in Chapters II and III, the highest alkali-alumina silicate reaction was taking place at 800°C. The porosity might decrease at high temperatures limiting the diffusion of KCl and K_2SO_4 aerosols into bentonite particles.

4.2 Methods of agglomerates investigation

In the previous chapter, the stability of fluidization against agglomeration and defluidization formation process was based on differential pressure and pressure

deviation performance had been measured. Furthermore, the maximum concentration of ash addition to maintaining fluidization state had also been identified. In this chapter, agglomerated bed material or bed residue would be investigated to know the kinds of alkali silicates or alkali alumina silicate components using XRD instrument, the microscopic appearance of agglomerate surfaces using SEM, and distribution pores of agglomerate using BET. The measurement was carried out on sieved agglomerates with typical size consisted of +350 µm as the biggest size, +88-125, and a sample of +125-177 µm as the highest mass and -88 µm as the smallest size.

4.2.1 X-Ray diffraction experiment

XRD is a non-destructive technique for analyzing the structure of the material. In this work, RINT 2100V/PC is XRD apparatus used to lead understanding of the structural characteristic of agglomerate. XRD relies on X-ray wavelengths. When X-rays scatter from a substance with structure at that length scale, interference can take place resulting in a pattern of higher and lower intensities. As the initial step for this measurement was size preparation for XRD measurement. Size preparation was only carried out on coarse agglomerated silica sand and bentonite particles by crushing process to obtain a smaller size in order that the particle could be fit to XRD plate.

During measurement, a beam of X-rays was directed towards a sample, scattered intensity was measured as a function of outgoing direction which the angle between the incoming and outgoing beam was 2Θ. All of the samples were analyzed from the 5-70° angle with the step size was 0.020^o and time per step 1.00^o/min. Interpretation of measured data was carried out by Jade 5 software. The parameter of interpretation consisted of measurement of organic and inorganic groups which the elements considered some elements based on XRF measurement such as K, Mg, S, Na, Ca, Al, P, Ti, Si, Cl, Fe, and others.

4.2.2 Pore size and volume analysis

This measurement used Belsorp mini II apparatus. The operation was started weighting to calculate the specific surface area of the object. Outgassing process as the following process on that sample which was carried out at 120°C for 3 hours under

nitrogen and helium atmospheres. After that, Helium was used to measure volume, and Nitrogen was used to measure adsorption for several hours. Some data would be obtained including specific surface area, distribution of pore radius, and pore volume based on the Barret-Joyner-Halenda (BJH) model. This model assumed capillary condensation of the liquid nitrogen within the pores and calculated from the relative pressures and the amount of nitrogen taken up at a given relative pressure of the sorption isotherm took place in the adsorbed layer of nitrogen and the capillary condensed nitrogen the pore size distribution. Pore size distribution in the BJH model was calculated by the amount of nitrogen adsorption measurement when the relative pressure is 0.99 (Li, *et.al.*, 2019). The formula for size distribution was as follows:

$$V_{pn} = \left(\frac{r_{pn}}{r_{kn} + \Delta t_n}\right)^2 \left(\Delta V_n - \Delta t_n \sum_{j-1}^{n-1} A_{cj}\right) \tag{18}$$

Where V_{pn} is the pore volume, r_{pn} is the maximum pore radius, r_{kn} is the capillary radius, V_n is capillary volume, t_n is adsorbed nitrogen layer thickness and A_{cj} is the area after the emptying. This study would measure porous diameter measurement for (1). Raw material (pure silica sand, bentonite, EFB ash), (2). Mixed of bed residue under $4.3U_{mf}$ and (3). $1.5\ U_{mf}$ at operational temperature 700, 750, 800°C.

4.2.3 Scanning Electron Microscope (SEM) measurement

Microscopic agglomerate figures were analyzed by using Hitachi Miniscope TM-1000 consisted of various sizes with various magnifications. Analyzed samples consisted of the biggest, the smallest, and the highest quantity samples after sieving treatment. The additional sample was also analyzed from the crushing of the biggest particle (+350 µm) to know more about the property according to agglomeration form and the structure of layers.

4.2.4 SEM-EDX measurement

This measurement was purposed to mapping the composition of elements that affected the agglomerate formation. Samples that had been analyzed consisted of a

mixture of silica sand and bentonite having sieved size +350 µm after treatment at 800℃. The instrument used here was Shimadzu SSX-550.

4.3   Result and discussion

4.3.1 Alkali-silicate identification on raw material

Identification of components using XRD apparatus consisted of silica sand, bentonite, and EFB ash particles. The measurement of silica sand and bentonite was carried out for different samples at room temperature, 700, 750, and 800℃. Meanwhile, measurement of EFB ash was only carried out for that sample which was obtained from the ash formation process at 700℃.

4.3.1.1 Alkali-silicate identification on normal and thermal silica sand

Identification was carried at normal temperature and thermal temperature at 700, 750, and 800℃. In the normal state, silica sand was dominated by quartz compound in which silica (SiO_2) structure dominated.
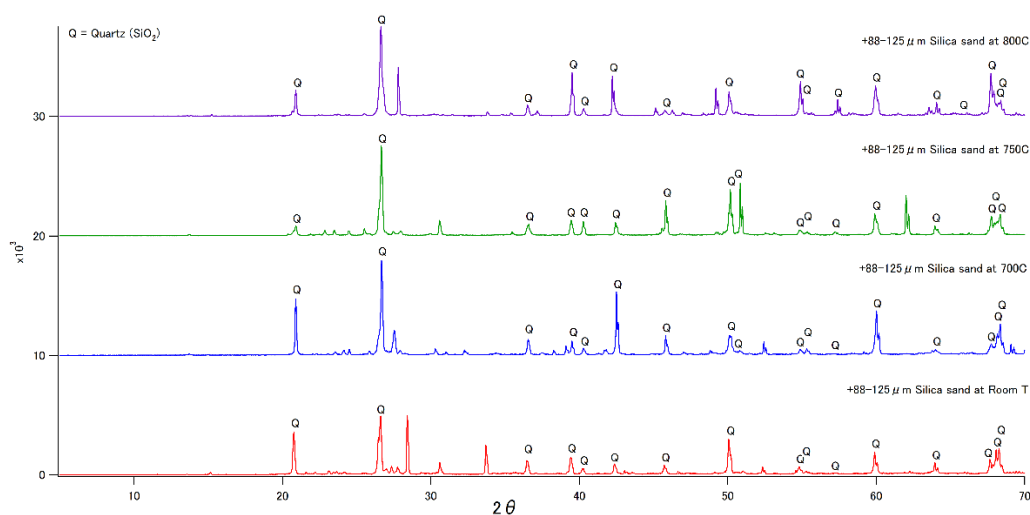
Figure 4-4. XRD analysis on silica sand particle at normal and thermal temperatures

Since thermal treatment had been applied, some peaks curve in **Figure 4-4** became fluctuating to achieve stability in several spots, the peaks could decrease or increase. The

increased temperature would lead to stability, from which the clearest bed particle could be seen after treatment at 800°C.

4.3.1.2 Alkali-silicate identification on normal and thermal bentonite

In normal conditions, peaks onset of bentonite consisted of cristobalite and quartz as silica structures. The heating process at 700°C resulted in the alkali-aluminosilicate formation such as sanidines ($K(Si_3Al)O_3$) and albite ($NaAlSi_3O_8$). Overall, those peaks did not significantly affect silica structures because those peaks were still clearly seen in **Figure 4-5**. At temperature 750°C, the change of cristobalite and quartz concentrations had taken place in which cristobalite and quartz had decreased as shown in some points in the curve. Meanwhile, alkali-aluminosilicate compounds including anorthide as newly identified compounds had also been formed. With the increasing temperature at 800°C, silica structures were looked stable. At some points, there was another alkali-aluminosilicate formation in the form of microline ($KAlSi_3O_8$). Therefore, based on this identification, the bentonite structure would significantly change in various temperature treatments.
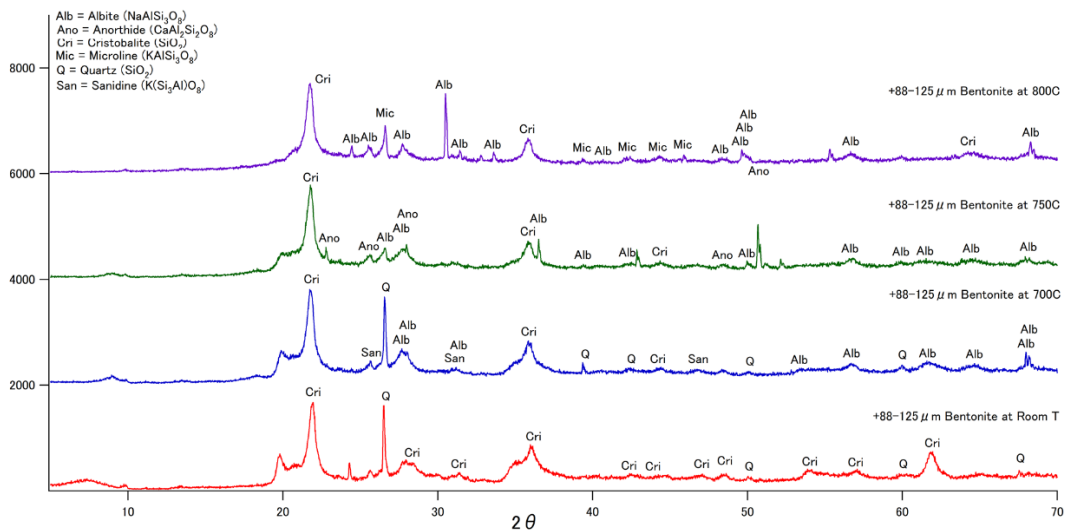
Figure 4-5. XRD analysis on bentonite particle at normal and thermal temperatures

4.3.1.3 Alkali-silicate identification on EFB ash at 700°C

Measurement of XRD showed that EFB ash was absolutely dominated by KCl. The presence of KCl became an important understanding that most agglomerates formation in this study were caused by the presence of that KCl. When compared to KCl particle from the synthetic process, the presence of KCl in ash had a clear similarity. The comparison between the KCl peak of EFB ash and synthesis was shown in **Figure 4-6**.
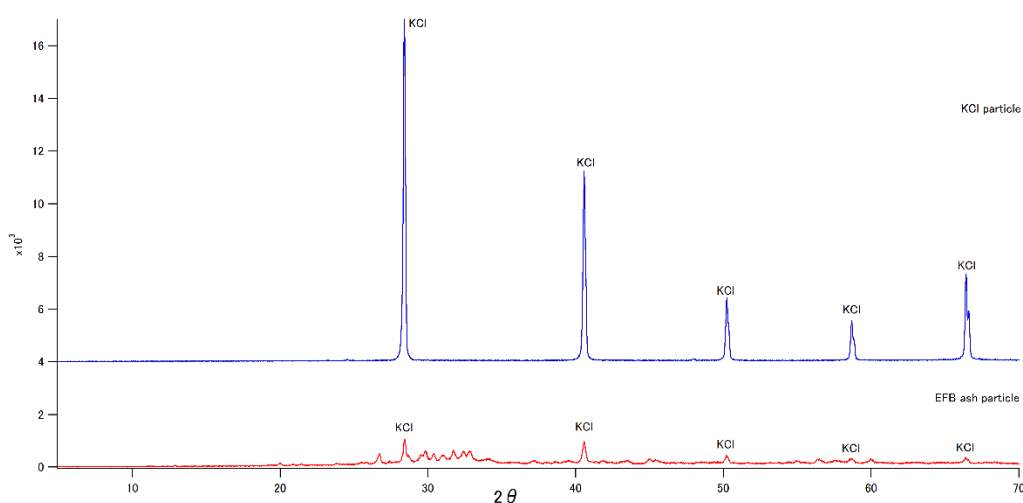
Figure 4-6. XRD analysis on EFB ash and synthetic KCl powder

4.3.2   Alkali-silicate identification on bed residue with 4.3U$_{mf}$ superficial velocity

The measurements were carried out on sieved bed residue particles consisted of +350 µm as the biggest size, -88 µm as the smallest size, and +88-125 µm as the highest mass. The highest mass with that size almost dominated all of bed residue samples.

4.3.2.1   Alkali-silicate identification on a mixture of silica sand at T= 700°C, 4.3 U$_{mf}$

The measurement would be compared to the XRD measurement of silica sand in the pure condition which could be mentioned as a normal state. XRD measurement on the particle with size -88µm showed that intensity of quartz components had decreased slightly which were confirmed by some alkali-aluminosilicates formation such as microline (K(Si$_3$Al)O$_8$) and anorthite (CaAl$_2$Si$_2$O$_8$). The presence of that aluminosilicates was clearly observed on measurement +88-125 µm as shown in **Figure 4-7**. On the

measurement of +350 µm particle, the concentration of quartz components was higher and clearer to be seen than other smaller sizes. Principally, operation at 700°C did not significantly affect quartz concentration change. Thus, the bed particle condition after thermal treatment was still in good condition which might be still dominated by the original size. Coating formation was taking place, but it might be small, even it had been already degraded during the fluidization process. On the measurement of +350µm bed particle, some alkali-silicate and alkali-aluminosilicates had been formed such as potassium gallium silicate ($KGaSi_3O_8$) and sanidine ($K(Si_3Al)O_8$).

Figure 4.7. XRD analysis on a mixture of silica sand from operation at 700°C, 4.3 U_{mf}

4.3.2.2 Alkali-silicate identification on a mixture of silica sand at T= 750°C, 4.3 U_{mf}

Measurement of -88 µm bed residue particle showed decrement of quartz concentration which was more significant than treatment at 700°C as shown by XRD curve in **Figure 4-8**. Some alkali-aluminosilicate components had been formed such as anorthide ($CaAl_2Si_2O_8$), microline ($KAlSi_3O_8$), sanidine ($K(Si_3Al)O_8$), albite ($NaAlSi_3O_8$) and potassium gallium silicate ($KGaSi_3O_8$). $NaAlSi_3O_8$ and $KGaSi_3O_8$ dominated those alkali-aluminosilicate components which had been formed. Measurement on +88-125 µm showed that concentration of quartz was higher than -88 µm particle size while the alkali-aluminosilicate composition was still the same to -88 µm mixture particle components. Meanwhile, measurement of +350 µm showed the highest concentration of quartz than other sizes. Agglomerates had been formed by

binding of some silica sand particles in an incomplete coating form which would be sintered each other to form large particles. Therefore, measurement XRD on these agglomerates showed that silica concentration was still high, even some alkali-aluminosilicates had been formed such as anorthite ($CaAl_2Si_2O_8$).
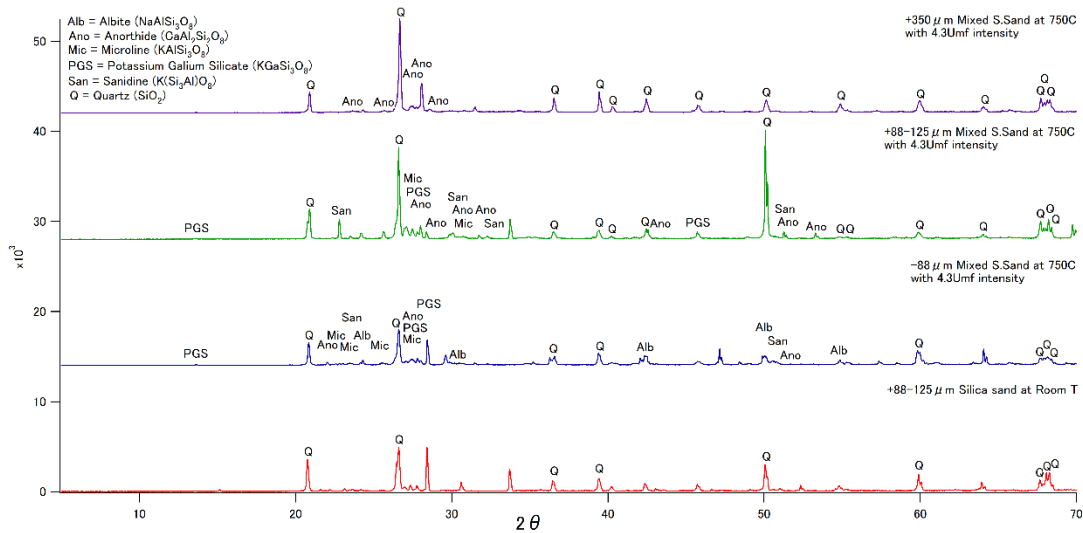
Figure 4-8. XRD analysis on a mixture of silica sand from operation at 750°C, 4.3 U_{mf}

4.3.2.3   Alkali-silicate identification on a mixture of silica sand at T= 800°C, 4.3 U_{mf}

On the measurement of -88µm, **Figure 4-9**, bed residue composition was dominated by high quartz. It elucidated that agglomerates were already formed in small intensity with potassium gallium silicate ($KGaSi_3O_8$) as that product.
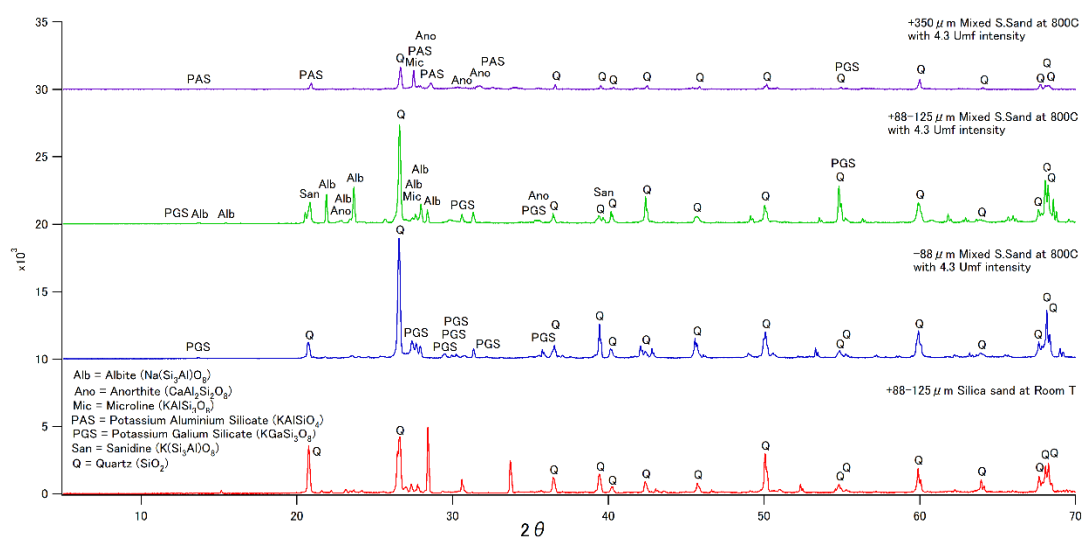
Figure 4-9. XRD analysis on a mixture of silica sand from operation at 800°C, 4.3 U_{mf}

On measurement -88 and +88-125 µm, quartz composition was still clear with high intensity as a normal state and alkali-aluminosilicate components including albite ($Na(Si_3Al)O_8$), sanidine ($K(Si_3Al)O_8$), and microlite ($KAlSi_3O_8$). The different condition was shown by measurement of +350µm. Some large agglomerates had been formed with the low amount of quartz material which indicated the coating formation as the reaction between alkaline and quartz might complete covering all of sand surfaces and sintering of coating as the substance of those agglomerates might completely be formed too. They consisted of microline ($KAlSi_3O_8$), potassium gallium silicate ($KGaSi_3O_8$) and anorthite ($CaAl_2Si_2O_8$).

4.3.2.4   Alkali-silicate identification on a mixture of bentonite at T= 700°C, 4.3 U_{mf}

Measurement in this section was carried out on all mixtures. XRD measurement in **Figure 4-10** showed the quartz still dominated all structures of bentonite particles. Therefore, operation bentonite in this condition should be run well.
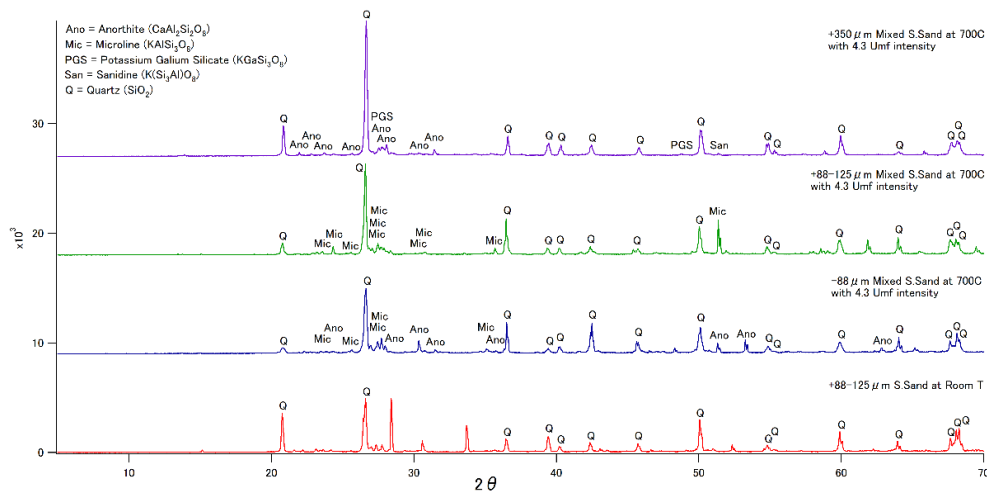
Figure 4-10. XRD analysis on a mixture of bentonite from operation at 700°C, 4.3 U_{mf}

4.3.2.5 Alkali-silicate identification on a mixture of bentonite at T= 750°C, 4.3 U_{mf}

On measurement -88 µm particle, the concentration of cristobalite had decreased starting from detector position at 20° to 70°. It was followed by agglomerate formation such as albite ($NaAlSi_3O_8$) as shown in **Figure 4-11**. Measurement of +88-125 µm size showed higher agglomerates consisted of anorthide ($CaAl_2Si_2O_8$), albite ($NaAlSi_3O_8$) as the two of highest intensities.
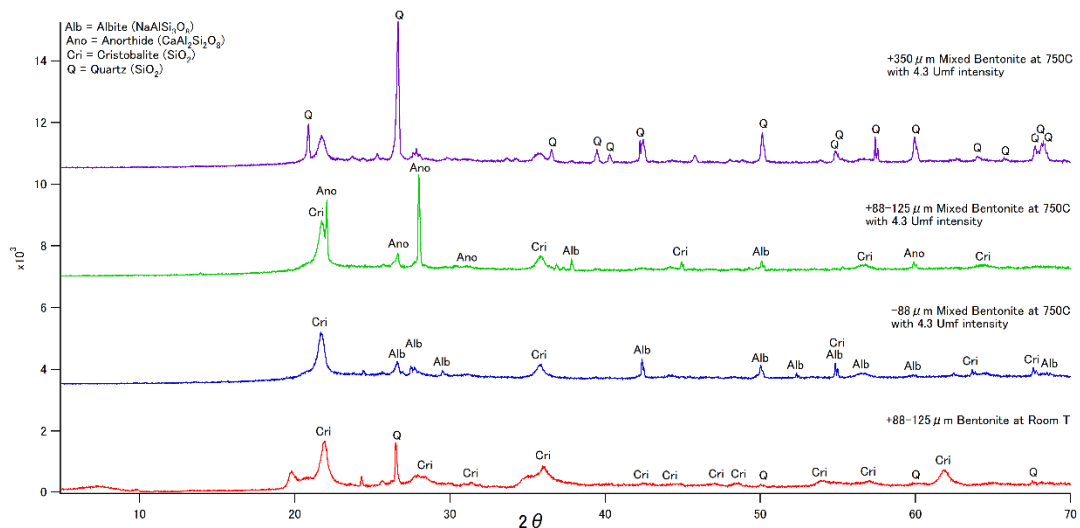
Figure 4-11. XRD analysis on a mixture of bentonite from operation at 750°C, 4.3 U_{mf}

While the low amount of cristobalite was still identified as having a lower concentration than the -88 µm mixture particle. On the measurement of +350 µm particle, no alkali-silicate or alkali-aluminosilicate formation was identified. On contrary, quartz peaks re-increased again and dominated all of the peaks. This behavior elutriated that the agglomerates were still dominated by a partial coating which had already got sintering process and formed large agglomerates but with weak bonding.

4.3.2.6   Alkali-silicate identification on a mixture of bentonite at T= 800°C, 4.3 U_{mf}

On measurement with higher temperature, 800°C, structure of -88 µm bed residue particles were like normal state and dominated by cristobalite. Change of structure could be observed by appearing of albite ($NaAlSi_3O_8$) and sodium aluminum silicate ($NaAlSiO_4$) in **Figure 4-12**. Since potassium concentration might be very low and ignored by XRD measurement, then the coating might be weak and easy to be degraded. Meanwhile, there were different structures again on +350 µm mixture particle, in which potassium element in agglomerates was high leading to form stickier structure. Furthermore, the presence of cristobalite components which already decreased significantly indicated that the presence of coating including sintered coating might completely form leading to construct larger agglomerates too.

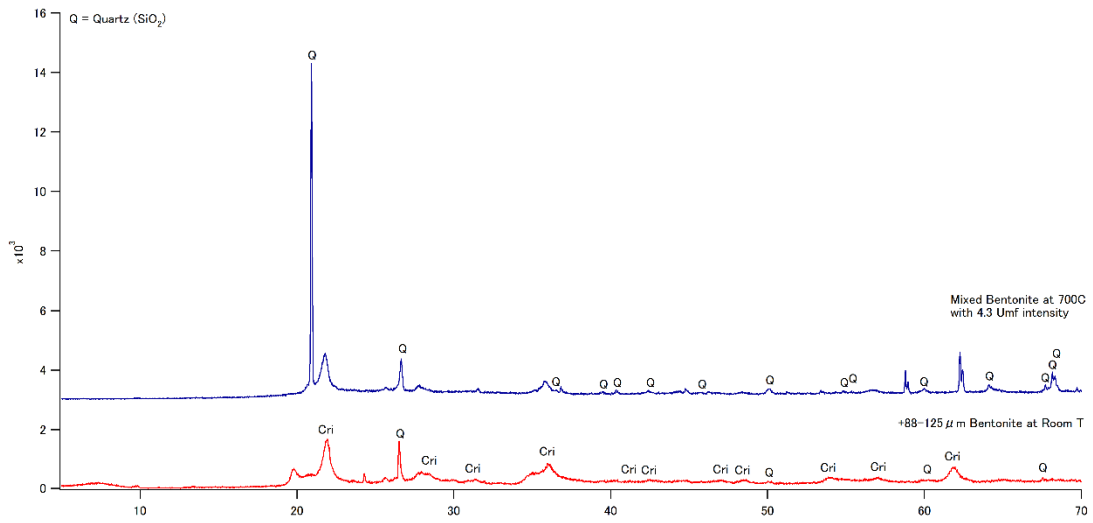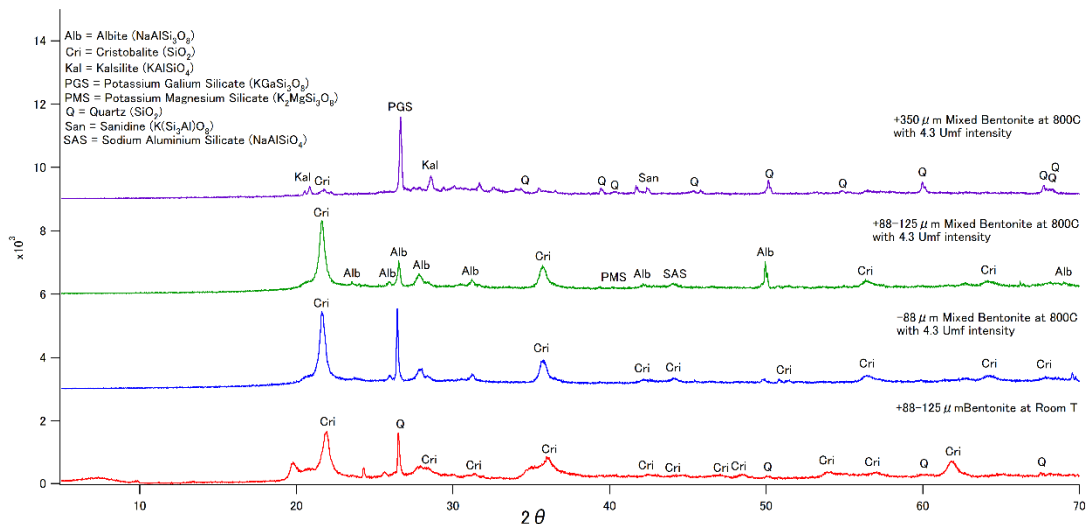**Figure 4-12.** XRD analysis on a mixture of bentonite from operation at 800°C, 4.3 U_{mf}

4.3.3 Alkali-silicate identification on bed residue with 1.5 U_{mf} superficial velocity

A similar method to operation with 4.3 U_{mf}, measurement was carried out on the biggest and smallest particle sizes including the heaviest mass after mechanical sieving treatment. As mentioned in chapter 1-3, fluidization with low velocity was needed to be observed as consideration to know the velocity effect against coatings and agglomerates formation. XRD measurement would support know silica concentration changes and the kinds of typical agglomerates formed.

4.3.3.1   Alkali-silicate identification on a mixture of silica sand at T= 700°C, 1.5 U_{mf}

The low-velocity adjustment might highly affect to form faster and higher alkali-aluminosilicate components. It was closely relevant to albite ($Na(Si_3AlO_8)$), anorthide ($CaAl_2Si_2O8$), and potassium gallium silicate ($KGaSiO_8$) formation which were already formed on the smallest size measurement (-88 µm). However, the concentration of quartz was high enough on that size indicating that coating or agglomerate formation was still very low formed.
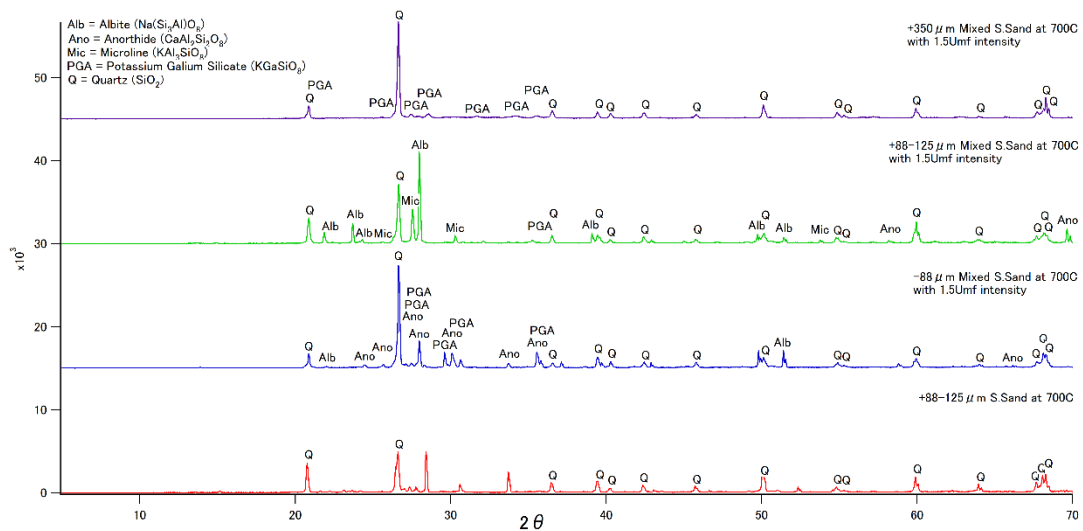
Figure 4-13. XRD analysis on a mixture of silica sand from operation at 700°C**,** 1.5U_{mf}

However, measurement on +88-125 µm particle resulted in a higher concentration of alkali-aluminosilicate and alkali-silicate materials above. XRD curve in **Figure 4-13** showed that there were some decrements of silica or quartz components even though

those decrements were not high. On the measurement of +350 μm mixture particle, quartz components were still detected on some degrees of detector record with insignificant intensity change. In this measurement, small amount of Potassium Gallium Silicate as the only one detected component which might coat on some spots of silica sand surfaces resulted in slight coating and weak agglomeration structure.

4.3.3.2 Alkali-silicate identification on a mixture of silica sand at T= 750°C, 1.5 U_{mf}

There were anorthite ($CaAl_2Si_2O_8$), potassium gallium silicate ($KGaSi_3O_8$), microline ($KAlSiO_3O_8$), sanidine ($K(Si_3Al)O_8$) formation besides silica components which kept remaining in high intensity like normal state as shown on -88 μm particle in **Figure 4-14**. The intensity of quartz was still high on +88-125 μm mixture particle with the domination of coating component consisted of albite ($NaAlSi_3O_8$), ortochlase ($KAlSiO_3O_8$), and $KGaSi_3O_8$. The high intensities of quartz elucidated that coating were low and agglomerates which might be already formed were still small. On the measurement of +350 μm particle, the quartz concentration had decreased significantly but the angle of detector degree with low intensity from 20 to 70° could still be identified. $KGaSi_3O_8$ and potassium aluminum silicate ($KAlSiO_4$) might be highly formed over measurement, from which those components were completely covered silica sand surfaces to make a sticky and strong agglomeration structure.

Figure 4-14. XRD analysis on a mixture of silica sand from operation at 750°C, 1.5 U_{mf}

4.3.3.3 Alkali-silicate identification on a mixture of silica sand at T= 800ºC, 1.5 U_{mf}

The concentration of silica was described as a quartz component whose intensity was stable enough at -88 µm particle size. In **Figure 4-15**, anorthide ($CaAl_2Si_2O_8$), potassium gallium silicate ($KGaSi_3O_8$), calcium aluminum silicate ($CaAl_2SiO_6$) were as main components of coating on silica sand surface. A similar structure had been formed on +88-125 µm particle but with lower intensity and coating might be formed with higher $KGaSi_3O_8$ and $CaAl_2SiO_6$.
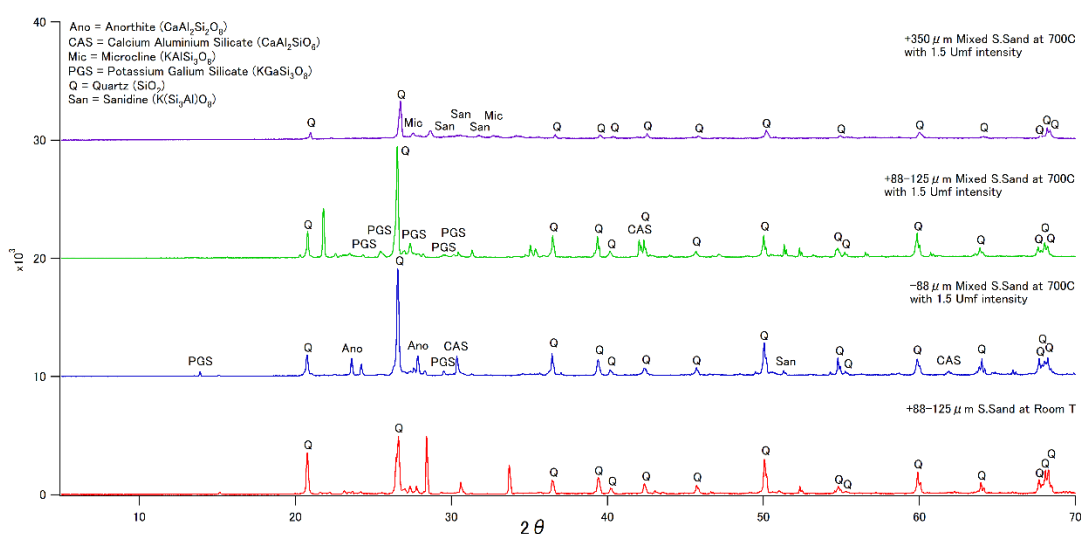
Figure 4-15. XRD analysis on a mixture of silica sand from operation at 800ºC, 1.5 U_{mf}

On +350µm particle, quartz concentration almost totally decreased. Some alkali-aluminosilicates which mainly consisted of potassium had been formed from detection between 20-40º but with low concentration. However, that agglomerates had a strong agglomerate structure, even stronger than operation at 750ºC. In this condition, most silica sand particles had been perfectly agglomerated to make stickier and stronger agglomerates. So, that was possible to reach a defluidization state in this condition.

4.3.3.4 Alkali-silicate identification on a mixture of bentonite at T= 700ºC, 1.5 U_{mf}

On particle -88µm, some cristobalites as silica spots got significant decrement from detection record between 20-60º when compared to the normal state in **Figure 4-16**. That decrement was closely related to albite formation even though in low concentration only.
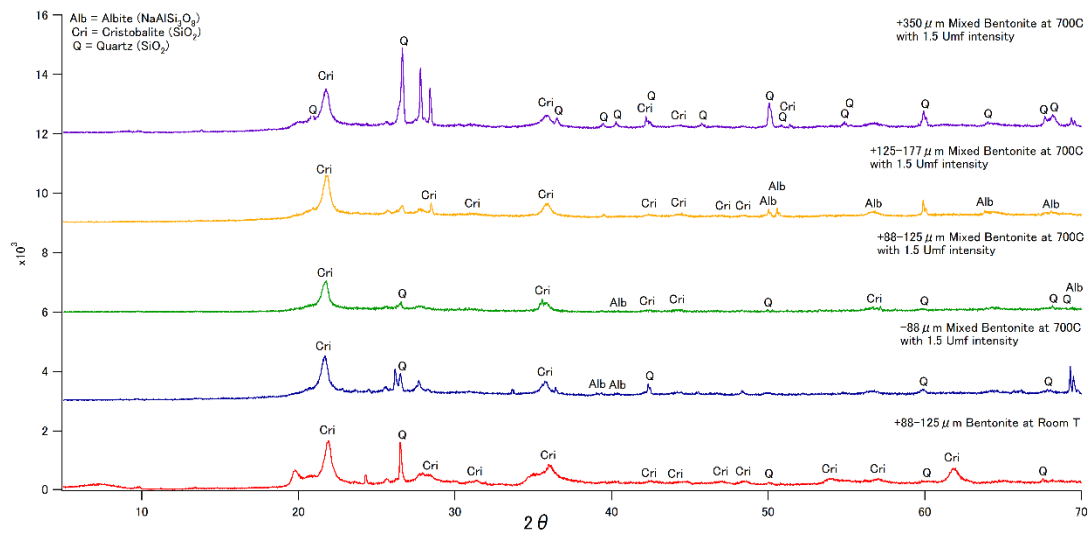
Figure 4-16. XRD analysis on a mixture of bentonite from operation at 700°C, 1.5 U_{mf}

On the measurement of bigger size, +88-125 µm, cristobalite, and quartz concentrations decreased. It was followed by higher albite ($NaAlSi_3O_8$) formation than -88 µm size. XRD measurement of +125-177 µm showed that the albite had been also produced, but cristobalite concentration in this sieving size was higher than -88 and +88-125 µm. On the measurement of the biggest sieved particle, +350 µm, the silica structure became clearer than the previous measurement. Cristobalite and quartz got significant increment with very low agglomeration which would be formed. Therefore, agglomeration structure on +350 µm particle got significant breakage leading to form smaller particle again which was still enable to support fluidization atmosphere.

4.3.3.5 Alkali-silicate identification on a mixture of bentonite at T= 750°C, 1.5 U_{mf}

On measurement -88 µm particle, cristobalite structure got slight decrement intensity. It was marked by anorthide presence on detector rotation after 20 until 50° in **Figure 4-17**. On particle +88-125 µm showed a similar trend that cristobalite concentration looked like -88 µm size. However, anorthide ($CaAl_2Si_2O_8$) was not identified again which might be already degraded even though in lower superficial velocity intensity. Meanwhile, on +350µm crystal structures of silica were changed and identified as quartz components whose intensity already significantly increased. It showed fluidization kept running well at this temperature.
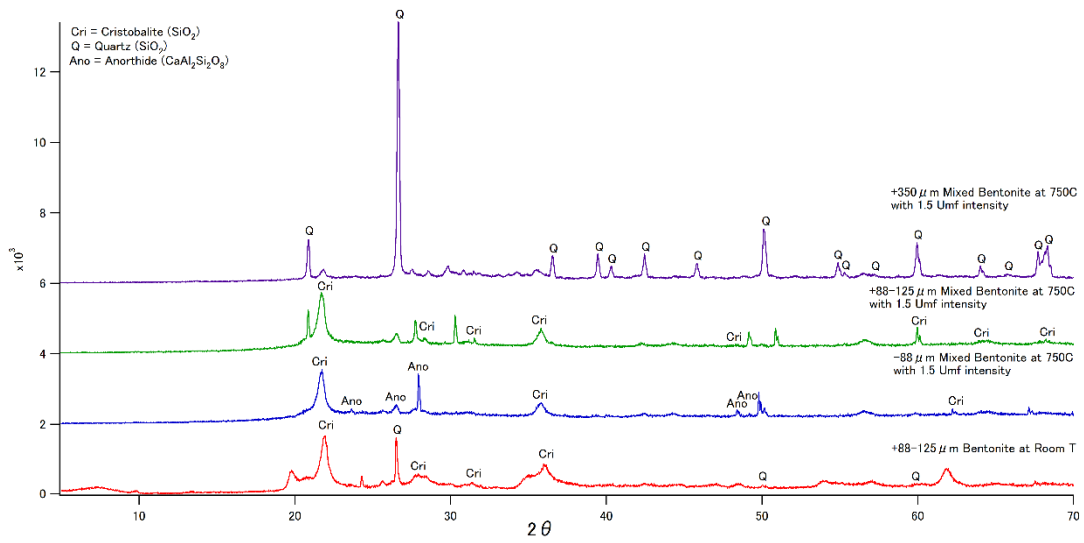
Figure 4-17. XRD analysis on a mixture of bentonite from operation at 750°C, 1.5 U_{mf}

4.3.3.6   Alkali-silicate identification on a mixture of bentonite at T= 800°C, 1.5 U_{mf}

Likewise, operation in section 4.3.1.2, cristobalite peaks on -88µm particle measurement decreased in some spots which should be appeared in high intensity as the normal state.
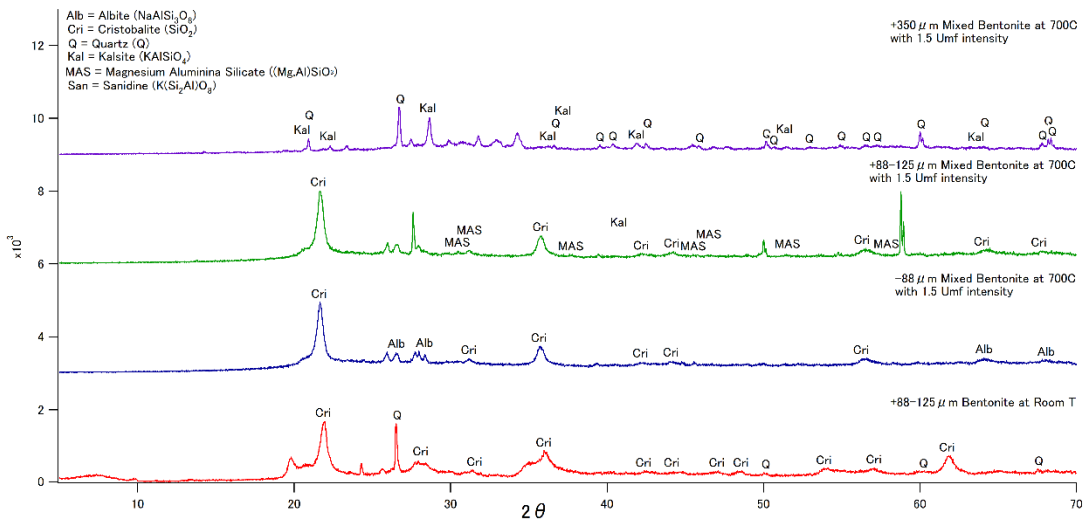
Figure 4-18 XRD analysis on a mixture of bentonite from operation at 800°C, 1.5U_{mf}

While albite peaks had also been detected from 20 until 70° as shown in **Figure 4-18**. On +88-125 µm gave a similar trend, from which the intensity of cristobalite was still high

enough. The slight coating was also identified by the presence of magnesium alumina silicate ((Mg.Al)Si.O$_3$). On +350 µm size, large agglomerates had been formed which might already have a sticky formation. The presence of kalsite (KAlSiO$_4$) contained potassium element would support to create an innermost layer as the basic structure to lead sticky agglomerates as mentioned in Chapter II. The high agglomerates formation was also proven by significant intensity decrement of quartz peak.

4.3.4 Pore measurement on raw material surfaces

Measurement of particle pores was carried out on the biggest, smallest particle size, and heaviest particle from the sieving treatment. Results from measurement were interpreted by the BJH method to know the radius, volume, and specific surface area of particle pores. **Table 4-1** showed maximum measurement including these average results.

Table 4-1 Pore characteristics on initial substances of bed particles

No.	Particle	Specific surface area (m^2.g^{-1})	Pore radius (nm)		Pore volume (cm^{3}g^{-1}nm^{-1})	
			Peak	Average	Peak	Average
A	Raw material					
	1.Silica sand at Room T	6.01	1.64	22.46	2.20E-03	5.23E-04
	2.Silica sand at 700ºC	0.59	12.24	22.46	1.65E-04	6.82E-05
	3.Silica sand at 750ºC	1.99	1.85	22.46	6.64E-04	1.99E-04
	4.Silica sand at 800ºC	0.63	10.65	22.46	1.54E-04	7.28E-05
	5.Bentonite at Room T	23.27	7.99	15.90	6.08E-03	2.94E-03
	6.Bentonite at 700ºC	26.15	10.65	14.22	6.19E-03	3.48E-03
	7.Bentonite at 750ºC	25.61	10.65	22.46	6.63E-03	2.85E-03
	8.Bentonite at 800ºC	13.10	12.24	12.73	4.69E-03	1.76E-03
	9.EFB ash at 700ºC	1.20	12.24	22.46	3.68E-04	1.22E-04

4.3.5 Pore measurement on normal and thermal silica sand surface

Table 4-1 and **Figure 4-19** showed the comparison of +88-125 µm silica sand at room temperature or normal state, 700, 750, and 800°C. Measurement at normal state resulted in the highest pore radius and volume, which were 1.64 nm and 2.20E-03 $cm^3g^{-1}nm^{-1}$. The lowest volume from measurement was 1.80E-05 $cm^3g^{-1}nm^{-1}$, while the specific surface area of this size was 6.0128 m^2g^{-1}. Significant differences resulted from measurement at 700°C, from which the highest pore radius increased to be 12.24 nm but with lower pore volume value became 1.65E-04 $cm^3g^{-1}nm^{-1}$. This operation measured specific surface area decrement became 0.5871 $m^2.g^{-1}$.
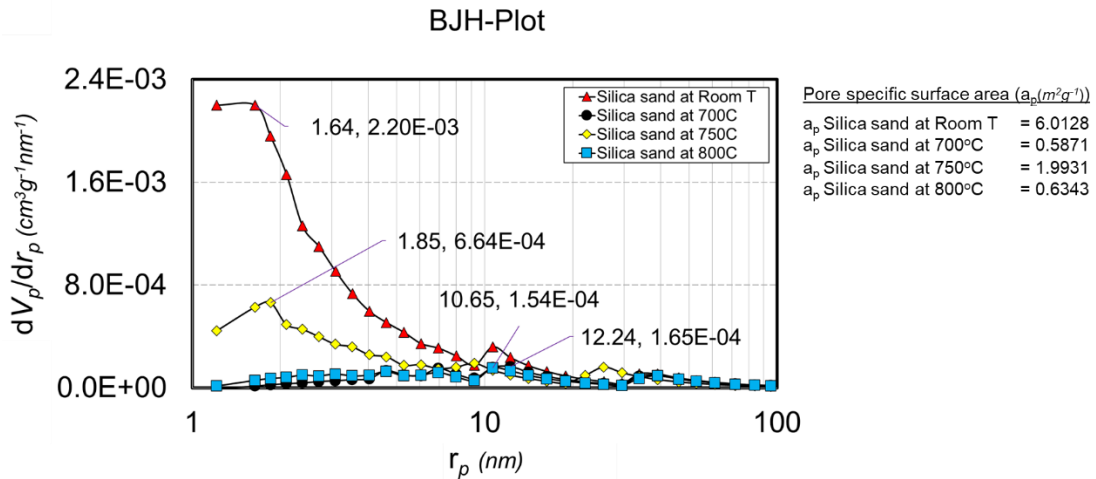
Figure 4-19. BJH analysis on silica sand particle at various temperature treatment

Increasing of temperature at 750°C caused decreasing in radius and volume of pores against normal state becoming 1.85 nm and 6.64E-04 $cm^3g^{-1}nm^{-1}$. The minimum volume over measurement was1.10E-05 $cm^3g^{-1}nm^{-1}$. Specific surface area also got significant decrement, but a bit higher than operation at 700°C in the amount 1.9931 $m^2.g^{-1}$. Operation at temperature 800°C resulted in higher pore radius but lower pore volume again than the normal state like the discussion at 700°C. They were 10.65 nm and 1.54E-04 $cm^3g^{-1}nm^{-1}$. The specific surface area got a significant decrement to be 0.6343 $m^2.g^{-1}$ as well. Silica sand mass was not degraded in various temperature treatments. It was relevant to the previous discussion in Chapter II based on TGA measurement. However, thermal treatments at 700, 750, and 800°C already gave a high effect on that particle

structure which significantly decreased on that specific surface area and pore volume particle properties.

4.3.6 Pore measurement on normal and thermal bentonite surface

Started from the measurement of +88-125µm bentonite particle at normal state, the highest pore radius and volume were 7.99 nm and 6.08E-03 $cm^3g^{-1}nm^{-1}$. That particle consisted of various pore radius, with the average value was 15.90 nm and the average pore volume was 2.94E-03 $cm^3g^{-1}nm^{-1}$ as shown in **Table 4-1** and **Figure 4-20**.
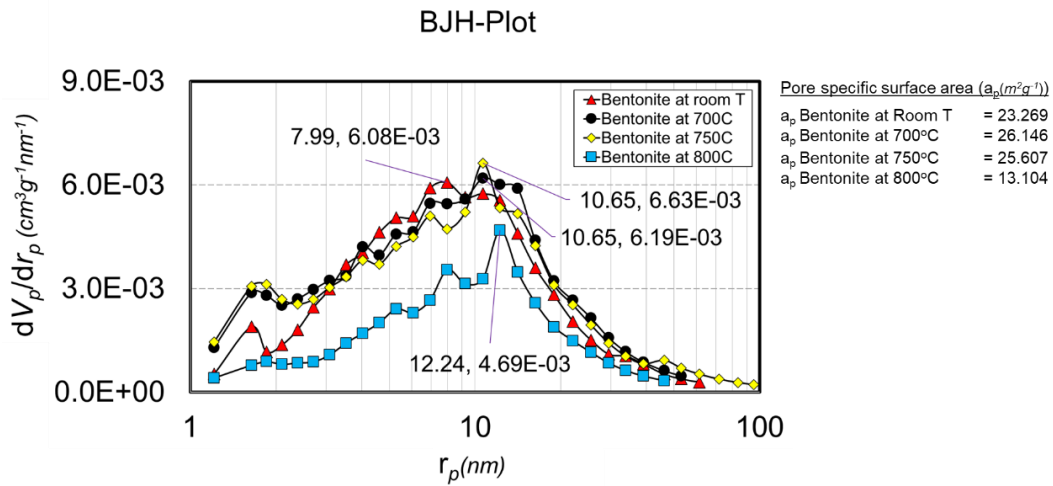
Figure 4-20. BJH analysis on bentonite particle at various temperature treatment

Measurement of bentonite porosity at 700°C obtained 10.65 nm and 6.19E-03 $cm^3g^{-1}nm^{-1}$ as the highest pore radius and volume which were already higher than the normal state. Minimum pore volume until the last measurement was 4.74E-04 $cm^3g^{-1}nm^{-1}$, while the average pore radius and volume were 14.22 nm and 3.48E-03 $cm^3g^{-1}nm^{-1}$.

On measurement at 750°C, maximum pore radius and volume were almost the same to 700°C values with a slight increase of pore volume only into 6.63E-03 $cm^3g^{-1}nm^{-1}$. Pore-specific area value increased when it was compared to normal state but slightly decreased against operation at 700°C into 26.146 m^2g^{-1}. The measurement at 800°C increased the highest pore radius into 4.69E-03 $cm^3g^{-1}nm^{-1}$ but decreased pore volume into 4.69E-03 $cm^3g^{-1}nm^{-1}$. The average pore radius and volume were 12.73 nm and 1.76E-03 $cm^3g^{-1}nm^{-1}$, with the minimum pore volume was 3.37E-04 $cm^3g^{-1}nm^{-1}$.

As mentioned in Chapter II, degradation of normal bentonite at 700°C made 10wt% of mass which was dominated by water molecule would be degraded completely. However, this measurement showed that some pores at the previous water location did not change significantly and bentonite form kept stable without getting significant shrinkage of initial size by thermal application.

4.3.7 Pore measurement on EFB ash surface at 700°C

Pore measurement on EFB ash had maximum pore radius and volume amount 12.24 nm and 3.68E-04 $cm^3g^{-1}nm^{-1}$. While average pore radius and volume in **Table 4-1** were 22.46 nm and 1.22E-04 $cm^3g^{-1}nm^{-1}$.
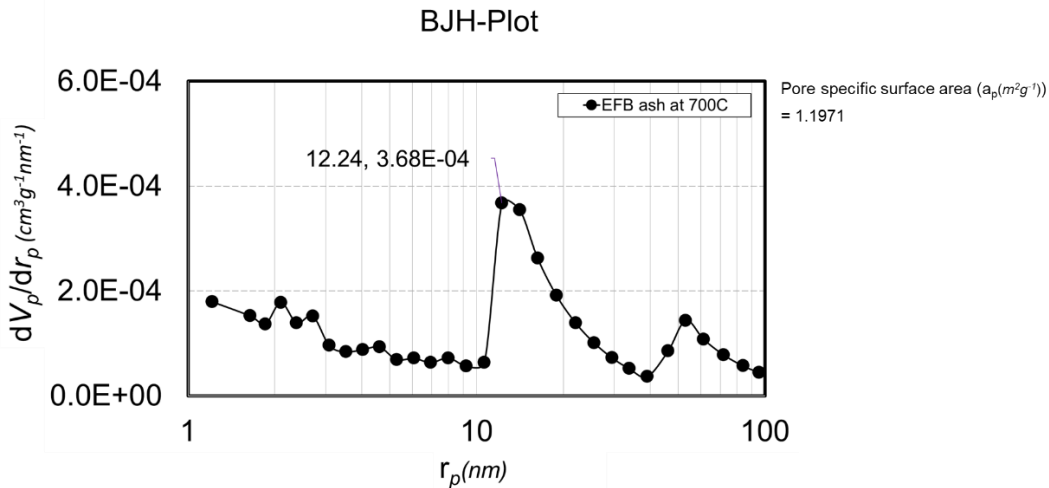
Figure 4-21. BJH analysis on EFB ash particle after temperature treatment at 700°C

Pore size distribution of EFB ash had certain homogeneity and heterogeneity which indicated the number of pores concentration. **Figure 4-21** showed most pore radius was concentrated under 10 nm but would be various for larger sizes. EFB ash had a small pore-specific area of 1.1971 m^2g^{-1}. The low of that surface area might be caused by transformation over thermal treatment which reduced much biomass mass significantly.

4.3.8 Pore measurement on bed residue particles surface with 4.3U_{mf} superficial velocity

The measurement was carried out on -88 as the highest particle, +88-125 as the lowest size particle, and +350µm as the highest mass particle. From this measurement,

the role of superficial velocity application would be observed to know porosity particle characterization. The resume of measurement could be seen in **Table 4-2** below.

Table 4-2 Pore characteristics on a mixture of particles from $4.3U_{mf}$ fluidization process

No.	Particle	Specific surface area $(m^2.g^{-1})$	Pore radius (nm)		Pore volume $(cm^3g^{-1}nm^{-1})$	
			Peak	Average	Peak	Average
B.	A mixture of s.sand with 4.3 U_{mf}					
	1.-88 µm at 700°C	0.52	10.65	22.46	2.45E-04	6.70E-05
	2.+88-125 µm at 700°C	5.55	1.64	22.46	2.12E-03	5.08E-05
	3.+350 µm at 700°C	1.50	1.64	17.84	6.33E-04	1.60E-04
	4.-88 µm at 750°C	0.57	12.24	22.46	1.69E-04	6.10E-05
	5.+88-125 µm at 750°C	6.20	1.64	22.46	2.38E-03	5.66E-04
	6.+350 µm at 750°C	2.67	1.64	14.22	1.22E-04	2.54E-06
	7.-88 µm at 800°C	0.52	12.24	22.46	1.42E-04	5.08E-05
	8.+88-125 µm at 800°C	1.64	1.64	12.73	6.30E-04	1.75E-04
	9.+350 µm at 800°C	0.62	1.64	15.90	2.60E-04	6.45E-05
C.	A mixture of bentonite with 4.3 U_{mf}					
	1.All mixtures at 700°C	15.94	9.23	22.46	3.51E-03	1.76E-03
	2.-88 µm at 750°C	7.03	10.65	22.46	1.91E-03	7.75E-04
	3.+88-125 µm at 750°C	7.09	10.65	22.46	2.15E-03	7.98E-04
	4.+350 µm at 750°C	4.30	1.85	22.46	8.97E-04	4.71E-04
	5.-88 µm at 800°C	3.11	12.24	22.46	1.24E-03	3.41E-04
	6.+88-125 µm at 800°C	5.57	12.24	22.46	1.26E-03	5.79E-04
	7.+350 µm at 800°C	1.28	12.24	22.46	4.24E-04	1.28E-04

4.3.8.1   Pore measurement on mixture of silica sand at T= 700°C, 4.3 U_{mf}

Pore measurement -88 µm consisted of the highest pore radius was 10.65 nm which was higher than +88-125 and +350 µm sizes as shown in **Table 4-2**. On the contrary, the peak of pore volume with the amount of 2.45E-04 $cm^3g^{-1}nm^{-1}$ was the lowest among the

others. The average pore radius on -88 and +88-125 µm was the same at around 22.46 nm but it slightly decreased on +350 µm of 17.84 nm. Distribution pore size on -88µm in **Figure 4-22** was heterogeneity concentrated in range 1.21 until 95.28 nm, but on +88-125 and +350µm were dominantly concentrated at radius within 10 nm which might indicate condensation of aerosols on those surfaces were already higher than -88 µm.

Figure 4-22. BJH analysis on a mixture of silica sand from treatment at 700°C, 4.3 U_{mf}

4.3.8.2 Pore measurement on a mixture of silica sand at T= 750°C, 4.3 U_{mf}

Measurement on -88 µm mixture particle in **Table 4-2** and **Figure 4-23** showed that the peak of pore radius was 12.24 nm with pore volume was 1.69E-04 $cm^3g^{-1}nm^{-1}$. Another lower spot was 39.01nm, 9.84E-05 $cm^3g^{-1}nm^{-1}$ as the second biggest radius in that size. The distribution of pore radius was concentrated in mesopore sizes by 10 nm. It was distributed in other bigger sizes, even though, with insignificant amount only.

Measurement on +88-125 µm showed that the highest radius was located at the peak 1.64 nm with volume 2.38E-03 $cm^3g^{-1}nm^{-1}$. The distribution size on +88-125 µm was concentrated within 20 nm, and the pore volume would gradually decrease with pore radius increment. Measurement on +350 µm showed a similar trend with +88-125 µm with the peak at radius 1.64 nm and volume 1.07E-03 $cm^3g^{-1}nm^{-1}$. The distribution of pore radius was concentrated from around 6 nm to 84 nm with pore volume within 2.04E-04 $cm^3g^{-1}nm^{-1}$. The pore-specific surface areas on those sizes were 0.57, 6.20, and 2.67 m^2g^{-1}. Normally, the pore-specific surface area would be high in large particles. However,

the measurement on +350 µm showed significant decrement which indicated the condensation of aerosols leading to form tight coatings and large agglomerates had been rapidly formed with higher concentration. This phenomenon was relevant to the agglomeration scheme from discussion in Chapter II in **Figure 2-11**.
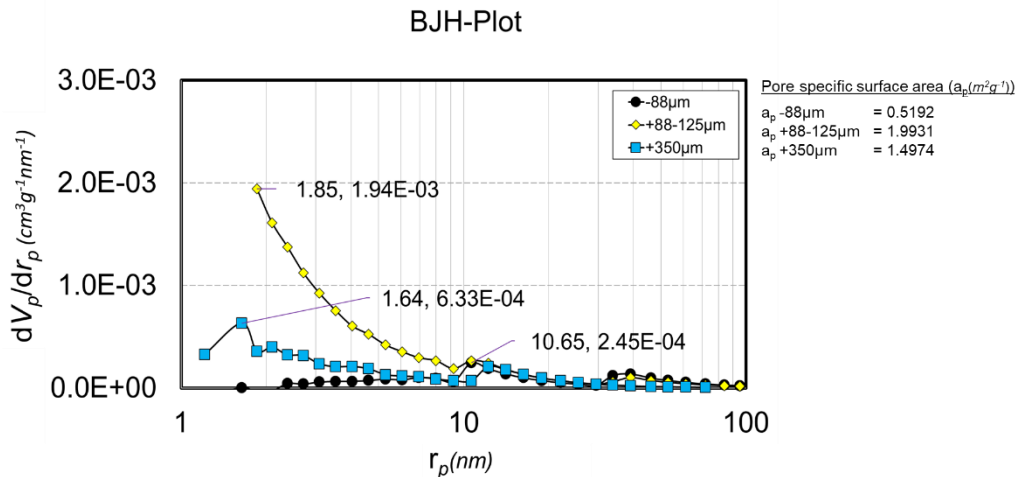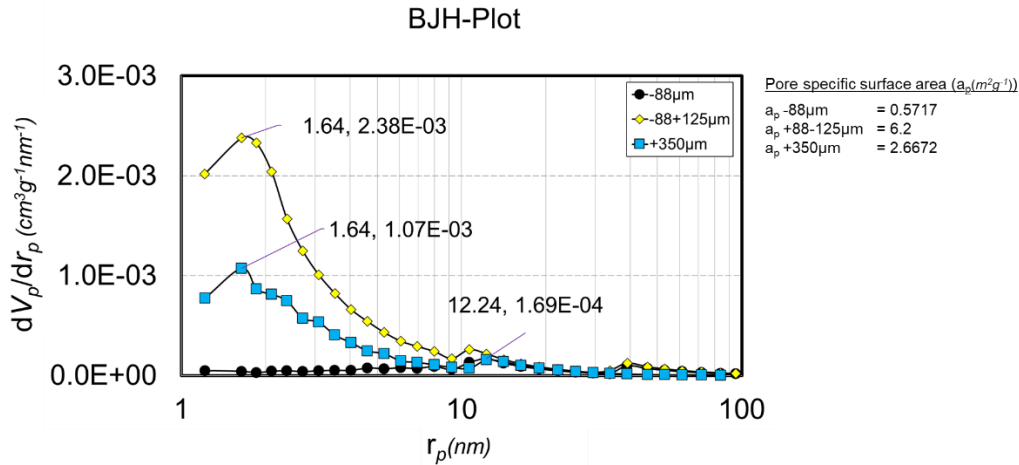

Figure 4-23. BJH analysis on a mixture of silica sand from treatment at 750°C, 4.3 U_{mf}

4.3.8.3 Pore measurement on a mixture of silica sand at T= 800°C, 4.3 U_{mf}

The highest concentration of pore radius on +88µm mixture silica sand was detected at 12.24 nm with pore volume 1.42E-04 $cm^3g^{-1}nm^{-1}$. Some spots in **Figure 4-24** with high enough volume was detected at radius 1.21 to 2.10, 7.99, 10.65 to 18.94, and 39.01 to 53.04 nm. Overall measurement showed the distribution of pore radius was dominated at radius by 10 nm with concentration by 5.0E-05. **Table 4-2** showed that the average pore radius and volume for this particle were 22.46 nm and 5.08E-05 $cm^3g^{-1}nm^{-1}$ with pore specific surface area was 0.52 m^2g^{-1}.

The next measurement was carried out on +88-125µm with the highest peak resulted in a lower pore radius such as 1.64 nm with pore volume 6.30E-04 $cm^3g^{-1}nm^{-1}$. Some radiuses with high volumes were concentrated from 1.21 to 5.29 nm, while overall particles dominantly distributed from 6 to 46 nm. The average pore radius was lower than -88µm particle; that was 12.73 nm with volume 1.75E-04 $cm^3g^{-1}nm^{-1}$. However, the specific surface area was 1.64 m^2g^{-1} which indicated that ash concentration on silica sand surface might increase when compared to initial silica sand in section 4.3.1.1.
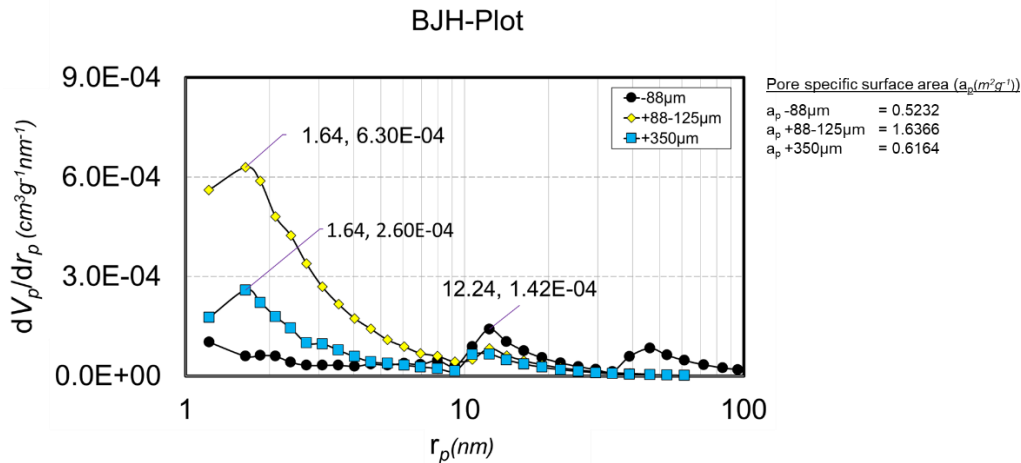
Figure 4-24. BJH analysis on a mixture of silica sand from treatment at 800°C, 4.3 U_{mf}

Measurement on +350 µm particle had a similar trend to +88-125 µm size. The pore radius peak was 1.64 nm with a volume of 2.60E-04 $cm^3g^{-1}nm^{-1}$. Some radiuses with high volume were distributed in the range of 1.21 to 4.03 nm, and 10.65 to 12.24 nm. While the concentration of pore radius was distributed in the range 4.61 to 61.31 nm with the pore volume within 5.0E-05 $cm^3g^{-1}nm^{-1}$. The average pore radius and volume for this size were 15.90 nm and 6.45E-05 $cm^3g^{-1}nm^{-1}$ with the pore-specific surface area was 0.62 m^2g^{-1}. Among pore-specific surface areas, the size of +350µm had a minimum value which was relevant to the most significant increment of coating mass formation on the silica sand surface.

4.3.8.4 Pore measurement on a mixture of bentonite at T= 700°C, 4.3 U_{mf}

Measurement was only carried out on the whole mixtures of bentonite which was depicted in the curve of **Figure 4-25**. The highest peak of pore radius was 9.23 nm with the pore volume was 3.51E-03 $cm^3g^{-1}nm^{-1}$. Overall observation showed that pore radius particles were distributed in several kinds which consisted of high enough concentration of pores volume concentrated at radius between 1.21 and 33.81 nm in, while small concentrations were distributed between 39.01 and 95.28 nm in stable enough concentration. From this measurement, the average pore radius and volume particles were 22.46 nm and 1.76E-03 $cm^3g^{-1}nm^{-1}$. The pore-specific surface area in **Table 4-2** showed that alkali-silicate or alkali-aluminosilicate particles which coated bentonite surface in

this measurement were relatively small when compared to the discussion in section 4.3.1.2.
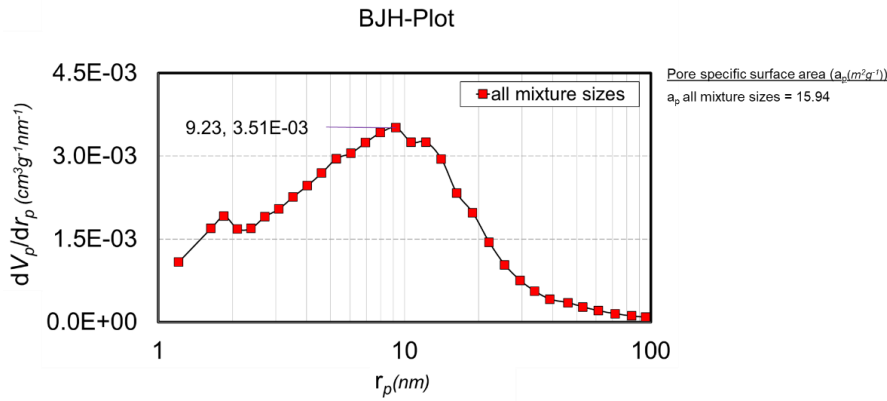
Figure 4-25. BJH analysis on a mixture of bentonite from treatment at 700°C, 4.3 U_{mf}

4.3.8.5 Pore measurement on a mixture of bentonite at T= 750°C, 4.3 U_{mf}

On the measurement of -88µm particle, the highest peak of pore radius was obtained at the radius of 10.65 nm with pore volume 1.91E-03 $cm^3g^{-1}nm^{-1}$. Another peak as the second-highest of pore radius was 14.13 nm with pore volume 1.77E-03 $cm^3g^{-1}nm^{-1}$. The distribution of pore size in **Figure 4-26** was similar to that at 700°C. It was concentrated in the range of mesopore size between 1.21 and 25.55 nm with a high enough concentration of pore volume, while a few spots with stable pore radius value was concentrated between 29.50 and 95.28 nm in a lower amount of pore volume value between 4.79E-04 and 3.21E-05 $cm^3g^{-1}nm^{-1}$. The average pore radius was obtained in the amount of 22.46 nm with an average pore volume was 7.75E-04 $cm^3g^{-1}nm^-1$ as shown in **Table 4-2**. Measurement of the pore-specific surface area was 7.03 m^2g^{-1} showing that the coating concentration was higher than operation at 700°C.

A similar trend to operation at 700°C had been shown by +88-125µm measurement, from which the highest peak of pore radius was 10.65 nm with pore volume was 2.15E-03 $cm^3g^{-1}nm^{-1}$. Heterogeneous distribution of pore size was concentrated at pores volume which higher than 5.00E-04 $cm^3g^{-1}nm^{-1}$, in the range of pore radius from 2.71 to 25.55 nm. While a few concentrations were less than 5.00E-04 $cm^3g^{-1}nm^{-1}$ located in the range of pore radius 1.21 to 2.38 nm and 29.50 to 95.28 nm. The average pore radius was similar

to the radius from operation at 700°C, namely 22.46 nm with pore volume 7.98E-04 $cm^3g^{-1}nm^{-1}$. The pore-specific surface area value was close to that operation, namely 7.09 m^2g^{-1}.
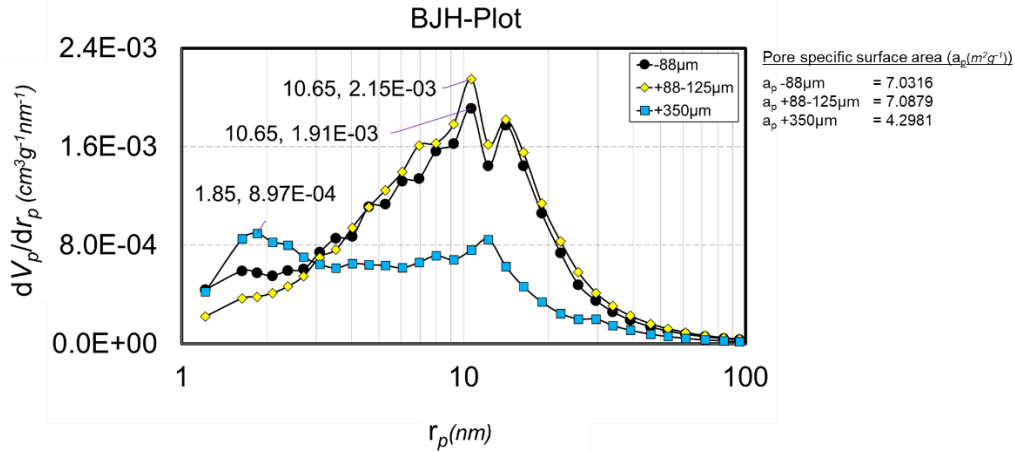
Figure 4-26. BJH analysis on a mixture of bentonite from treatment at 750°C, 4.3 U_{mf}

The highest peak of pore radius from +350 µm mixture size was 1.85 nm, pore volume = 8.97E-04 $cm^3g^{-1}nm^{-1}$. It was followed by a radius of 12.24 nm with pore volume 8.48E-04 $cm^3g^{-1}nm^{-1}$. Other concentrations having high pores radius were concentrated between 33.81 and 95.28 nm with pores volume less than 2.00E-04 $cm^3g^{-1}nm^{-1}$. The average pore radius was the same as particles from previous measurements, namely 22.46 nm with the pore volume was 4.71E-04 $cm^3g^{-1}nm^{-1}$. Meanwhile, measurement of the pore-specific surface area showed more significant decrement than previous measurements which elucidated that concentration particle had coated higher bentonite than measurement on other particles.

4.3.8.6 Pore measurement on a mixture of bentonite at T= 800°C, 4.3 U_{mf}

The highest peak on the -88 mixture of particles in **Figure 4-27** was located at pore radius 12.24 nm, pore volume = 1.24E-03 $cm^3g^{-1}nm^{-1}$. Distribution of particle was dominated on concentration with pore volume less than 2.00E-04 $cm^3g^{-1}nm^{-1}$ in the range of pore radius 1.21 to 4.61 nm, and 46.13 to 95.28 nm. Distributions of pores radius were higher than 2.00E-04 $cm^3g^{-1}nm^{-1}$ had pores volume concentration between 5.29 and 39.01

nm. Average pores radius and volume in **Table 4-2** were 22.46 nm and 3.41E-04 $cm^3g^{-1}nm^{-1}$. The pore-specific area had significantly decreased when compared to the measurement at operation 700 and 750°C in the same particle size, namely 3.11 m^2g^{-1}.

Measurement on +88-125 µm as the third highest peak of pores radius was 12.24, 1.85, and 18.96 nm with pores volume were 1.26E-03, 1.19E-03, and 1.14E-03 $cm^3g^{-1}nm^{-1}$ respectively. The distribution of pores radius was more heterogeneous than -88 µm size. It was concentrated in the range of radius between 1.21 and 39.01 nm. While pores radius between 46.13 and 95.28 were concentrated in lower pores volume which was less than 2.00E-04 $cm^3g^{-1}nm^{-1}$. The average pore radius value was the same as the pore radius of -88µm, with average pore volume was 5.79E-04 $cm^3g^{-1}nm^{-1}$ and pore specific area was 5.75 m^2g^{-1}. The pore specific area was higher than the -88 µm mixture of particles which showed that accumulated coating concentration on the bentonite might be small, even it was lower than the coating concentration on -88 µm particle too.

Measurement on +350 µm particle resulted in the highest peak of pore radius that was the same as -88 and +88-125 µm particle size but with a significant decrement of pores volume into 4.24E-04 $cm^3g^{-1}nm^{-1}$. Most pores size had been distributed at a concentration less than 2.00E-04 $cm^3g^{-1}nm^{-1}$, consisted of pores radius 1.21 to 6.95, 9.23, 22.07 to 33.81, and 46.13 to 95.28 nm. While larger pore sizes were only located at pore radius around 7.99, 10.65 to 16.29, and 39.01 nm.
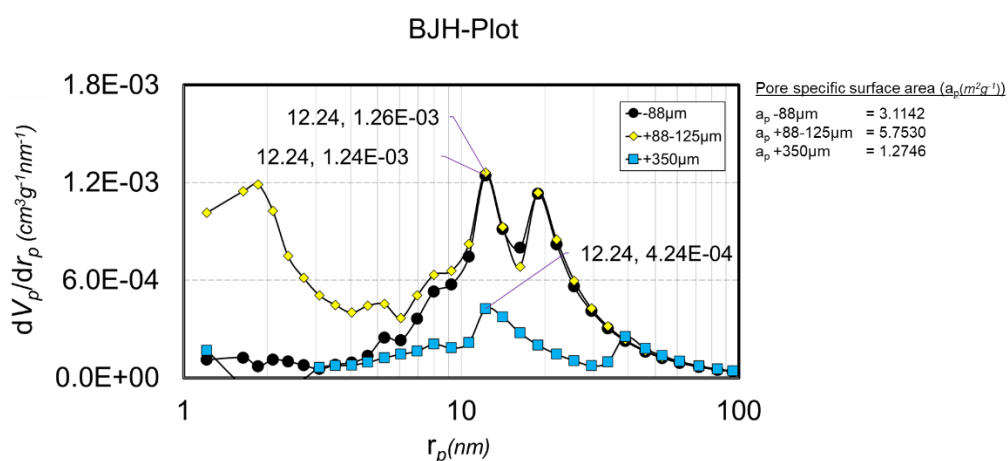

Figure 4-27. BJH analysis on a mixture of bentonite from treatment at 800°C, 4.3U_{mf}

The average pore radius was the same as the measurement on the -88 and +88-125µm particle but with a more significant decrement of pores volume, which was 1.28E-04 $cm^3g^{-1}nm^{-1}$. Furthermore, the pore-specific surface area had highly decreased by 1.28 m^2g^{-1} that shown coating formation might be already tightly and completely formed on the whole bentonite surface.

4.3.9 Pore measurement on bed residue particles surface with 1.5 U_{mf} superficial velocity

Kinds of sieved particles in this measurement were the same as the measurement on 4.3 U_{mf}. Table 3.3 was the resume of measurement which would be explained in detail in the next sections.

Table 4-3 Pore characteristics on a mixture of particles from 1.5U_{mf} fluidization process

No.	Particle	Specific surface area $(m^2.g^{-1})$	Pore radius (nm)		Pore volume $(cm^3g^{-1}nm^{-1})$	
			Peak	Average	Peak	Average
D.	A mixture of s.sand with 1.5 U_{mf}					
	1.-88 µm at 700ºC	0.60	12.24	22.46	2.06E-04	6.62E-05
	2.+88-125 µm at 700ºC	0.84	1.64	22.46	2.30E-04	1.01E-04
	3.+350 µm at 700ºC	0.52	1.21	22.46	3.02E-04	3.38E-05
	4.-88 µm at 750ºC	0.30	12.24	22.46	1.84E-04	4.00E-05
	5.+88-125 µm at 750ºC	4.75	1.64	22.46	1.81E-03	4.28E-04
	6.+350 µm at 750ºC	2.73	1.64	14.22	9.68E-04	2.94E-04
	7.-88 µm at 800ºC	1.42	1.64	22.46	4.12E-04	1.31E-04
	8.+88-125 µm at 800ºC	1.90	1.21	22.46	7.79E-04	1.55E-04
	9.+350 µm at 800ºC	1.41	1.66	22.75	5.80E-04	1.40E-04
E.	A mixture of bentonite with 1.5 U_{mf}					
	1.-88 µm at 700ºC	18.28	10.65	14.22	4.38E-03	2.39E-03
	2.+125-177 µm at 700ºC	20.55	9.23	18.43	4.64E-03	2.49E-03
	3.+350 µm at 700ºC	9.41	1.64	15.91	2.99E-03	9.54E-04

4.-88 µm at 750ºC	8.10	10.65	15.90	2.26E-03	9.71E-04
5.+88-125 µm at 750ºC	14.94	1.64	14.22	3.12E-03	1.74E-03
6.+350 µm at 750ºC	0.59	12.22	12.80	2.58E-04	7.66E-05
7.-88 µm at 800ºC	7.14	10.65	22.46	1.94E-03	7.80E-04
8.+88-125 µm at 800ºC	10.49	1.64	22.46	2.35E-03	1.03E-03
9.+350 µm at 800ºC	2.38	1.64	12.73	9.17E-04	2.74E-04

4.3.9.1 Pore measurement on mixture of silica sand at T= 700ºC, 1.5 U_{mf}

On the -88 µm particle, the highest peak of pore radius was 12.24 nm with pore volume 2.06E-04 $cm^3g^{-1}nm^{-1}$. Another observed high peak was 39.01 nm with the pore volume was 1.08E-04 $cm^3g^{-1}nm^{-1}$. The sizes of pores were homogenously distributed with average pore radius and volume were 22.46 nm and 6.62E-05 $cm^3g^{-1}nm^{-1}$ as shown in **Table 4-3** which the increase of velocity did not significantly affect the characteristic of -88 µm particle.

The next measurement on +88-125 µm showed that the highest peak of pore radius was 1.64 nm with pore volume 2.30E-04 $cm^3g^{-1}nm^{-1}$. It was also followed by 12.24 and 10.65 nm as other pores radius with high pores volume. **Figure 4-28** showed that the distribution of pores volume decreased while pores radius increased. Based on **Table 4-3**, the average pore radius was the same as -88 µm particle with average pore volume was 1.01E-04 $cm^3g^{-1}nm^{-1}$, and pore specific surface area was 0.84 m^2g^{-1}. That specific surface area was very different to section 4.4b in the same condition which indicated superficial velocity with 1.5 U_{mf} application had a high tendency to decrease pore specific surface area.

Measurement on the +350µm mixture of particles showed that the highest peak of pore radius was 1.21 nm with peak volume 3.02E-04 $cm^3g^{-1}nm^{-1}$. Distribution size was dominated at pores radius between 6.95 and 95.28 nm with pores volume was less than 2.00E-05 $cm^3g^{-1}nm^{-1}$. Pore specific surface area was 0.52 m^2g^{-1} that showed accumulated coating in 1.5 U_{mf} was higher than 4.3 U_{mf} application.
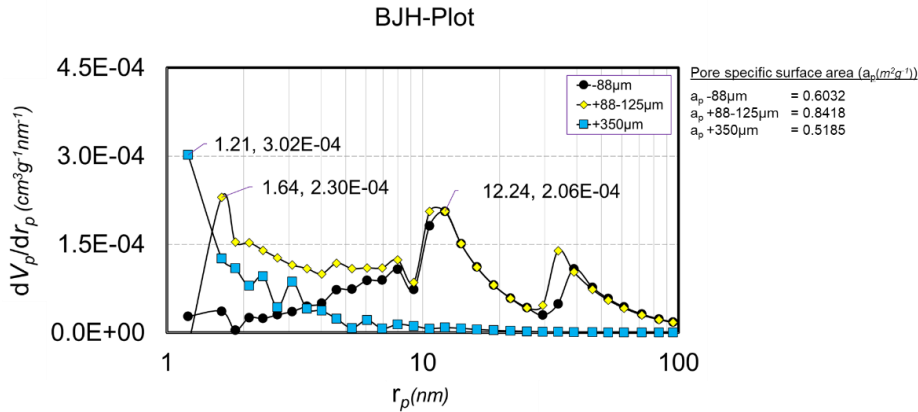
Figure 4-28. BJH analysis on a mixture of silica sand from treatment at 700°C, 1.5 U_{mf}

4.3.9.2 Pore measurement on a mixture of silica sand at T= 750°C, 1.5 U_{mf}

The highest peak of pore radius from -88 µm particle measurement in **Figure 4-29** was 12.24 nm with pore volume = 1.68E-04 $cm^3g^{-1}nm^{-1}$. Another peak radius with almost the same volume concentration was 10.65 nm with volume 1.68E-04 $cm^3g^{-1}nm^{-1}$. The concentration of distribution size was located at pore volume less than 5.00E-05 $cm^3g^{-1}nm^{-1}$ consisted of some different pore radius, like 1.21 to 6.95, 9.23, 25.5 to 33.81, and 61.31 to 95.28 nm. Meanwhile, the average pore radius in this size was the same as the measurement at 700°C in the same condition with pore volume 1.84E-04 $cm^3g^{-1}nm^{-1}$. Measurement of pore specific area was lower than measurement with 4.3 U_{mf} application, namely 0.30 m^2g^{-1}.

The next measurement on the +88-125 µm particle showed a different peak of pore radius namely 1.64 nm with pore volume = 1.81E-03 $cm^3g^{-1}nm^{-1}$. Distribution of pore size was concentrated at some radius, that was 7.99 to 12.24 and 16.29 to 95.28 nm with pores volume less than 2.00E-04 $cm^3g^{-1}nm^{-1}$. The average pore radius was the same as the previous measurement on -88µm particle with a higher average pore volume around 4.28E-04 $cm^3g^{-1}nm^{-1}$ as shown in **Table 4-3**. Pore specific surface area for this size was 4.75 m^2g^{-1} which was lower than the measurement on 4.3U_{mf} fluidization amount 6.20 m^2g^{-1}. It proved coating formation might be easily formed during fluidization with superficial velocity 1.5 U_{mf}.

Measurement on +350 µm particle showed that the highest peak had the same radius as measurement on +88-125 µm with lower pore volume amount 9.68E-04 $cm^3g^{-1}nm^{-1}$.

Distribution of pores radius had been dominated at interval size 6.06 to 10.65 nm and 16.29 to 53.04 nm. Average pores radius showed a smaller value than previous measurements, that was 14.22 nm with average pore volume = 2.94 cm^{3}g^{-1}nm^{-1}. Meanwhile, the result of the pore-specific surface area measurement was lower than the measurement with velocity 4.3 U$_{mf}$, which was 2.73 m^{2}g^{-1}. It showed that different velocity intensities did not give significant difference typically on a large mixture of the particle with size +350 µm at operation 700ºC. It might be caused by decreasing velocity intensity which would reduce collisions and alkali-silicate or alkali-aluminosilicate reaction during fluidization of bed particles. Therefore, the mixture of particles could not be completely formed in this state.
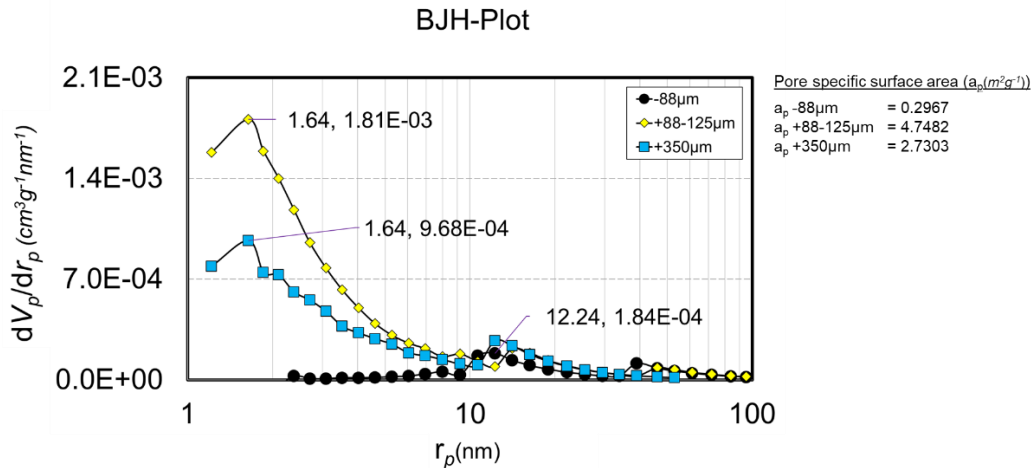
Figure 4-29. BJH analysis on a mixture of silica sand from treatment at 750ºC, 1.5 U$_{mf}$

4.3.9.3 Pore measurement on a mixture of silica sand at T= 800ºC, 1.5 U$_{mf}$

Measurement was started from -88 µm with the highest peak of pore radius was 1.64 nm and pore volume equaled to 4.12E-04 cm^{3}g^{-1}nm^{-1}. The concentration of pores radius was heterogeneously distributed in the range 1.21 to 95.28 nm with the minimum pore volume was 3.5E-05 cm^{3}g^{-1}nm^{-1} in **Figure 4-30**. The average pore radius from **Table 4-3** was 22.46 nm, and the average pore volume was 1.31E-06 cm^{3}g^{-1}nm^{-1}. While the pore-specific surface area was obtained in the amount of 1.42 m^{2}g^{-1}. Related to pore surface area discussion in normal silica sand at section 4.3.5, specific surface area from

this mixture was higher than the normal state which indicated that accumulation of coating of bed particle surface might be very low.

Measurement of +88-125 µm particle size resulted in the same highest peak of pore radius as the -88 µm mixture of particles which the pore volume was 7.79E-04 $cm^3g^{-1}nm^{-1}$. The average pore radius was the same as the -88µm measurement that average pore volume had increased to become 1.90 m^2g^{-1}. It showed that the accumulation of coating formation on the silica sand surface in this condition was still small. The distribution of pore particles was homogenous, and it was distributed in the range between 4.61 and 95.27 nm.
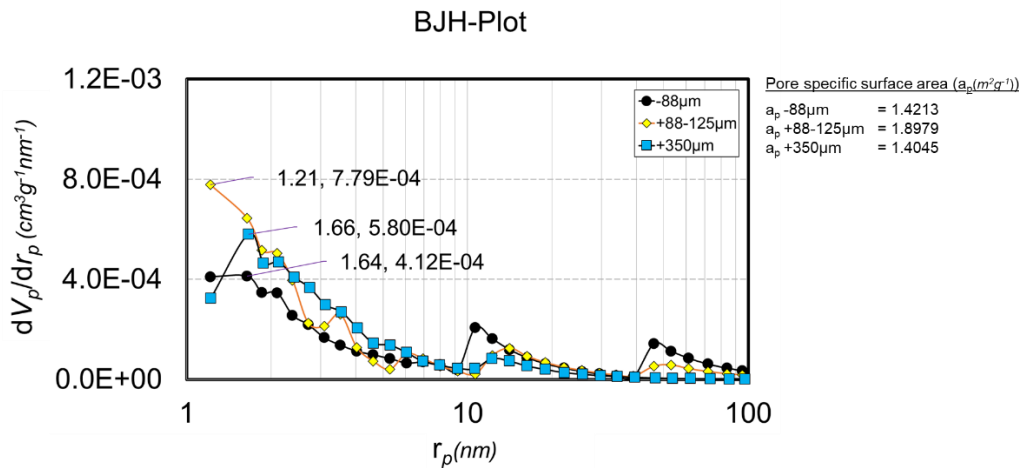
Figure 4-30. BJH analysis on a mixture of silica sand from treatment at 800°C, 1.5 U_{mf}

Analysis on the +350 µm mixture of particles showed that the highest peak of pore radius was1.21 nm and maximum pore volume was 5.80E-04 $cm^3g^{-1}nm^{-1}$. Distribution particle had a similar trend to +88-125 µm size which was stably concentrated between 6.94 and 97.45 nm with pore volume was less than 1.0E-04 $cm^3g^{-1}nm^{-1}$. The average pore radius was 1.40E-04 $cm^3g^{-1}nm^{-1}$. Measurement on the pore-specific surface area had lower coating formation when compared to fluidization with 4.3 U_{mf}, namely 1.41 m^2g^{-1}. It could be concluded that fluidization condition with velocity 1.5 U_{mf} reduced intensity of particles collision and decreased potency and coating formation rate.

4.3.9.4   Pore measurement on a mixture of bentonite at T= 700°C, 1.5 U$_{mf}$

Beginning measurement on -88 µm mixture of bentonite showed that the highest peak was located at pore radius 10.65 nm with maximum pore volume 4.38E-03 cm^{3}g^{-1}nm^{-1} as shown by the curve in **Figure 4-31**. The distribution of pore radius was not homogenous with a minimum pore volume was 3.99E-04 cm^{3}g^{-1}nm^{-1}. The distribution of particles was concentrated at pore volume concentration which was less than 2.00E-03 cm^{3}g^{-1}nm^{-1}. The pore radius was there in the range 1.21 to 3.09 and 22.07 to 53.04 nm. Distribution pore radius was also concentrated in the range 3.53 to 18.94 nm with pores volume between 2.00E-03 and 4.38E-03 cm^{3}g^{-1}nm^{-1}. **Table 4-3** showed that the average pore radius was 14.22 nm with the average pore volume concentration was 2.93E-03 cm^{3}g^{-1}nm^{-1}. The pore-specific surface area was high enough, namely 18.27 m^{2}g^{-1}. So, the accumulation of coating in this condition was likely very small.

Measurement on +125-177 µm, as the sieved particle with the highest mass, showed that the highest peak of pore radius was 9.23 nm with pore volume 4.64E-03 cm^{3}g^{-1}nm^{-1}. The average pore radius was 18.43 nm with pore volume 2.49E-03 cm^{3}g^{-1}nm^{-1}. Distribution pore size was highly concentrated in high pore volume concentration in the range of pore radius from 1.21 to 29.50 nm with pore volume from 1.00E-03 to 5.00E-03 cm^{3}g^{-1}nm^{-1}. The small amount of distribution size was concentrated in the range of radius between 33.81 and 71.90 nm with pore volume less than 1.00E-03 cm^{3}g^{-1}nm^{-1}. Measurement on the pore-specific surface resulted in a high enough value around 20.55 m^{2}g^{-1}. It showed that accumulation of coating formation on bentonite might be low caused by not so different value with the specific surface area of normal bentonite as mentioned in section 4.3.6.

Measurement for the biggest size bed particle, +350 µm, showed that the highest peak of pore radius was located at 1.64 nm with pore volume 2.99E-03 cm^{3}g^{-1}nm^{-1}. The average pore radius based on that measurement was 15.91 nm with the average pore volume of 9.45E-04 cm^{3}g^{-1}nm^{-1}. The trend of pore particle distribution slowly decreased by increasing pore radius. From which pores radius particle was dominantly accumulated in the range 1.21 until 9.23 nm with pores volume range between 5.00E-04 and 3.00E-03 cm^{3}g^{-1}nm^{-1}. Some pores radiuses had been already concentrated in pores volume less than 5.00E-04 cm^{3}g^{-1}nm^{-1} which their pores radius ranged from 10.65 to 61.31 nm. Pore

specific surface area was 9.41 m^2g^{-1}. It showed the drastic decrement of porosity condition. The coating in this state might be already highly accumulated on the bentonite surface.
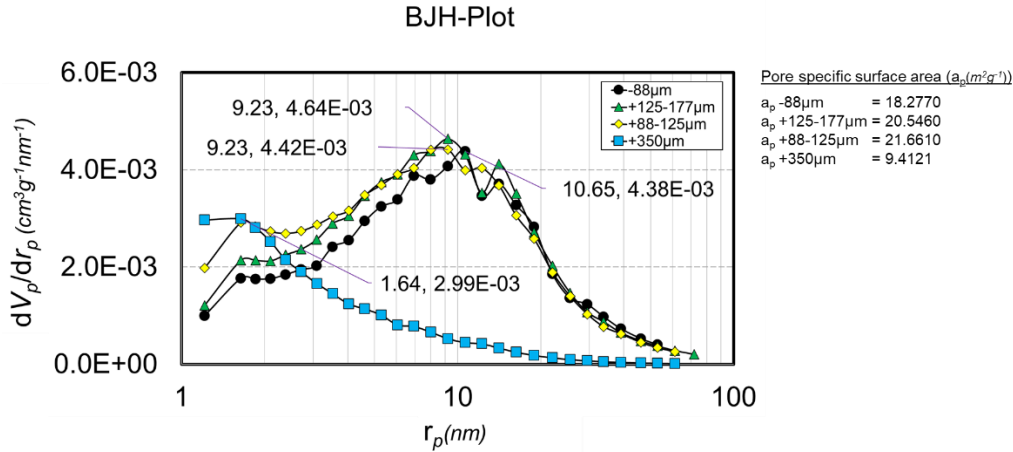
Figure 4-31. BJH analysis on a mixture of bentonite from treatment at 700°C, 1.5 U_{mf}

4.3.9.5 Pore measurement on a mixture of bentonite at T= 750°C, 1.5 U_{mf}

Measurement on -88µm mixture of bentonite at 750°C treatment showed that the highest of peak radius and pore volume in **Figure 4-32** were located at coordinate 10.65 nm and 2.26E-03 $cm^3g^{-1}nm^{-1}$. Another peak having a lower pore volume concentration was 16.29 nm and 2.06E-03 $cm^3g^{-1}nm^{-1}$. Distribution of pore size was mainly concentrated in pore radius 1.21 to 1.64 nm, 2.38 to 4.03 nm, and 25.55 to 29.50 nm in the range of pore volume between 5.0E-04 to 1.0E-03 $cm^3g^{-1}nm^{-1}$. Lower concentration had distributed in several radiuses of pores, as (1). 4.61 to 6.06 nm, 22.07 nm with pores volume between 1.00E-03 to 1.50E-03 $cm^3g^{-1}nm^{-1}$; (2). 6.95 to 9.23 nm, 18.94 nm with pores volume between 1.50E-03 to 2.00E-03 $cm^3g^{-1}nm^{-1}$; and (3). 10.65 to 16.29 nm with pores volume between 2.00E-03 to 2.50E-03 $cm^3g^{-1}nm^{-1}$. The average pore radius from **Table 4-3** was 15.90 nm with the average pore volume was 9.71E-04 $cm^3g^{-1}nm^{-1}$. The pore-specific surface area was already lower than normal bentonite in section 3.4.2, namely 8.10 m^2g^{-1}. It elucidated that few numbers of the agglomerates had been formed and coated bentonite particle surfaces.

On the measurement of +88-125 µm mixture of bentonite, the two highest peaks of pore radius were 1.64 nm and 14.23 nm with pore volumes were 3.12E-03 and 2.66E-03

$cm^3g^{-1}nm^{-1}$. Distribution pore volume gradually decreased with pore radius increment which was mainly concentrated in the range between 2.71 and 7.99 nm; 12.24 nm; and 18.94 nm with pores volume between 1.50E-03 to 2.00E-03 $cm^3g^{-1}nm^{-1}$. The average pore radius was 14.22 nm and the average pore volume was 1.74E-03 $cm^3g^{-1}nm^{-1}$. The pore-specific surface area had been formed in a lower amount than normal bentonite, which was 8.10. The pore-specific surface area from measurement was 14.94 m^2g^{-1} that indicated coating formation had been formed in low concentration.
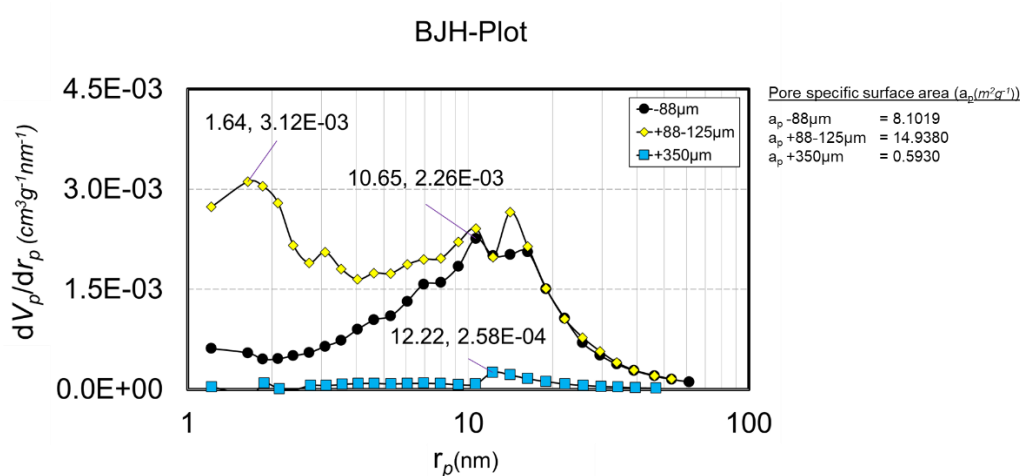
Figure 4-32. BJH analysis on a mixture of bentonite from treatment at 750°C, 1.5 U_{mf}

In the measurement on the largest particle, +350 µm, the highest peak of pore radius was 12.22 nm with pore volume 2.58E-04 $cm^3g^{-1}nm^{-1}$. Distribution pore size was dominated in the range of pore volume between 5.00E-05 to 1.00E-04 $cm^3g^{-1}nm^{-1}$ with pores radius 1.88 nm, 2.74 to 10.63 nm, and 22.11 and 25.69 nm. The averages pore radius and pore volumes were 12.80 nm and 7.66E-05 $cm^3g^{-1}nm^{-1}$ while pore specific surface area showed a very significant decrement becoming 0.59 m^2g^{-1}. It elucidated that accumulation of agglomerates coating bentonite surface had existed in high concentration.

4.3.9.6 Pore measurement on a mixture of bentonite at T= 800°C, 1.5 U_{mf}

The highest peak of pore radius from measurement on the -88 µm mixture of bentonite at 800°C was 10.65 nm with pore volume 1.94E-03 $cm^3g^{-1}nm^{-1}$. Another high peak observed from **Figure 4-33** was 16.29 nm with pore volume 1.75E-03 $cm^3g^{-1}nm^{-1}$.

The distribution of pores was dominantly located in the range of pore volume between 0 and 50E-04 $cm^3g^{-1}nm^{-1}$ having a larger pores radius between 29.50 and 95.28 nm. Another concentration was highly distributed in the range of pore volume between 5.00E-04 and 1.00E-03 $cm^3g^{-1}nm^{-1}$ with the pore radius between 1.21 and 4.61 nm. Some pores radius consisted of 5.29 to 9.23 nm, 14.13 nm, and 18.94 nm had been distributed in the range pores volume between 1.00E-03 and 1.50E-03 $cm^3g^{-1}nm^{-1}$. The average pore radius from **Table 3-3** was 22.46 nm and average pore volume 7.80E-04 $cm^3g^{-1}nm^{-1}$, while pore specific surface area was 7.14 m^2g^{-1}. That specific surface area value was lower than operation at 700 and 750°C using the same sizes. Therefore, the accumulation of agglomerates might have been already formed on the bentonite surface.

On the measurement of the +88-125 µm particle, the highest peak of pore radius was 1.64 nm with pore volume 2.35E-03 $cm^3g^{-1}nm^{-1}$. Distribution pores volume was concentrated between 1.0E-03 to 1.5E-03 $cm^3g^{-1}nm^{-1}$ with pores radius, such as 2.38 to 9.23 nm and 18.94 nm. Several pore radiuses had been concentrated in another range of pore volume 0 to 5.00E-04 $cm^3g^{-1}nm^{-1}$ too. The average pore radius was the same as the -88µm mixture of particles with the average pore volume was 1.03E-03 $cm^3g^{-1}nm^{-1}$. Pore specific surface area of this measurement was 10.49 m^2g^{-1}. Previous measurements at different temperatures resulted in different concentrations of coating. Since this measurement had a lower pore-specific surface value than others, then the highest accumulation of coating formation might be already produced.

Porosity measurement of +350 µm particle resulted in the highest peak of pore radius was 1.64 nm with pore volume 9.17E-04 $cm^3g^{-1}nm^{-1}$. The distribution particle was concentrated in the range of pore volume between 0 to 2.00E-04 $cm^3g^{-1}nm^{-1}$ with the pore radius 6.06 to 46.13 nm. The average pore radius had drastically decreased becoming 12.73 nm which was lower than -88 and +88-125 µm measurements, while the average pore volume was 2.74E-04 $cm^3g^{-1}nm^{-1}$. The pore-specific surface area from measurement was 2.38 m^2g^{-1} which had drastically decreased than results from operation with -88 and +88-125 µm particle. However, it was higher than the result from $4.3U_{mf}$ treatment in section 4.4.6 that indicated that coating formation might be lower on bentonite with $1.5U_{mf}$ treatment. However, collisions among particles in lower velocity application would be weaker than higher velocity. So, degradation of agglomerates would be slower to be eroded during fluidization was taken place. Therefore, the fluidization with low

superficial velocity intensity (1.5 U_{mf}) application had a higher risk to lead larger agglomerates formation than operation with 4.3 U_{mf}.
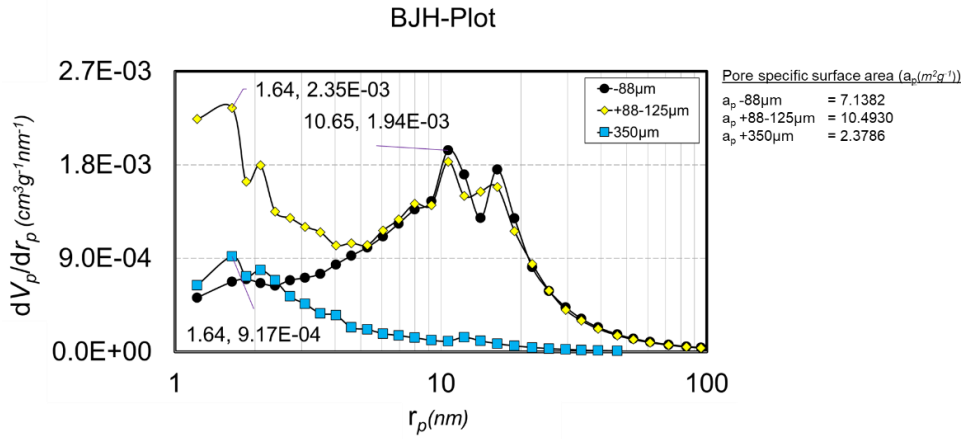
Figure 4-33. BJH analysis on a mixture of bentonite from treatment at 800°C, 1.5 U_{mf}

4.3.10 Microscopic observation on raw material and bed residue particles

The observation of raw material was conducted on +88-125 µm and fine particle sizes. While measurement on bed residue consisted of 3 typical sizes, that were -88, +88-125 or +125-177, +350µm for the largest sieved size, the heaviest mass, and the smallest sieved particle respectively.

4.3.10.1 Microscopic observation on raw material

Silica sand particle had a solid and hard shape with small pores on the surface. That structure in **Figure 4-34** showed that the high endurance of that particle would be difficult to be degraded when physical contact or collision of particle taken place.

+88-125 µm silica sand   +88-125 µm bentonite   EFB ash
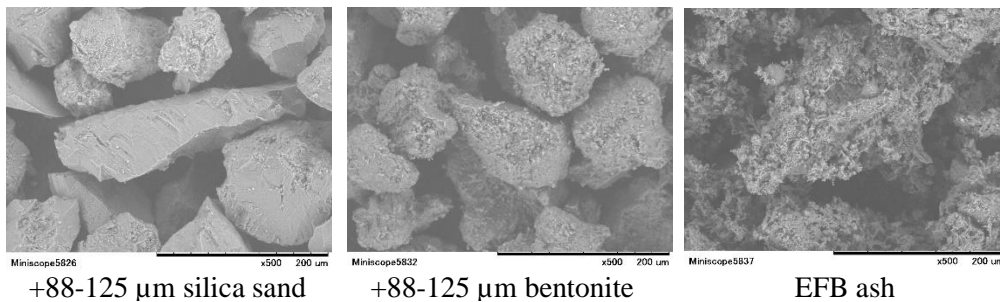
Figure 4-34. SEM images of silica sand, bentonite and EFB ash

Observation on bentonite showed that porous structure on the surface had an unclear shape which made that structure looked weak. While EFB ash structure looked very weak with high porosity. That porosity showed a number of large masses had been lost during the ash formation process at 700°C.

4.3.10.2 Microscopic observation on a mixture of silica sand at T= 700°C with 4.3 U_{mf}

A small coating had been formed on the -88µm mixture of silica sand surface in **Figure 4-35**. While on +88-125 µm, the coating was not clearly formed.

-88 µm

+88-125 µm

+350 µm

Incomplete melting of ash

Incomplete coating of S.sand

+350 µm
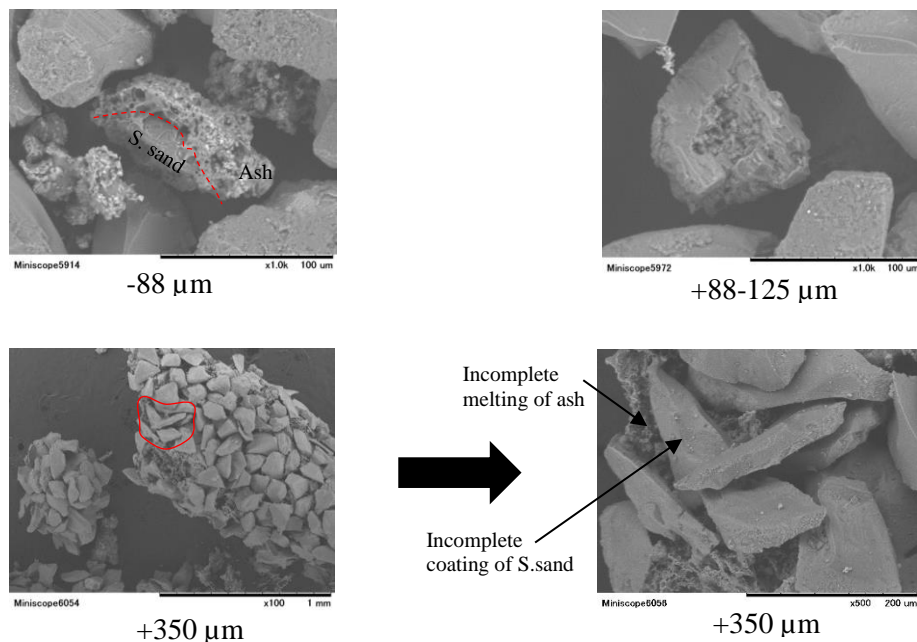
Figure 4-35. SEM images on a mixture of silica sand, from operation at T=700°C, 4.3 U_{mf}

Some incomplete coatings, incomplete melting of ash had been formed and sintered on +350 µm size to form a larger size. Since structure coating was not completely formed, then the agglomerate would be easily eroded and degraded into a smaller structure.

4.3.10.3 Microscopic observation on a mixture of silica sand at T= 750°C with 4.3 U_{mf}

Figure 4.36 showed that small deposits had been accumulated on the silica sand surface. While on +350 µm, that coating had been thicker than measurement at 700°C.

However, the structure of agglomeration was still completely formed which was mainly dominated by an incomplete coating of silica sand and incomplete melting of ash enabling degradation of agglomerates into small sizes again.
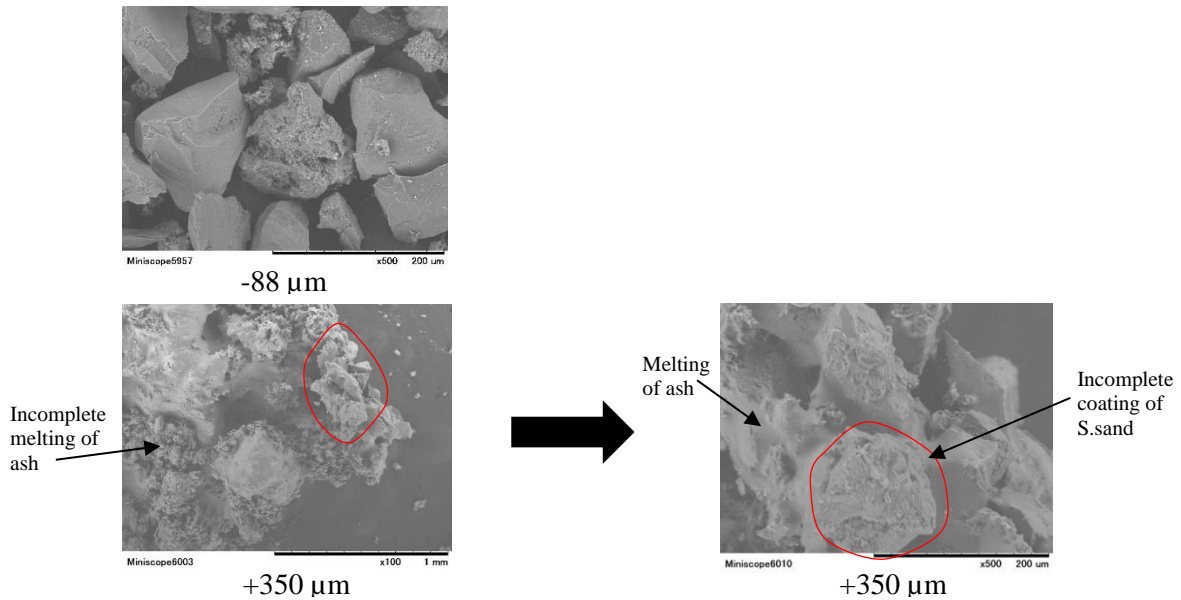
Figure 4-36. SEM images of the mixture on silica sand, from operation at T=750°C, 4.3 U_{mf}

4.3.10.4 Microscopic observation on a mixture of silica sand at T= 800°C with 4.3 U_{mf}

Observation on -88 and +88-125 µm showed that small agglomerates had been deposited on silica sand surface with very low concentration, but on +350 µm was bound completely. Most silica sand surfaces had been coated by agglomeration coming from EFB ash which had reacted, melted, and adhered completely on that surface. **Figure 4-38** showed that there were some bright layers between silica sand and ash border that showed innermost layer formation as the strongest form of alkali-alumina silicate reaction consisted of potassium, alumina, and silica components.

+350 µm   +350 µm
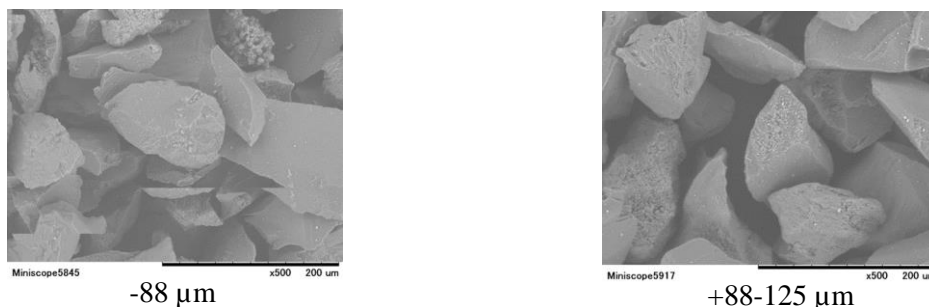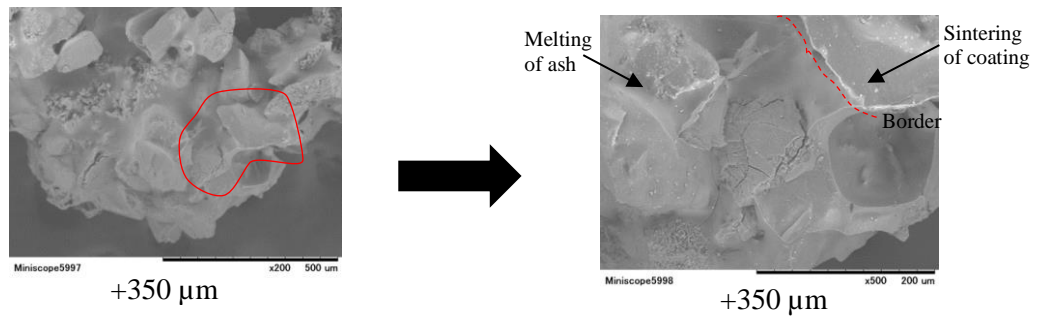
Figure 4-37. SEM images on a mixture of silica sand, from operation at T=800°C, 4.3 U_{mf}

4.3.10.5 Microscopic observation on a mixture of bentonite at T= 700°C with 4.3 U_{mf}

In this observation, the structure of bentonite was still clearly observed and large agglomerate formation in this figure was not formed.
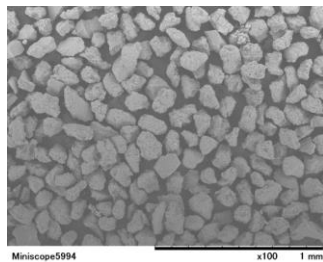
All size

Figure 4-38. SEM images on a mixture of bentonite, from operation T=700°C, 4.3 U_{mf}

4.3.10.6 Microscopic observation on a mixture of bentonite at T= 750°C with 4.3 U_{mf}

Some agglomerates had been formed on bentonite surface but insignificant as in **Figure 4-39**. It showed that most of the bed particles likely could be fluidized well in the bubbling column.

+88-125 µm
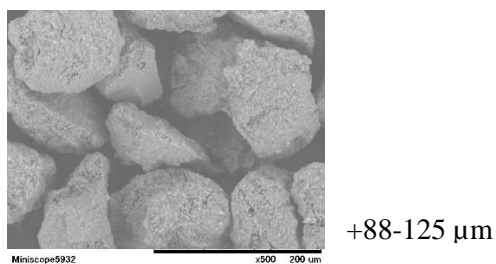
Figure 4-39. SEM images on a mixture of bentonite, from operation at T=750°C, 4.3 U_{mf}

4.3.10.7 Microscopic observation on a mixture of bentonite at T= 800°C with 4.3 U$_{mf}$

Analysis of particles -88 and +88-125 µm showed that some small agglomerates had been contained on bentonite surfaces, but their concentrations were still insignificant. However, thick coatings had been formed on +350 µm size. In **Figure 4-40**, both EFB ash and bentonite shapes were difficult to be identified because those bindings had been formed completely. However, in some spots of large agglomerates, there were ashes in some spots which were still formed in highly porous form and still not melted on bentonite surface. While the other spots looked melted completely. The complete coating would lead to achieving strong binding between condensed ash and bentonite. Therefore, since the coating formation on bentonite was not complete as silica sand, then the stickiness of largely agglomerated bentonite was likely to be weaker than silica sand in the same operation condition, section 4.3.10.4.

-88 µm

+88-125 µm

+350 µm

+350 µm
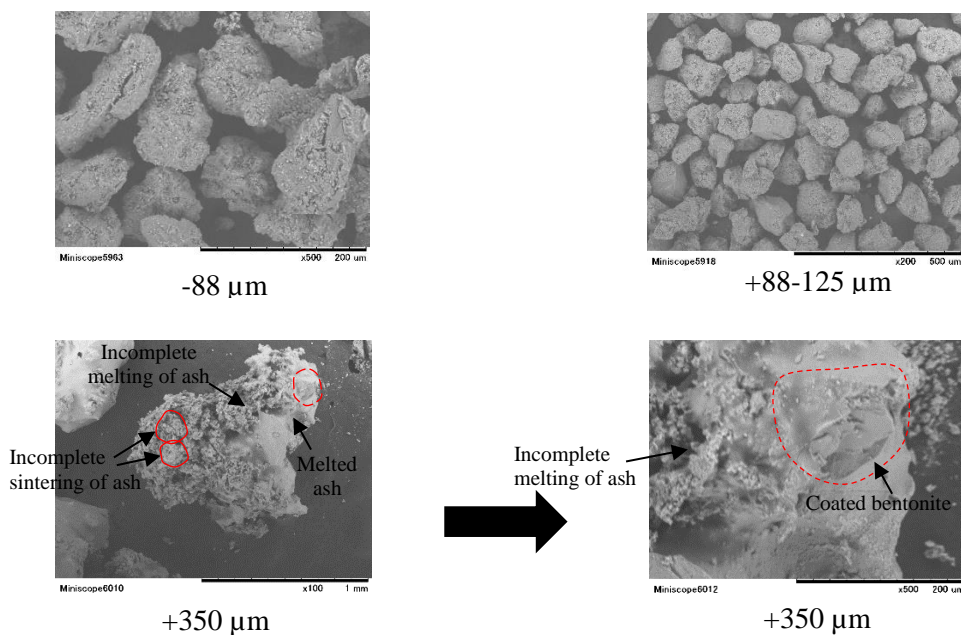
Figure 4-40. SEM images on a mixture of bentonite, from operation at T=800°C, 4.3 U$_{mf}$

4.3.10.8 Microscopic observation on a mixture of silica sand at T= 700°C with 1.5 U$_{mf}$

Observation on -88 and +88-125 µm showed that those characteristic surfaces looked clear and almost the same as the initial condition of silica sand before treatment. Therefore, fluidization would be possible to run well if the condition of bed particles were

like this state, **Figure 4-41**. On the +350 µm, the agglomeration had been formed on the silica sand surface where some spots on the silica sand surface were not completely coated by silicate products.
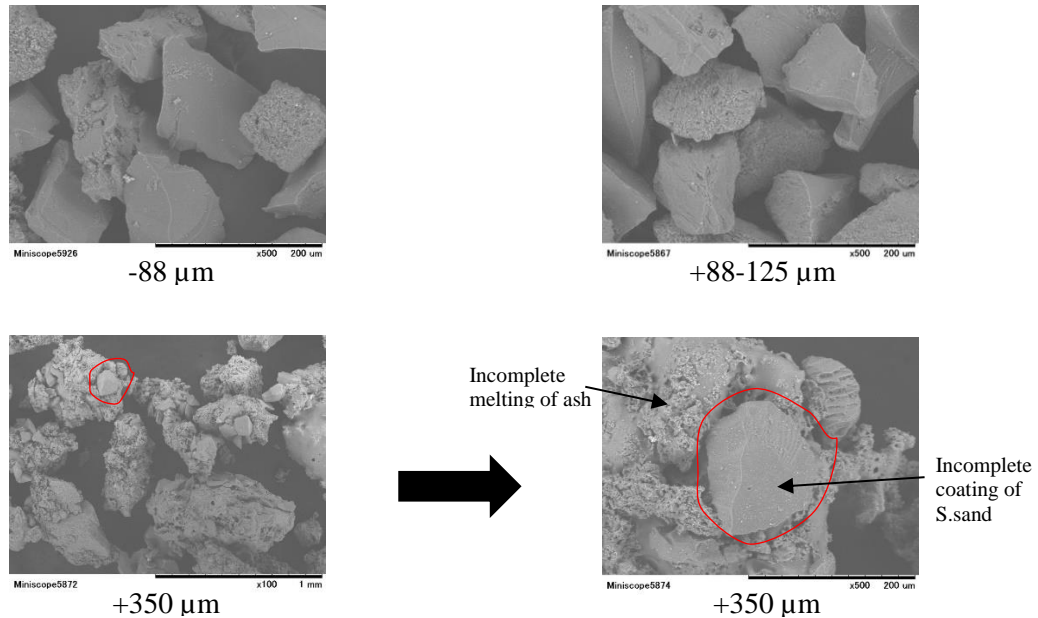
Figure 4-41. SEM images on a mixture of silica sand, from operation at T=700°C, 1.5 U_{mf}

This result was different when compared to analysis in the same condition but in different velocities (4.3 U_{mf}) in section 4.3.10.2. From which, the effect of higher velocity would decrease larger coating formation. Therefore, defluidization state would be likely faster to be formed with velocity 1.5 U_{mf}.

4.3.10.9 Microscopic observation on a mixture of silica sand at T= 750°C with 1.5 U_{mf}

On the -88 µm mixture of silica sand, some small agglomerates had been poorly coated on some silica sand. Some deposits had also been accumulated on the +88-125 µm surface. However, both sizes looked still possible to be fluidized as in the normal state. Analysis on +350 µm showed that most silica sand surfaces had been coated by silicate layers. Compared to the agglomeration process with higher fluidization intensity 4.3 U_{mf}, then agglomeration in this structure looked stronger to be degraded during fluidization. EFB

ashes still had a porous structure, and it looked as if they did not melt completely with silica sand.
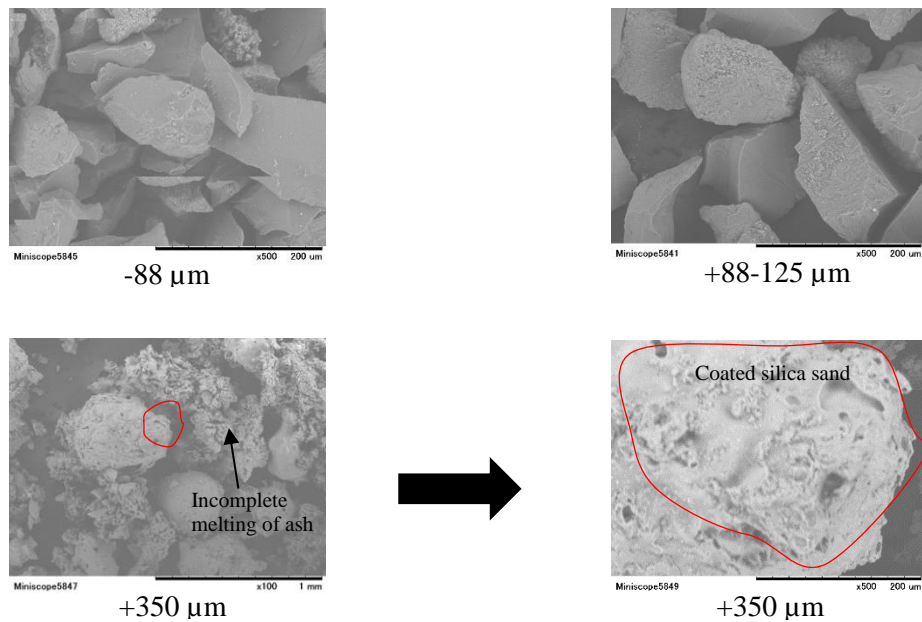
Figure 4-42. SEM images on a mixture of silica sand, from operation at T=750°C, 1.5 U_{mf}

Compared to the agglomeration process with higher fluidization intensity 4.3 U_{mf}, then agglomeration in this structure looked stronger to be degraded during fluidization. EFB ashes still had a porous structure, and it looked as if it did not melt completely with silica sand. So, in this condition complete agglomeration was only formed in some spots making all of the agglomerates in that figure might be not so strong as silica sand. However, application lower velocity would inhibit the degradation process of agglomerates making the coating looked bigger.

4.3.10.10 Microscopic observation on a mixture of silica sand at T= 800°C with 1.5 U_{mf}

Different from the previous measurement with 4.3 U_{mf}, several flakes in **Figure 4-43** had been accumulated on the -88 µm particle surface where the shape of deposits looked solid, hard, and strong. Observation on +88-125 µm showed that small deposits had been formed but not as many as -88 µm. While on +350 µm, the coating had been completely formed where the concentration of ash and silica sand had been mixed

completely even though incomplete coating was still available in some spots. The effect of lower velocity would minimize particle collision and made some coatings that were not homogenously formed on the surface.
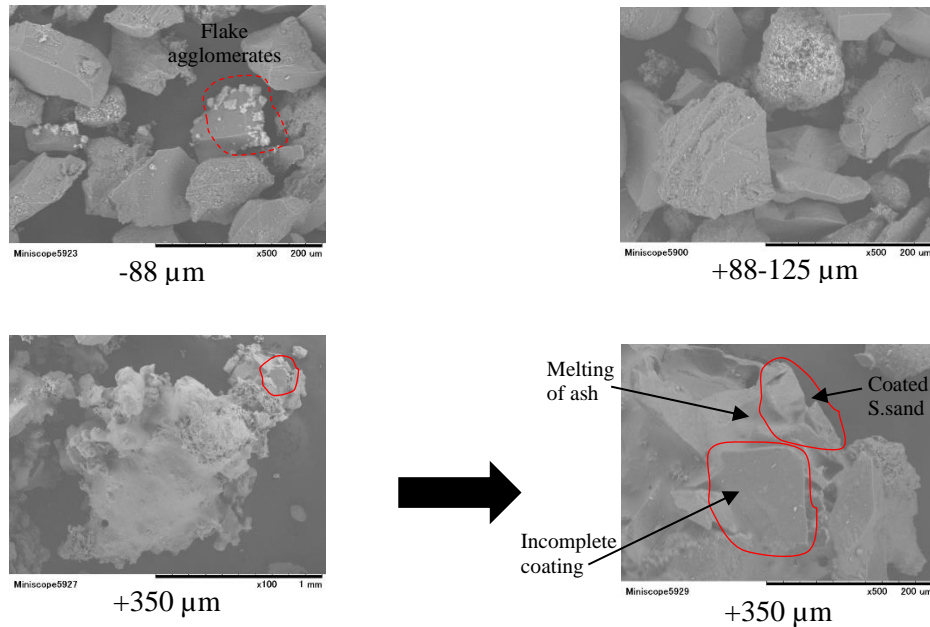
Figure 4-43. SEM images on a mixture of silica sand, from operation at T= 800ºC, 1.5 U_{mf}

4.3.10.11 Microscopic observation on a mixture of bentonite at operation 700ºC with 1.5 U_{mf}

Observation on -88 and +125-177 µm showed a very low number of agglomerates had been accumulated on their surfaces. It was different from the +350 µm observation showing that large agglomerates had mostly coated all of the bentonite surfaces. However, that structure looked weak with large porous. Condensed ashes were not melted completely on bentonite. Therefore, the bentonite and ash still could be distinguished based on shape differences in **Figure 4-44** which were still clear enough to be observed visually. The thickness of agglomerates was high. It might be caused by the low-velocity intensity used in the process. It made the agglomerates more difficult to be degraded during the fluidization process.
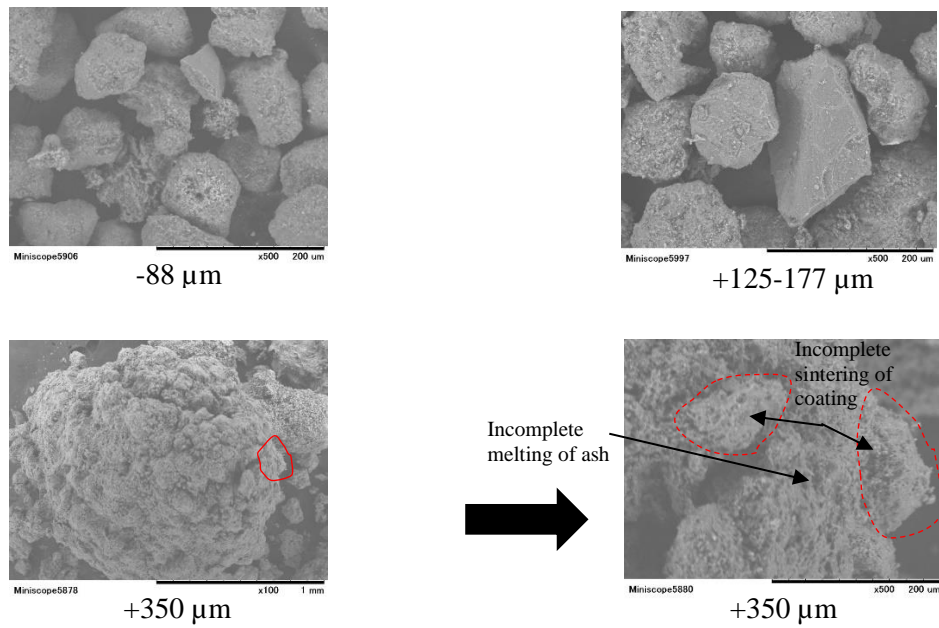
Figure 4-44. SEM images on a mixture of bentonite, from operation at T= 700°C, 1.5 U_{mf}

4.3.10.12 Microscopic observation on a mixture of bentonite at T= 750°C with 1.5 U_{mf}

Similar to the operation at 700°C, accumulated agglomerates on particle -88 and +88-125µm looked too small but the sintering of silicate at operation 750°C and coating formation on the surface increased. The condition of those particles in this process as shown in **Figure 4-45**.
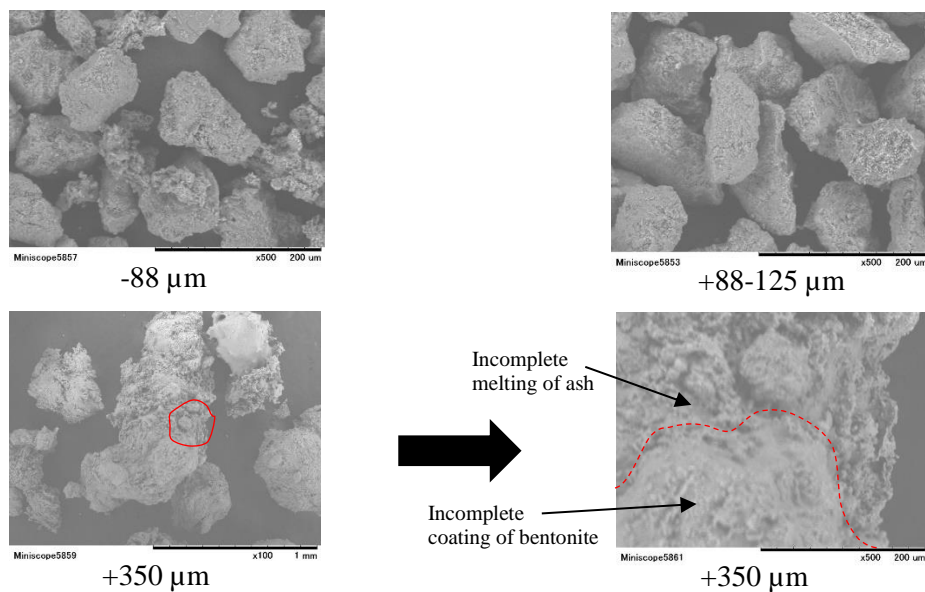
Figure 4-45. SEM images on a mixture of bentonite, from operation T= 750°C, 1.5 U_{mf}

4.3.10.13 Microscopic observation on a mixture of bentonite at T= 800°C with 1.5 U$_{mf}$

The particle with sizes -88 and +88-125 µm showed the similar condition to operations at 700 and 750°C. In **Figure 4-46**, most of the ashes had been completely melted on bentonite surface at temperature 800°C to contribute to the strong and hard agglomerate structures formation as shown by the +350 µm figure.
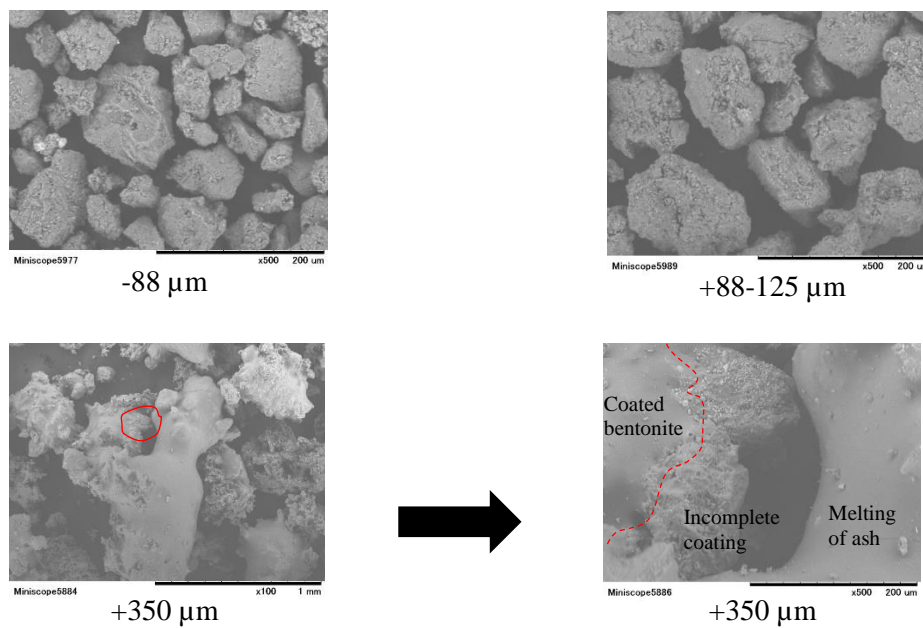
Figure 4-46. SEM images on a mixture of bentonite, from operation at T=800°C, 1.5 U$_{mf}$

Condensation of ashes had largely formed, and it had been bound to create silicate binding on bentonite surface in the form of complete and incomplete coatings of bentonite surface areas.

4.3.11 Distribution of condensed aerosols and alumina related to the uncoated formation of agglomerates

The measurement uses SEM-EDX was carried out on bed residue as a mixture of silica sand and a mixture of bentonite from thermal treatment to obtain data regarding the surface structure and morphological feature based on analysis in some points on sample surfaces. **Table 4-4 and 4-5** explained elemental mass concentration from raw data which would be analyzed in section 4.3.11.1 and 4.3.11.2

Table 4-4 Mass of elements in mixture of silica sand for spot 1 (left) and 2 (right)

Elements (wt%)	Point 1	Point 2	Point 3	Point 4
O	40.54	44.27	52.06	36.73
Na	0.46	0.40	0.66	0.50
Mg	--	0.32	7.82	0.32
Al	5.10	7.03	23.57	8.09
Si	30.96	23.72	1.30	30.10
P	0.54	0.22	--	0.74
K	19.47	21.51	13.26	21.53
Ca	1.38	1.32	1.03	0.90
Fe	1.57	1.22	0.31	1.08

Elements (wt%)	Point 1	Point 2	Point 3	Point 4	Point 5
O	36.996	25.968	37.830	37.944	39.924
Na	0.662	0.622	0.738	1.109	0.931
Mg	--	0.366	0.303	0.314	0.232
Al	11.460	7.934	11.209	12.091	11.734
Si	28.273	23.793	28.418	29.961	27.962
P	1.231	0.470	0.711	1.039	0.932
K	14.066	23.435	12.974	10.738	11.280
Ca	6.363	8.96	6.419	5.722	6.183
Fe	0.949	8.452	1.398	1.082	0.822

Table 4-5 Mass of elements in a mixture of bentonite for spot 1 (left) and 2 (right)

Elements (wt%)	Point 1	Point 2	Point 3	Point 4	Point 5
O	58.215	42.728	44.904	50.985	56.062
Na	1.688	0.613	0.369	1.337	1.002
Mg	1.388	0.774	0.307	1.259	1.572
Al	3.68	2.16	0.521	2.983	6.353
Si	28.336	47.514	47.666	34.878	30.258
P	2.809	2.438	2.880	2.403	--
K	1.377	1.933	2.299	2.011	1.602
Ca	0.516	0.192	0.160	1.094	1.520
Fe	1.991	1.648	0.894	0.453	7.569

Elements (wt%)	Point 1	Point 2	Point 3	Point 4	Point 5
O	48.642	50.306	37.163	39.902	23.286
Na	0.793	1.758	0.815	0.988	0.962
Mg	0.497	3.064	3.975	2.717	2.824
Al	1.350	7.332	7.632	5.597	8.801
Si	43.340	29.538	35.383	38.137	44.032
P	2.579	--	1.029	1.064	--
K	1.718	1.655	1.978	2.030	2.546
Ca	0.336	--	--	0.276	--
Fe	0.745	6.347	12.025	9.289	17.549

Measurement of both mixtures of particles was carried out on two different spots on that sample surface. Kinds of samples were obtained from the bubbling fluidization process with $4.3U_{mf}$ fluidization intensity at 800°C. It considered that alkali-silicate or alkali-alumina silicate reaction between EFB ash and sand or bentonite was completely much higher formed in that condition. Furthermore, operation at 800°C made the agglomeration form much clearer to be observed.

4.3.11.1 Mapping elements on +350 µm sieved mixture of silica sand at T= 800°C, 4.3 U_{mf}

Figure 4-47 showed that silica sand surfaces had mostly completed being covered by coatings. The structure of the coating looked solid, in which only a few areas of the coating layer were not completely covered. When compared to the EFB ash structure based on microscopic observation in section 4.3.10.1, the amount of ash that stuck on silica sand surfaces had been already formed in a different structure. It had completely melted and tightly tied over silica sand surfaces.

Analysis on a mixture of silica sand structures was elucidated by **Figure 4-47**, in which the sampling was carried out on 2 different spots, as spots 1 and 2. Each spot consisted of some detected points, in which points 1 to 4 were for spot 1 and point 1 to 5 were for spot 2. Information of those points was as followed: (*Area 1*), as locations of

silica sand which had mostly coated (i.e. spot 1-point 1, 2 and 4; spot 2-point 1,2 and 3 too).
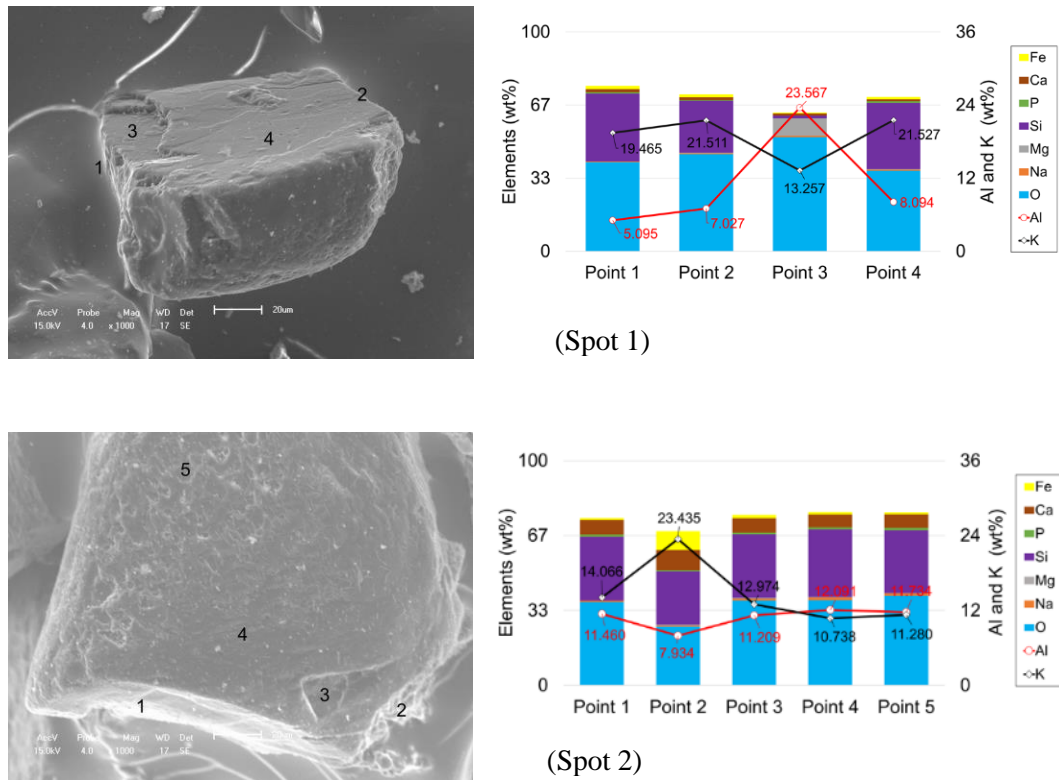
(Spot 1)

(Spot 2)

Figure 4-47. Mapping mixture of silica sand elements on spots 1 and 2

While (*Area 2*), as locations were not completely coated (i.e. spot 1-point 3; spot 2-point 4 and 5). Elemental analysis was carried out by considering the main elemental components that built up silica sand structure based on XRF and CHN measurements data in Chapters 2 and 3 discussions. Those main elements were K, Al, Na, Mg, Si, P, Ca, Fe, and O. This measurement focused to compare the concentration between Al and K which would strongly affect alkali alumina silicate reaction leading to agglomerates formation.

As shown in reactions 1 to 11, the presence of alumina concentration would be involved in binding formation if that structure was available in alumina silicate form. Since all points contained aluminum elements, thus all reactions would result in alkali-alumina silicate products. It was relevant to the results which had shown those peaks in previous XRD measurement. The binding would be much stronger when alumina

decreases leading to form stickier agglomerates. Based on **Table 4-4** and the curve of **Figure 4-47**, the concentration of K was high in *Area 1* in the range 12.97 to 23.44 wt% but having low Al concentration between 5.10 and 11.46 wt%. *Area 1* was proven by bright spots in **Figure 4-47 (a) and (b)**. Meanwhile, low K but high Al concentrations in the range of 10.74 to 13.26 wt% and 11.73 to 23.57 wt% respectively were shown in *Area 2* which had been dominated by dark spots. Therefore, the coating layers around *Area 2* looked slight.

4.3.11.2 Mapping elements on +350µm sieved mixture of bentonite at T= 800°C, 4.3 U_{mf}

Mapping of elements in **Figure 4-48** showed coating formation on bentonite surfaces. That formation looked weak which the coatings were not adhered to and melted perfectly. When compared to the agglomerated mixture of silica sand, coating layers were not homogenously distributed on bentonite.
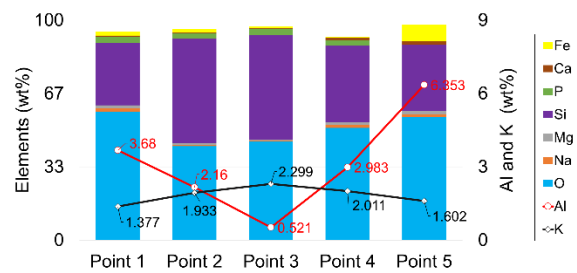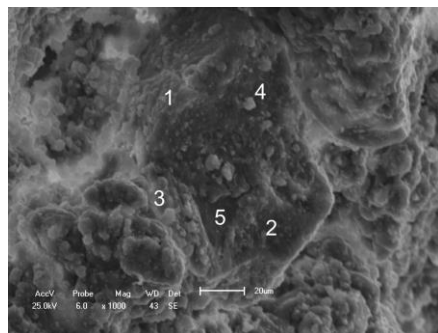
(Spot 1)
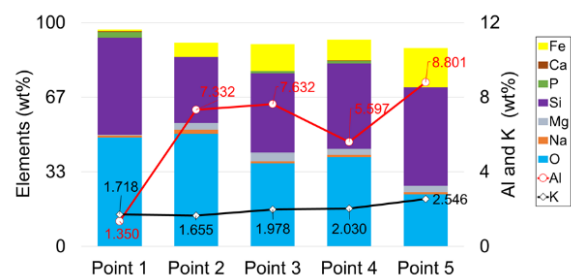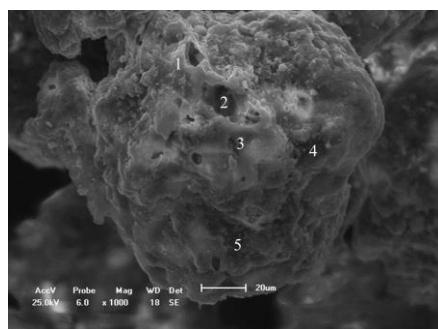
(Spot 2)

Figure 4-48. Mapping mixture of bentonite elements on spot 1 and 2

It could be seen in that figure that different thicknesses had dominated bentonite surfaces. As mentioned in chapter 2 and 3, application high superficial velocity with 4.3 U_{mf} fluidization intensity on the agglomerated mixture of bentonite would be easier to be degraded than a mixture of silica sand. It was caused by all binding formation highly contained aluminum as an inhibitor of agglomeration. For this reason, the binding became weak and easy to be eroded by collision during fluidization was taken place. Some strong coatings just formed in some spots on bentonite having few aluminum contents. It would gradually increase by ash concentration increment to form incomplete coatings which would be sintered to form large agglomerate particles having high porosity.

This measurement was carried out to clear up that reason by samplings on two different spots on bentonite surfaces based on the same definitions as section 4.6.1. Those samplings consisted of *Area I* for spot 1 consisted of points 3 and 6, while spot 2 was for point 1. *Area II* referred to spot 1 consisted of points 1,2, 4, and 5, while spot 2 was for points 2,3,4, and 5.

In the curve of **Figure 4-48,** the high of potassium in *Area 1* was marked by bright spots as coating layers consisted of K concentration in the range 1.72 to 2.30 wt.% and Al concentration between 0.52 and 1.35 wt.%. The dark spots showed slight coating on bentonite surfaces that consisted of K between 1.38 and 2.55 wt.% while Al concentration between 2.16 and 8.80 wt.%.

4.4 Agglomeration mechanisms of silica sand or bentonite particles with EFB ash

Defluidization of bed particle had been formed on silica sand and bentonite at 800°C and 1.5 U_{mf} superficial velocity treatment. However, on silica sand, it had only been formed in treatment with velocity 4.3 U_{mf}. Therefore, the increase of velocity significantly supported to inhibit defluidization state on bentonite. Operation at 800°C had a higher risk to form melting of ash because the amount of molten EFB ash that had been dominated by KCl would be easier to melt at a temperature between 750 and 800°C. That melting product would form larger agglomerates simultaneously with the sintering of coatings processes. Therefore, the large agglomerates had been mostly formed on treatment at 800°C. Theoretically, alkali-alumina silicate formation only involved a reaction between bentonite particle and alkaline in the form of KCl, K_2SO_4, and KOH.

However, the kind of alkaline might be involved in that reaction was KCl only as shown by XRD measurement in **Figure 4-6** resulting in some products such as kalsite (KAlSiO4), leucite (KAlSi$_2$O$_6$), albite (NaAlSi$_3$O$_8$), and anorthide (CaAl$_2$Si$_2$O$_8$).

In XRD analysis, the increase of temperature would also decrease the intensity of the initial silica peak contained in quartz or cristobalite as the main element of bed particles. While temperature increment stimulated some formations of alkali silicate and alkali alumina silicates peaks which were highly affected by the loss of bentonite structure such as hydroxyl at temperature 450 to 500°C. That hydroxyl might be previously bound up to alkaline like potassium and natrium contained in the initial bentonite. When dihydroxylation was formed by 800°C, eutectic alumina silicate would be formed to attain the balance of chemical structure, as sanidines (K(Si$_3$Al)O$_3$) and albite (NaAlSi$_3$O$_8$). During agglomeration formation, the quartz of bentonite was still much higher peak intensity than silica sand with temperature increment at 800°C as shown in **Figures 4.9, 4.12, 4.15,** and **4.18**. It showed that a small amount of silicate which was also contained in bentonite had reacted with alkali metals in the lower amount as shown in +350μm mixture of silica sand particles both 4.3 and 1.5 U$_{mf}$ application. Therefore, measurement on bentonite resulted in low agglomerates formation. It was proven by the comparisons of the peak intensity of quartz and cristobalite in bentonite which was still higher than silica sand particles.

Distribution pores on silica sand were dominated by a radius of 1.64 nm, while 10.65 nm on bentonite. The increase of temperature significantly decreased the pore volume and pore specific surface on both particles after thermal treatment by 800°C as shown in **Figures 4.19** and **4.20**. The coating layer had been formed after feeding some ashes. Comparison of pore volume on both mixture of bed particles after treatment at 800°C as shown in **Figure 4.24, 4.27, 4.30, 4.33** were also insignificant that indicated the high potency of agglomeration formation having larger and stronger appearance had been formed.

The distribution of Al element on a mixture of bed particles had been shown in **Figures 4.47** and **4.48** by SEM-EDX measurement in which some uncoated spots referred to a higher concentration of aluminum than potassium**.** That elemental mapping showed that most silica sand surfaces had been completely coated by agglomerates. Based on elemental composition, the concentration of potassium was roughly higher than that of

aluminum was. Incomplete coatings indicated the presence of high Al concentration could inhibit alkali-alumina silicate reaction on bentonite surface. Therefore, those coatings were only formed on the spots having low Al concentration. Since the coatings were incomplete, it made the structure of agglomerates on bentonite were weaker and easier to be degraded than silica sand by high-velocity application.
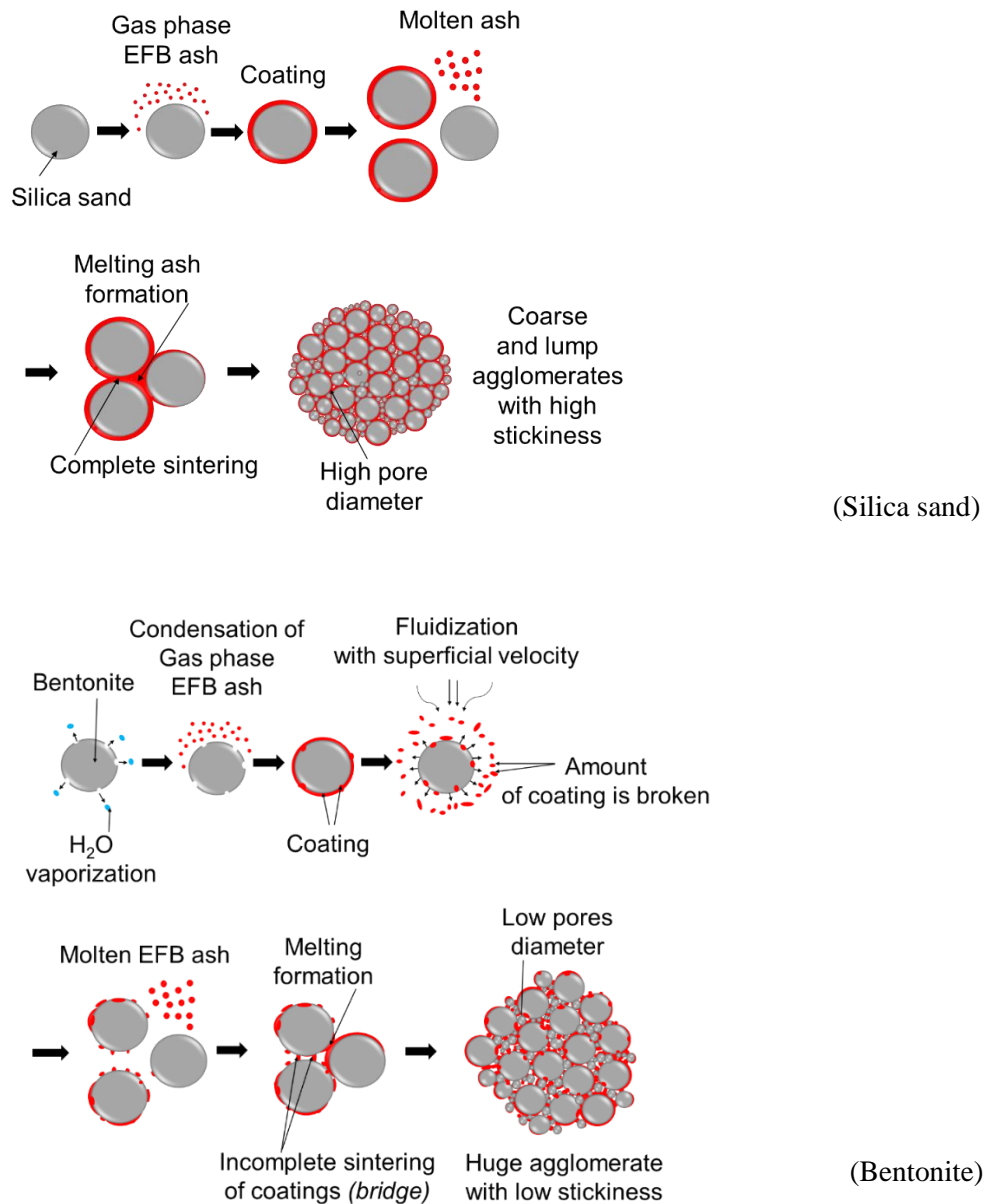

(Silica sand)

(Bentonite)

Figure 4-49 Agglomerate formation scheme of silica sand and bentonite during fluidization in thermal operation

The mechanism of agglomeration formation on silica sand and bentonite was illustrated by **Figure 4-49**. During heating up, silica sand particle was stable but dehydration amount of water in bentonite had carried out. Thermal treatment by 750°C would completely remove it to remain empty pores of water and increase pore specific surface area in bentonite during that treatment which was relevant to measurement as shown in **Table 4-1**. When condensation of aerosol took place, alkaline concentration in aerosol form would be bound on silica sand surface to form coating layer which the thickness would gradually increase by increasing temperature because Al concentration was low and had equal homogenous distribution. It would be different for bentonite which condensation was not only formed on some spots of the surface but also in empty pores space. Since Al concentration in bentonite was high, the structure of the coating might be weak. Some spots with low Al concentration kept withstanding to form gradual coating and sintering of coating process, leading to produce large agglomerates. However, since those agglomerates were partially concentrated in some spots, then the structure was not so strong like the agglomerated mixture of silica sand which all surfaces had been coated completely. It made agglomerated bentonite easy to be degraded during fluidization into primary or smaller size again. This phenomenon was proven by comparing the bubbling fluidization with 4.3 and 1.5 U$_{mf}$, from which the higher superficial velocity application at 800°C made the fluidization on agglomerated bentonite particles was possible by applying high superficial velocity.

4.5   Conclusion

Analysis of a mixture of bed particles showed that peak concentration of silica in the form of quartz or cristobalite would significantly decrease during silicate reaction involving alkali from EFB ash, alumina, and silica in silica sand or bentonite particles at treatment 800°C. It was relevant to the comparison of microstructure between silica sand and bentonite structures showing that pore-specific surface area on agglomerate should increase during the increasing of particle size. However, pore measurement decreased at 800°C that indicated bed particle surfaces had been filled and bound out by the amount of ash. The presence of Aluminum, based on mapping elements on bed particle surfaces, had a significant contribution to inhibit agglomeration, from which bentonite particle had

higher Al concentration, even though that element distribution was not homogenous on bentonite surface. Therefore, microstructure observation on bentonite at treatment 800ºC showed incomplete coating and sintering phenomena supporting the benefit of bentonite application in fluidization.

References

Sabiha, A.B., and Kheloufi, A., and Boutarek, N., and Aissa, K., and Fouad, K. (2016). *Characterization of silica quartz as raw material in photovoltaic applications*. 1758. 030043. 10.1063/1.4959439.

Valchev, A., and Marinov, M., and Grigorova, I., and Nishkov, I. (2011). *LOW IRON SILICA SAND FOR GLASSMAKING*.

Mahdaoui, T., and Bouaouadja, N., and Madjoubi, A., and Bousbaa, C. (2007). *Study of the Effects of Sand Blasting on Soda Lime Glass Erosion*. International Review of Mechanical Engineering. 1. 11.

McLaws, I.J. (1971): U*ses and specifications of silica sand;* Research Council of Alberta, RCA/AGS Earth Sciences Report 1971-04, 67 p.

Bowdish, F.W. (1967): *Opportunities in the beneficiation of feldspathic sands*; Proc.3rd Forum on Geology of Industrial Minerals, Geol. Surv. Kansas. Spec. Distrib. Pub.34, p.126-37

Weems, J.B. (1903). *Chemistry of Clays*. Iowa Geological Survey Annual Report, 14, 319-346. https://doi.org/10.17077/2160-5270.1076

Al Ani, T., and Sarapää, O. (2008). *Clay and clay mineralogy*. Geological Survey of Finland, Report M19/3232/2008/41, Espoo.

Bailey, SW, 1980a, *Structures of layer silicates*. In: Brindley GW & Brown G ed. Crystal structures of clay minerals and their X-ray identification. London, Mineralogical Society, pp 1–123. Available at: http://www.minsocam.org/msa/collectors_corner/arc/nomenclaturecl1.htm.

Bailey SW. and Chairman, 1980b, *Summary of recommendations of AIPEA [Association International Pour lettuce des Argyles nomenclature committee on clay*. Am Mineral, 65: 1– 7.

Bailey, S.W., 1988. *Odinite, a new dioctahedral-trioctohedral Fe3+-rich 1:1 clay mineral*: Clay Minerals, v. 23, p. 237–247.

Moore, D. and R.C. Reynolds, Jr., 1997. *X-Ray Diffraction and the Identification and Analysis of Clay Minerals*, 2nd ed.: Oxford University Press, New York.

Murray H., 2002. *Industrial clays case study. Report of the Mining, Minerals and Sustainable Development Project vol. 64*, International Institute for Environment and Development and World Business Council for Sustainable Development, UK.

Haydn H. Murray. *Developments in Clay Science*, volume 2, Elsevier Science, Amsterdam, 2007, 180 + viii pp. ISBN-13: 978-0-444-51701-2, ISBN-10: 0-444-51701-4.

Öhman, M., and Nordin, A. (2000). *Bed Agglomeration Characteristics during Fluidized Bed Combustion of Biomass Fuels*. Energy & Fuels - ENERG FUEL. 14. 10.1021/ef990107b.

Boström, D., and Grimm, A., and Boman, C., & Björnbom, E., and Öhman, M. (2009). *Influence of Kaolin and Calcite Additives on Ash Transformations in Small-Scale Combustion of Oat*. Energy & Fuels - ENERG FUEL. 23. 10.1021/ef900429f.

Steenari, B., and Lundberg, A., and Pettersson, H., and Wilewska-Bien, M., and Andersson, D. (2009). *Investigation of Ash Sintering during Combustion of Agricultural Residues and the Effect of Additives*. Energy & Fuels - ENERG FUEL. 23. 10.1021/ef900471u.

Li, X., and Gao, Z., and Fang, S., and Ren, C., and Yang, K., Wang, F. (2019). *Fractal Characterization of Nanopore Structure in Shale, Tight Sandstone and Mudstone from the Ordos Basin of China Using Nitrogen Adsorption*. Energies. 12. 583. 10.3390/en12040583.

Chapter V

General conclusion

5.1. Conclusion

Agglomeration and defluidization particles are important issues resulted from the alkali-silicate reaction involving alkaline of Empty Fruit Bunch (EFB) ash and silicon (SiO_2) which are dominantly contained in silica sand and bentonite bed particles. EFB is a solid residue of Crude Palm Oil (CPO) production that is categorized as waste material. One of the treatments to enhance EFB is thermochemical conversion like gasification to convert it to become renewable energy resources and chemicals. In this study, the thermal treatment process was carried out at temperatures 700, 750, and 800°C as selected temperatures to obtain high syngas quality and high efficiency as in similar processes to gasification plant development in Indonesia as the largest producer of CPO in the world. Alkali reaction was dominated by KCl as the dominant component contained in EFB ash as shown from XRD measurement in **Figure 4-6**.

From this study, agglomeration on the bed material surface was determined by the increase of $\overline{\Delta P}_{loss}$ between $\overline{\Delta P}$ resulted from theoretical measurement based on equation 1 and 2 calculation and experimental measurement coming from logging system, and the decrease of $\overline{\Delta P}_{deviation}$ based on equation 3 leading to reach similar differential pressure as fixed bed state indicating the defluidization state had been achieved. The formation of silicate would gradually increase during the increase of operational temperature. **Figure 2-19** showed that the defluidization state on silica sand particle had been reached after the feeding of ashes was 1.55 wt% with fluidization intensity 4.3 U_{mf} at temperature 800°C. While the bentonite still could be fluidized even though with smooth fluidization only. Meanwhile, the defluidization with intensity 1.5 U_{mf} had been reached after total concentration of ashes in fluidized bed were 3.87 and 0.35 wt.% for silica sand and bentonite applications as shown in **Figure 3-12** and **3-24** respectively. It showed that the increase of velocity gave a significant contribution to reducing defluidization formation at operation 800°C. While fluidization kept running normally at operation 700 and 750°C,

decreasing performance was much higher reached with fluidization intensity 1.5 U_{mf} though.

Alkali-silicate product in agglomerated both bed particle mixtures consisted of alkaline, alumina, and silica components as proven by XRD measurement in **Figure 4.7– 4.18,** which the alumina concentration was much higher in bentonite than silica sand. The alkali-silicate formation was proven by decreasing silica peaks like quartz and cristobalite as the main components contained in silica sand or bentonite. The concentration of aluminum in bentonite was distributed heterogeneously, while silica sand was distributed more homogenous on bed material surfaces. Therefore, the whole silicate formation in this study was available in the form of low melting point of eutectic alkali-alumina silicate. High aluminum concentration had contributed to inhibit and avoid the alkali-silicate reaction. However, it was still possible to form silicate formation as a coating on the bed particle surface at low aluminum concentration. The 4.3 U_{mf} superficial velocity application had strongly affected the degradation of the coating. Furthermore, sintering of coating would be difficult to be completely formed caused by the bridge as the platform of the coating was so thin. So, agglomerates from a mixture of bentonite were not so sticky, and it could be easy to be eroded to become similar to the original particle size again. However, some silicates involving silica sand were strongly bound up to each other to build sticky agglomerates which were difficult to be degraded, even though by 4.3 U_{mf} treatment. That sticky agglomerates had been analyzed by agglomeration indicators measurement (I_1-I_3) which showed a very significant difference between the theoretical standard value of agglomeration from equations 3-5 and experiment resulted in Chapters II and III. Bed particle endurance was also analyzed according to elemental mass particle calculation based on equation 6.

Thermal treatment showed that the initial silica sand structure was stable, because of no mass degradation of quartz as the main compound with the stable peak of XRD intensity at temperatures 700 to 800°C as shown in **Figure 4-4**. However, there were few masses degradation and silicates formation on initial bentonite with some decrement of silica intensity peak contained in quartz and cristobalite components as shown in **Figure 4-5**. Therefore, thermal fluidization was important for initial bentonite treatment to avoid melting of bed material process during the heating up process. In the mixture of silica sand, some alkali-alumina silicates had been formed starting from operation at 700 until

800°C in both fluidization intensity 4.3 and 1.5 U_{mf}. While the silicates in a mixture of bentonite had only been formed at operation 800°C with 1.5 U_{mf} velocity.

Measurement of pore size distribution on silica sand showed that there were no significant changes of pore radius and pore specific surface area during operation at 700 to 800°C which most of those changes were lower than bentonite. The significant change was only taking place on the pores volume that would decrease when temperature increased. Meanwhile, the decrease of bentonite pore-specific surface area was significant with temperature increment. The trend would increase at temperature 750°C mainly caused by the loss of water layers. However, it significantly decreased at 800°C mainly caused by melting and crystallization substances to achieve the stability of the initial bentonite structure. Analysis of a mixture of bed residue showed that the larger the sieved mixture of bed size particle was, the lower pore specific surface area resulted in. On the largely sieved bed residue, most of the pores of bed particle had been occupied by coating layer making pore specific surface area increased too. The effect of temperature increment decreased the pore specific surface area caused by sintering of coating and melting of molten EFB ash would completely form. The higher superficial velocity adjustment would simultaneously support to decrease pore specific surface area too. Higher velocity would lead to completely reach direct contact among of bed particles to build coating layer. The coating had been formed in stronger binding formation than lower velocity because the bridge that indicated the pore condition had been strongly formed in that agglomerates.

Observation from SEM measurement showed a significant difference between operations 4.3 and 1.5 U_{mf}. Accumulation of agglomerates on silica sand and bentonite surfaces both -88 and +88-125 µm was small. However, a significant difference could be clearly observed on +350 µm sieved bed residue particles. The images showed accumulated agglomerates coming from sintering of coating and melting of ash were the highest and clearest at temperature 800°C. Some portions in bentonite agglomerates showed partial or incomplete sintering of the coating process, even though the melting of ash was not so different from silica sand.

As mentioned before, the presence of aluminum would give a positive impact to inhibit agglomeration. It was shown by the elemental mapping particle using SEM-EDX in **Figures 4-47** and **4-48**, from which the dark points indicated rich aluminum, but the

bright points were rich with potassium. Most points on the bentonite contained higher Al than K, so the silicates formation was low. Some silicates would be formed in the area that contained lower Al concentrations having weak silicate structures. They were confirmed by XRD measurement for 4.3 and 1.5 U_{mf} superficial velocity at 800°C like kalsilite ($KAlSiO_4$), sanidine ($K(Si_3Al)O_8$), and potassium gallium silicate ($KGaSi_3O_8$) as shown in **Figure 4-12** and **4-18**. Overall measurements based on pressure difference analysis, elemental and component measurement, and microstructure observation between bentonite and silica sand particles showed that the bentonite had better performance to extend longer fluidization state than silica sand according to that capability to keep being fluidized during EFB ash increment that had been accumulated in bed column. The utilization of bentonite bed particles became a promising prospect to be developed and be implemented in the thermal EFB fluidization process both in 4.3 and 1.5 U_{mf} fluidization intensity that ideally operated within temperature 800° and 750°C, respectively. However, since the intensity of velocity application that was needed in the bubbling fluidization system should be high, and application of fluidization velocity should be the same as gasification plant located in Indonesia, so the utilization of 4.3 U_{mf} was preferable and better than 1.5 U_{mf}. Based on comparison between silica sand and bentonite related to the capability to extend fluidization state, then the bentonite had resulted in better performance based on that durability which kept being fluidized in operation until 800°C.

List of presentation and publication non-journal

- Title: Analysis of Particle Circulation Performance during
  Circulating Fluidized Bed (CFB) Conversion Process
  Conference name: 12th International Symposium on Green Energy (ISGE) 2018
  Venue: August 29th-31st, 2018/Ota, Japan
  Activity : Poster presentation

- Title: An Influence of Alkaline Accumulation on Defluidization of a Clay Particle
  Fluidized Bed
  Conference name: The 24th SCEJ Symposium on Fluidization & Particle Processing
  Venue: December 5-7th, 2018/ Hachioji, Japan
  Activity: Poster Presentation and Publication paper

- Title: An Influence of Alkaline Accumulation on Defluidization of a Clay and
  Silica sand Particles Fluidized Bed/ Oral presentation
  Conference name: 第１４回バイオマス科学会議
  Venue: January 16-17th, 2019/ Higashihiroshima, Japan
  Activity: Oral presentation and Publication paper

- Title: Defluidization Investigation on Bubbling Fluidized Bed Particle against
  Alkaline Addition during Pyrolysis Process/ Oral presentation
  Conference name: 18th Asia Pacific Confederation of Chemical Engineering
  Congress (APCChE) 2019
  Date/Venue: September 23rd-27th, 2019/ Sapporo, Japan
  Activity: Oral presentation and Publication paper

List of publication in the journal

- Title: Agglomeration and Defluidization of Silica Sand and Bentonite Particles during Empty Fruit Bunch (EFB) Ash Addition in Bubbling Fluidized Bed (BFB) Processes

  Journal name: Journal of Chemical Engineering of Japan (JCEJ)

  Status: Accepted